Titre: Title:	Development of Polypropylene Microporous Hydrophilic Membranes Through Cast Extrusion and Stretching
Auteur: Author:	Amir Saffar
Date:	2014
Type:	Mémoire ou thèse / Dissertation or Thesis
Référence: Citation:	Saffar, A. (2014). Development of Polypropylene Microporous Hydrophilic Membranes Through Cast Extrusion and Stretching [Thèse de doctorat, École Polytechnique de Montréal]. PolyPublie. https://publications.polymtl.ca/1445/

UNIVERSITÉ DE MONTRÉAL

DEVELOPMENT OF POLYPROPYLENE MICROPOROUS HYDROPHILIC MEMBRANES THROUGH CAST EXTRUSION AND STRETCHING

AMIR SAFFAR

DÉPARTEMENT DE GÉNIE CHIMIQUE

ÉCOLE POLYTECHNIQUE DE MONTRÉAL

THÈSE PRÉSENTÉE EN VUE DE L'OBTENTION

DU DIPLÔME DE PHILOSOPHIAE DOCTOR

(GÉNIE CHIMIQUE)

JUILLET 2014

UNIVERSITÉ DE MONTRÉAL

ÉCOLE POLYTECHNIQUE DE MONTRÉAL

Cette thèse intitulée:

DEVELOPMENT OF POLYPROPYLENE MICROPOROUS HYDROPHILIC MEMBRANES THROUGH CAST EXTRUSION AND STRETCHING

présentée par : SAFFAR Amir

en vue de l'obtention du diplôme de : Philosophiae Doctor

a été dûment acceptée par le jury d'examen constitué de :

Mme HEUZEY Marie-Claude, Ph.D., présidente

M. AJJI Abdellah, Ph.D., membre et directeur de recherche

M. CARREAU Pierre, Ph.D., membre et codirecteur de recherche

M. KAMAL Musa, Ph.D., membre et codirecteur de recherche

M GRMELA Miroslav, Ph.D., membre

M. HATZIKIRIAKOS Savvas, Ph.D., membre

DÉDICACE

To my beloved mother and sisters

ACKNOWLEDGEMENTS

First of all, I would like to express my deep and sincere gratitude to my supervisors, Prof. Abdellah Ajji, Prof. Pierre J Carreau and Prof. Musa R Kamal. Their patience, warm encouragements, confidence in me and insightful suggestions have been of great value for me. I truly appreciate their precious comments, constructive remarks and significant efforts for improving the quality of the papers. I really feel lucky for having the rare opportunity to do my PhD under supervision of these famous world-class researchers.

Special thanks to all technical staff of the chemical engineering department, particularly Mr. Guillaume Lessard, Ms. Claire Cercle and Ms. Melina Hamdine.

I would also like to deeply thank Claire Cercle for her warm and quick response to my request for translating parts of this thesis to French.

I warmly thank Mr. Ebrahim Jalali Dil and Mr. Hesamoddin Tabatabaei, for their valuable advice, friendly help, and extensive discussions during this study. I would like to extend my gratitude to all my friends in Montreal for their unforgettable favors and for all the memorable moments I had with them; very special thanks to Ebrahim, Khalil, Hesam, Abbas, Amirhossein, Farhad, Arash, Ramin, Jaber, Ahmad, Hamed (Mahdi) and Vahid who were always there, ready to hear me and help me.

Finally, with all my heart, I would like to express my undying gratitude to my beloved mother and sisters for the overwhelming support they provided and for sacrifices they made throughout my life; there will never be a right word to express my feeling of appreciation for their unconditional love.

RÉSUMÉ

Grâce à ses excellentes propriétés, le Polypropylène (PP) a connu un regain d'intérêt au cours de ces dernières années dans la fabrication de membranes microporeuses. Une des techniques utilisées pour fabriquer des membranes poreuses de PP sans utiliser de solvant ou de particule est basée sur l'étirement d'un film précurseur ayant une structure cristalline lamellaire. Cependant, malgré la popularité du PP à être utilisé dans la production de membranes, il est difficile de le faire adhérer à la plupart des substrats hydrophiles en raison de son caractère hydrophobe. Ce désavantage limite son utilisation dans de nombreuses applications. L'objectif de cette étude est donc de développer des membranes microporeuses hydrophiles à base de PP. Les caractéristiques des résines de PP (modifiées), ainsi que les conditions de recuit et d'étirement sont des facteurs clés pour générer des films précurseurs ayant de bonnes propriétés cristallines et par conséquent, de bonnes membranes microporeuses. C'est ainsi que différents grades commerciaux de PP modifiés, c'est-à-dire greffés soit avec de l'anhydride maléique (PP-g-MA), soit avec de l'acide acrylique (PP-g-AA) ont été mélangés avec du PP vierge par extrusion de film cast. Il a été montré que l'addition des PP modifiés (PP-g-MA ou PP-g-AA) a changé la structure cristalline lamellaire du film précurseur. La perméabilité à la vapeur d'eau augmente de façon significative même à de basses concentrations de PP modifié par rapport à celle du PP vierge. Ceci est attribué à la présence d'une concentration suffisante de groupements polaires à la surface du film tout en ne modifiant la structure cristalline que de façon minimale.

Dans la deuxième partie de cette étude, afin d'améliorer les propriétés hydrophiles de la membrane, des nanoparticules de dioxyde de titane (TiO_2) ont été utilisées. Les analyses FTIR-ATR (IRTF-ATR, InfraRouge à Transformée de Fourier en réflexion) et de XPS (Photo spectrométrie à Rayon X) ont montré que les segments hydrophiles du PP modifié (amphiphile)

agissent comme des groupements fonctionnels et se greffent avec les particules de TiO2 sur la surface du film précurseur. Les résultats ont indiqué que l'hydrophilicité des membranes en PP modifié a été améliorée sans affecter la structure poreuse.

Enfin, dans les troisièmes et quatrièmes parties de ce travail, les changements de la structure cristalline et les performances membranaires ont été étudiés en détails afin d'optimiser les conditions de recuit et d'étirement. Il a été montré que le recuit améliore les propriétés physiques du film en générant un réarrangement des chaines et en créant des lamelles secondaires dans la zone amorphe. Les films recuits ont montré deux seuils d'écoulement sur les courbes de traction et une relation linéaire a été établie entre la force associée au second seul d'écoulement et la quantité de lamelles secondaires. Il a également été observé que la taille des pores et la porosité de la membrane augmentaient avec l'augmentation du temps et de la température du recuit. Pour ce qui a trait à l'étirement, une étape d'étirement à froid a permis de générer une interconnexion entre les pores. Le ratio d'étirement optimal pour l'étirement à froid se trouve en dessous de la déformation correspondant à l'apparition du second seuil d'écoulement du polymère. Au delà de ce second seuil, une diminution de la perméabilité est observée et ceci s'explique par la fragmentation des lamelles. Il a également été montré de façon quantitative qu'appliquer une déformation à basse vitesse d'allongement permet d'obtenir des membranes avec de meilleures propriétés de perméabilité.

ABSTRACT

Due to the outstanding properties of polypropylene (PP), this polymer has been widely used for the production of microporous membrane. One of the techniques to make porous membranes from PP without using solvent and/or particles is based on the stretching a precursor film containing a row-nucleated lamellar structure. However, despite the popularity of PP as a membrane material, PP is difficult to adhere to many hydrophilic substrates because of its intrinsic hydrophobic nature. This limits its performance in many membrane applications. The aim of the present study is to develop polypropylene microporous hydrophilic membranes. Resin characteristics of the modifiers as well as annealing and stretching conditions are the key factors for the production of the appropriate crystalline morphology in precursor films and consequently microporous membranes. In this regard, different commercial maleic anhydride and acrylic acid grafted polypropylene (PP-g-MA and PP-g-AA) were melt blended with PP using cast film extrusion. Investigating the blending of modifiers showed that the addition of the modifiers changed the crystalline lamellar structure of the precursor film. It was found that water vapor permeability was increased significantly at low concentrations of the modifiers, compared to neat PP. This was attributed to the presence of a sufficient concentration of polar groups on the surface with a minimal change in the crystalline structure.

To increase even further the hydrophilic properties of the membrane, in the second part of this study, titanium dioxide (TiO_2) nanoparticles was employed. ATR-FTIR and XPS analyses showed that the hydrophilic segments of an amphiphilic modifier can act as surface functional groups and graft with TiO_2 nanoparticles on the precursor film surface. The results indicated that the hydrophilicity of the modified PP membranes was improved without affecting the pore structure.

In the third and fourth parts of this research, changes in the crystalline structure and membrane performance were investigated in details to optimize annealing and stretching conditions. It was shown that annealing improved the physical properties of the films by promoting chain rearrangement and creating secondary lamellae in the amorphous region. Annealed films exhibited double yield points in the tensile deformation curves and a direct linear relationship between the strength of the second yield point and the fraction of the lamellae was reported. It was also observed that by increasing annealing time and temperature, the pore sizes and porosity of the membrane increased. Regarding stretching, the cold stretching step was found to be the important one to promote interconnection between the pores. The optimum stretch ratio for the cold stretching step was found to be below the strain corresponding to the second yield point of the polymer; beyond that strain, a reduction in the permeability was observed and explained in terms of lamellae fragmentation. It was also shown quantitatively that applying a low strain rate improved the permeability of the membranes.

TABLE DES MATIÈRES

LIST OF TABLES

LIST OF FIGURES

CHAPTER 1 INTRODUCTION

Microporous membranes are commonly used in separation processes such as filtration, battery separators and medical applications to control the permeation rate of chemical components. Due to the wide range of chemical structures, optimum physical properties and low cost of polymers, these materials are known as the best candidates for the fabrication of microporous membranes.

Three commercially available processes are used for making microporous membranes: solution casting followed by phase separation (also known as extraction process), particle stretching, and dry-stretching. In the phase separation process, the polymeric raw material is mixed with processing oil or plasticizer and this mixture is extruded, then, the plasticizer is removed by extraction (Gozdz et al. 1997). In the particle stretching process, the polymeric material is mixed with solid particles, this mixture is extruded, and pores are formed during stretching at the interface between the polymer and solid particles (Aoyama et al. 1990). Processing cost, pore size control and solvent or particle contaminations are the main drawbacks of the solution and particle stretching techniques. The process to develop membranes by stretching, without using a solvent or extra component, has been introduced since 30 years ago for some semi-crystalline polymers.The dry-stretch process, which is the method used in this study, is based on stretching of a polymer film containing a row-nucleated lamellar structure. This method is relatively less expensive in comparison to the other methods and there is no solvent contamination. The major disadvantage of this method is low tear resistance of the final membranes in the stretching direction.

Three consecutive stages are carried out to obtain porous membranes by this technique: (1) creating a precursor film containing the desired lamellar morphology, i.e., an oriented shish-kebab structure, through shear and elongation-induced crystallization of the polymer having

proper molecular weight and molecular weight distribution, (2) annealing the precursor film at elevated temperatures to improve the crystalline structure, and (3) stretching at room temperature to create the pores by lamellar separation and then, stretching at a high temperature to enlarge them (Sadeghi 2006; Tabatabaei 2009; Liu et al. 2013). To produce microporous membranes by the stretching technique, obtaining precursor films with an adequate orientation and alignment of the crystal lamellae are needed (Sadeghi 2006; Tabatabaei 2009). The type of resin and applied processing conditions are the key factors for the production of the precursor films with controlled type, orientation, and connection of the crystals, which in turn control the final membrane structure.

Semi-crystalline polypropylene (isotactic PP) is one of the most commonly used polymers today in a variety of applications due to its outstanding properties, such as low cost, easy processing, good mechanical properties, chemical stability and non-toxicity (Xu et al. 2010). Despite its popularity as a membrane material, PP does not adhere to many substances such as water or to hydrophilic substrates because of its intrinsic hydrophobic nature. This limits its applications in wastewater treatment, desalination of sea water, electrode separators in batteries and biomedical applications (Bongiovanni et al. 1998; Hester et al. 1999; Fang et al. 2009; Xu et al. 2010).

Hydrophobic membranes are also prone to fouling when used in treating aqueous solutions containing natural organic matter, e.g., oil droplets or macromolecular species. Organic matter is easily adsorbed onto the membrane surface or pore walls and results in the deterioration of the membrane performance. Subsequently, replacement and maintenance costs of membrane modules are increased (Hester et al. 1999; Fang et al. 2009; Li et al. 2009). Membrane fouling can be divided into reversible and irreversible fouling. Reversible fouling caused by reversible organic matter adsorption, which occurs in a hydrophilic surface, can be fully or partly removed.

Irreversible fouling is caused by irreversible organic matter adsorption on the hydrophobic surface and can only be eliminated by chemical or biochemical cleaning (Meier-Haack et al. 2004; Zhang et al. 2010). The cause for irreversible fouling is the lack of hydrogen bonding interactions between the hydrophobic membrane and water in the boundary layer, which leads to the spontaneous process of the repulsion of water molecules away from the surface. By contrast, membranes with a hydrophilic surface are able to form hydrogen bonds with the surrounding water molecules (Li et al. 2013). It is difficult for hydrophobic solutes to approach the water boundary and break the orderly structure due to the energy required to remove the water boundary and expose the membrane surface (Meier-Haack et al. 2004; Zhang et al. 2010). Furthermore, the presence of a spontaneous and permanent wettable surface is a basic requirement for a battery separators to accommodate the aqueous electrolyte solution and prevent solvent leakage, which often causes the deterioration and reduces the life of a battery (Goel et al. 2009; Kim et al. 2010). Accordingly, increasing the hydrophilicity of the membrane surface is the general approach used to prevent irreversible membrane fouling and, as well, to improve the surface properties, such as adhesion and printability (Bongiovanni et al. 1998; Zhang et al. 2010).

Despite this drawback, hydrophobic materials have higher mechanical and chemical stability than hydrophilic materials, which are used in membrane applications (Hester et al. 1999; Meier-Haack et al. 2004). Thus, the ideal membrane would combine the superior bulk properties of hydrophobic materials with the surface chemistry of hydrophilic materials (Hester et al. 1999; Datla 2008).

Different strategies have been carried out to improve hydrophilicity of the membrane surface, i.e., increasing the amount of surface polar groups and maximizing hydration. However, blending of

polymers is by far one of the most efficient techniques to generate new materials with desired properties while satisfying the economic aspects (Datla 2008).

The main motivation of this study is improving hydrophilic properties of microporous polypropylene membranes through cast extrusion. To achieve this goal, in the first phase of this study, different commercial amphiphilic modifiers, i.e., maleic anhydride and acrylic acid grafted polypropylene (PP-g-MA and PP-g-AA), were melt blended at different concentrations with PP to examine the hydrophilicity and crystalline structure of the PP based microporous membranes. In the next step, the hydrophilic properties of the microporous membranes are enhanced through grafting TiO_2 with COOH groups on the surface. Having obtained an understanding of the membrane process, the last phase of the thesis looks in depth at the influence of annealing and stretching conditions on the crystalline structure and membrane performance. Understanding these mechanisms is important to prepare membranes with the desired performances.

This dissertation is based on four articles that have been published or submitted to scientific journals, and consists of the following chapters:

- Chapter 2 provides a literature review considering the related issues.
- The objectives are introduced in Chapter 3.
- In Chapter 4, the organization of the articles is described.
- Chapters 5-8 include the four articles describing the main results obtained in this study.
- Chapter 9 presents a general discussion about the results presented in previous chapters.

- Finally, Chapter 10 summarizes the most important conclusions of this thesis and outlines some recommendations for the future works in this area.

CHAPTER 2 LITERATURE REVIEW

2.1 Polypropylene structure

Polypropylene was discovered in the early 1950s by Giulio Natta. It is prepared by polymerizing propylene in the presence of a catalyst under carefully controlled heat and pressure. Propylene as a gaseous by-product of petroleum refining is an unsaturated hydrocarbon, containing only carbon and hydrogen atoms. Depending on the catalyst and the polymerization method used, the molecular configuration can be altered to produce three types of polypropylenes: atactic, isotactic, and syndiotactic configurations. The Ziegler-Natta catalyst, which was developed in the 1950s, makes the isotactic formation possible with a high level of crystallinity and different molecular weights (Datla 2008). Isotactic polypropylene (iPP) is one of the most commonly used polymers today in many different applications due to its outstanding properties, such as low cost, easy processing, good mechanical properties, chemical stability and non-toxicity (Van der Meer 2003; Xu et al. 2010). Nowadays, the commercially available polypropylene grades usually show a very high fraction of isotacticity; therefore, the term "PP" refers to isotactic polypropylene in the following discussion.

The crystal forms of PP are quite complicated and highly dependent on the processing conditions. PP possesses four crystal forms: α, β, γ, and smectic forms. All of these forms involve the same 3_1-helix conformation as shown in Figure 2-1, but packed differently when folded into lamellae (Lin 2008).

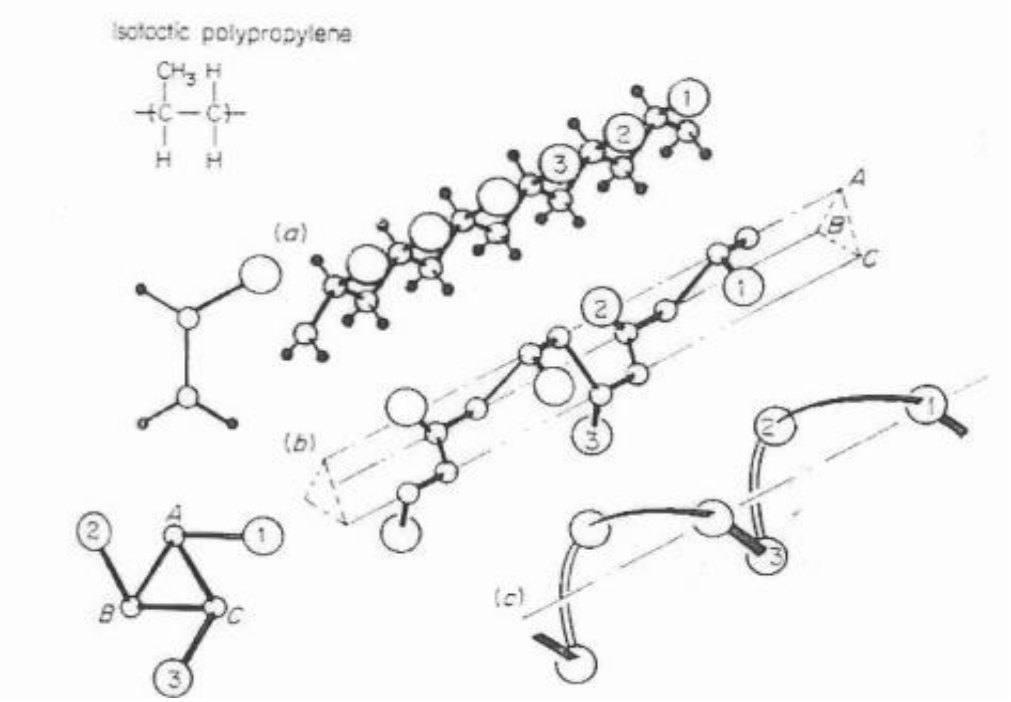

Figure 2-1: (a) Isotactic Polypropylene, (b) The 3_1-helix, (c) The 3i -helix with only showing methyl groups (Lin 2008).

The α-phase: The most common crystalline form encountered in conventional processing conditions, such as under a slow cooling and high stress, is the α-form (Lin 2008). The monoclinic unit cell of α form has the following parameters a = 6.65Å, b = 20.96Å, c = 6.5Å and β=99.62°. The overall density is 0.946 g/ cm^3 and melt at about 160 ^oC (Van der Meer 2003).

The β-phase: The β-form can be found in some specific processing conditions such as large temperature gradient or fast cooling or use of β-nucleating agents (Van der Meer 2003). The β-form is thermally unstable with a melting temperature of 152 °C, and can transform to the α-form at elevated temperature or under stress (Lin 2008). The β phase has a trigonal unit-cell with lattice parameters a = b = 11.0 Å, c = 6.5Å, β = 120° and density = 0.922 g/cm^3.

The γ-phase: The γ crystal structure is tetragonal (a=6.38 Å , c = 6.33 Å , N =1, density = 0.939 g/cm^3) and may be formed in low molecular weight PPs or when crystallization is performed under high pressure. In this unit cell the c-axis is not parallel with chain axis direction and have an angle of + or - 40° with the normal direction of the lamellae (Van der Meer 2003; Lin 2008).

Smectic form: The smectic form presents a state of order intermediate between amorphous and crystalline states (a transition crystallographic state). This form found under very rapid cooling and transforms into the α-form at elevated temperatures (Lin 2008). The smectic-to-α form transition can be characterized with an apparent exotherm peak at a temperature from 65 to 120 °C (Lin 2008).

2.2 Crystallization process

When a semi-crystalline polymer crystallizes, the polymer chains tend to pack and form a crystalline layer called lamellae. The thickness of the lamella varies from approximately 4 nm for the crosshatched lamellae to several tens of nanometers for primary grown lamellae. Since the typical polymer chain length is about 1000 nm, the only explanation for the conformation of the polymer chains in the lamellar structure is chain folding (Lin 2008). Lateral dimensions of the lamellae may reach several micrometers. The lamellae are separated by amorphous layers while its thickness is usually in the order of the thickness of lamellae (Van der Meer 2003).

It is known that strain can accelerate the crystallization kinetics of the polymer, increase the nucleation rate and change the crystalline morphology. Therefore, the crystallization of polymers can be divided into the following regimes:

2.2.1 Quiescent crystallization: Spherulites

In an unstressed state, crystallization usually starts at some kind of isolated and discontinuous nuclei and lamellae grow radially along the growth direction and form the spherulitic morphology (see Figure 2-2a). Spherulites do not have the oriented regularity on a lamellar scale along the extrusion direction (Zhou 1997; Van der Meer 2003).

2.2.2 Flow induced crystallization (FIC)

Flow-induced oriented molecular chains markedly increase the nucleation rate and the crystal growth rate of the polymer and form a different morphology with respect to quiescent conditions (Lamberti 2011). Basically, a polymer can be under the influence of an elongational flow (stretching flow) or a shear flow, even though in most processing operations both elongational and shear fields are applied on melts (Steenbakkers 2009). Compared to shear flow, the elongational flow is much more effective in inducing chain extension and orientation. A major consequence of chain extension is the decrease in conformational entropy and a corresponding increase in the free energy. This means an increase in the driving force for crystallization at a fixed processing temperature (Zhou et al. 2010). Also, we can consider that a simple shear flow may be represented as the superposition of a purely elongational flow and a purely rotational flow. The rotational and elongational components in a simple shear flow are equal, such that the polymer cannot attain a stable fully stretched condition: the extensional component orients and stretches the molecules, whereas the rotational component causes a fluctuation in the extension (Iervolino 2006). Therefore, shear flow is considered a weak flow that is less efficient than elongational flow in obtaining orientation or stretching. Although numerous studies have been conducted on the effect of shear flow on the crystallization of various resins, very little has been

reported on the role of elongational flow. This lack of investigations is due to the difficulties to measure the extensional material functions. For instance, it is still impossible to reach very large strains and deformation rates with the existing elongational rheometers. Elongational flow can be created in many devices and geometries including two roll and four roll mills, converging flow and cross-slot device.

Under elongational flow, certain polymer chains are extended; therefore, thermodynamically as well as kinetically, these portions of the chains can crystallize faster and form row-nucleated fibril crystals. The first-formed row-nucleated fibril crystals can then serve as nuclei for the later development of chain-folding lamellar crystals (Zhou 1997). Combination of the above two structures is commonly refereed as shish-kebab or row morphology (see Figure 2-2b).

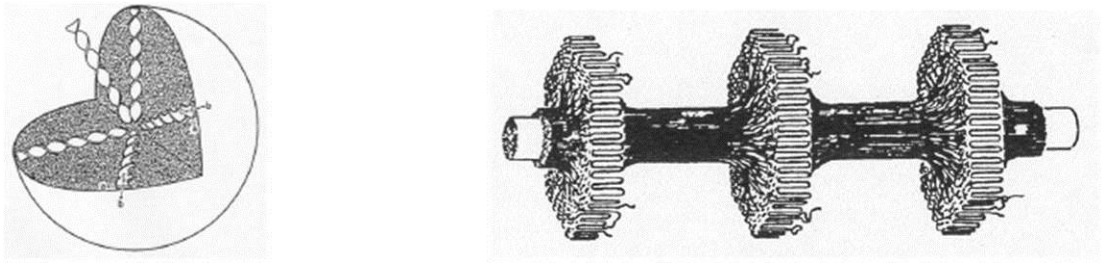

(a) (b)

Figure 2-2 : Schematic of a) a spherulitic and b) a shish-kebab structure (Bashir et al. 1986).

The flow induced crystallization process to produce shish kebab structure can be summarized as follows:

Initially, the molecular chains of polymers are presented as random coils in the melt (Figure 2-3a). After applying a steady deformation, the chains are stretched slightly (Figure 2-3b), which aggregates each one to form a bundle structure and promotes the formation of stable nuclei.

These stable nuclei align tightly in the direction of flow to form the fibrillar-like skeleton structure (oriented crystal nuclei) (Figure 2-3c). Subsequently, these aligned nuclei grow by absorbing the neighboring molecular chains. The nuclei grow perpendicularly to the direction of flow, which leads to the 2-dimensional growth of polymer crystals (Figures 2-3d and e). The final result is the shish–kebab crystal structure: the oriented nuclei aggregate tightly and form the shish-like fibrillar crystal skeleton, while the lamellae grow epitaxially around it (Zhang et al. 2008).

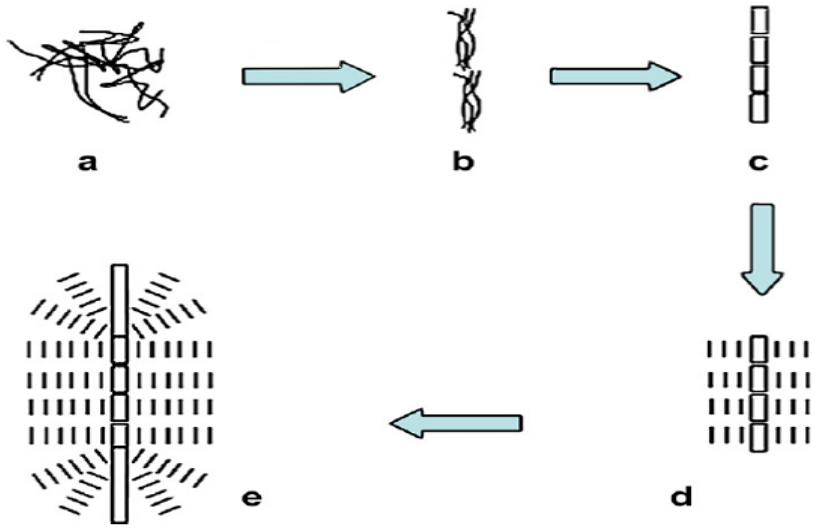

Figure 2-3: Schematic picture of flow-induced crystallization: (a) amorphous molecular chains in melt, (b) flow-induced molecular chain orientation, (c) formation of oriented crystal nuclei, and (d and e) 2-dimensional growth of crystal (Zhang et al. 2008).

According to the mechanism of flow-induced crystallization of polymer melts, if the linear row nuclei or shish did not form, the subsequent growth of kebabs, i.e., lamellae perpendicular to the flow direction would not be possible. The processing parameters as well as resin characteristics

(e.g. molecular weight, molecular weight distribution and long chain branching) are the key factors for controlling the morphological features of the extruded precursor films (Sadeghi 2006; Tabatabaei 2009). Also, die temperature, die gap, rate and position of the air cooling unit, chill roll temperature, and draw ratio are the major processing parameters that need to be optimized depending on the resin.

The crystalline morphology of films is dependent on the stretch ratio. If the deformation applied in a flow is strong enough, highly oriented structures can be observed. This factor is controlled by the melt and stretch speeds. The ratio of stretch speed to the melt velocity determines the value of draw ratio (DR). Lower DRs result in fully spherulitic structures. By increasing DR, the radius of the spherulite decreases and the spherulite gradually becomes smaller and deforms. With a further increase in DR, the polymer melt stretchs faster so that severely deformed spherulites are now dominant and develop a fiber-like structure. The rate of increase of the orientation is relatively high with an increase of DR. When the DR becomes even larger, spherulites are difficult to form and most chains are oriented and later introduced into the shish structures. As a result, the shish (or shish kebab) structure becomes dominant (see Figure 2-4) (Zhou et al. 2010).

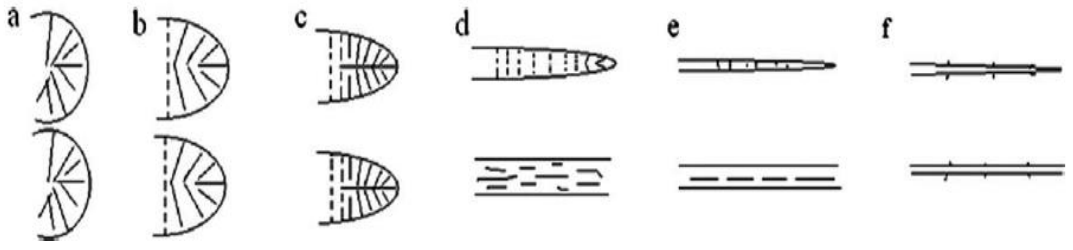

Figure 2-4: Model interpretation of the morphology evolution with the increase of DR (Zhou et al. 2010).

Tabatabaei (2009) and Sadeghi (2006) also observed that the draw ratio in polypropylene cast films improved the orientation along the machine direction. They reported a linear relationship between the orientation function and draw ratio. Also, they showed that at low draw ratios the lamellae are not well aligned perpendicularly to the flow direction, but as DR increases, the lamellae align themselves perpendicularly to the machine direction (MD).

As mentioned above, the process for the formation of such a lamellar structure is based on the elongation of the chains in the melt state followed by a rapid crystallization. It is obvious that the chains should preserve their elongated form to be able to act as initial nuclei. The relaxation time of the chain is also the other important factor for this stage. Based on experimental evidence, a critical deformation or elongation rate needs to be exceeded to change from the spherulitic to the oriented crystallization regime where fibrillar growth occurs (Bischoff White et al. 2012; Custodio et al. 2009; Steenbakkers 2009). In the absence of flow, the elongated chains will relax to random coils. So, there is a competition between these two factors, i.e., deformation and relaxation. If the length of an elongated chain is larger than the size of a critical bundle nucleus, it is possible for nucleation to progress. On the other hand, nucleation cannot progress. This is the reason why critical deformation exists for the formation of shish. It is to be noted here that critical deformation may depend on the characteristics of the polymer, and decreases with the addition of long chains which has the largest relaxation time (Yamazaki et al. 2005).

Somani et al. (2000) followed the orientation development upon applying different shear rates. They found that the deformation rate must be high enough to orient and align the polymer chains in the melt to form stable nuclei in the flow direction. At a given shear rate, only those molecules having a chain length (molecular weight) above a critical value can form stable oriented row nuclei, while the rest of the molecules will remain un-stretched. Then the result would be a

bimodal distribution of chain molecules represented by a dual population of oriented and non-oriented chains. Their findings showed that increasing shear rate did not enhance the chain extension, but increased the amount of chains that became oriented. Then a structure with a bimodal population of oriented and non-oriented chains was created as can be seen in Figure 2-5. This figure shows that the "critical molecular weight" (*M**) on the curve shifts to a higher values at low deformation rates, as showed by the lines (1- low shear rate and 2- high shear rate). The area under the MWD curve represents the fraction of material above or below the critical molecular weight. It was claimed that the value of *M** is more sensitive at low shear rates than at higher ones, reaching a plateau at high shear rates (Somani et al. 2000).

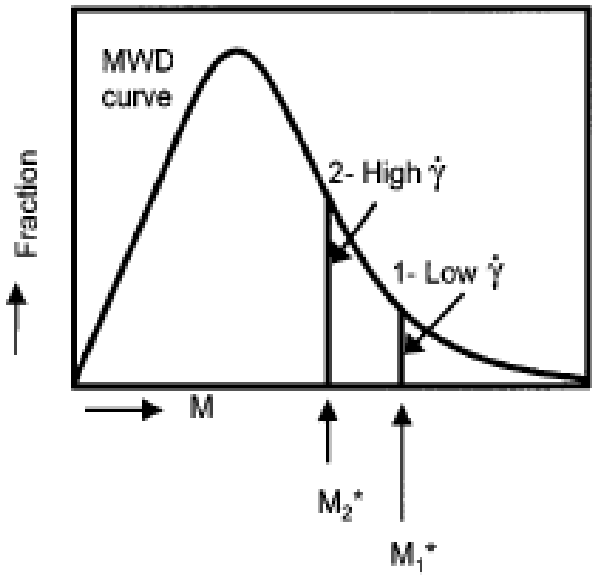

Figure 2-5: Schematic showing the effect of imposed shear conditions on the shift in the location of the critical molecular weight *M** (Somani et al. 2000).

Nogales et al. (2001) proposed a method to calculate the critical molecular weight for orientation. They considered the oriented structure based on the change in the radius of gyration and the

degree of chain extension is represented as the ratio of the radius of gyration of the extended chain to that of non-oriented chain. The comparison between the radius of gyration in direction parallel to the deformation field and the radius of gyration in the perpendicular direction to the deformation field can represent finally the orientation.

Under isothermal conditions, the molecular weight and chain architecture are expected to play major roles in governing the extent of elongation and stability of the oriented structures after cessation of shear. Longer chains and branched molecules both take a longer time to relax after deformation than shorter ones, and thus, have a better chance of being oriented. The longer chains from the high molecular weight tail would give rise to orientation-induced nuclei due to higher orientation compared to the shorter chains. The short chain molecules relax in a very short time after deformation and hence cannot form nuclei under flow. But, it has been shown that temperature dependency of the relaxation time is much stronger than that of the zero shear viscosity (Somani et al. 2000).

The die temperature (the extrudate temperature) affects the relaxation of the molecules. Low temperature will slow down the chain relaxation, leading to an increase probability for the formation of lamellae by the low molecular weight chains. However, very low extrusion temperatures prevent the mobility of the molecules, which results in a non-appropriate row-nucleated lamellar structure. Therefore, an optimum temperature needs to be selected for each polymer. Tabatabaei (2009) reported that the overall effect of moving towards lower temperature is more deteriorating than processing at higher temperature. Their results showed that the use of air cooling in addition to chill rolls helps flow induced crystallization to occur at lower temperatures for PP and HDPE monolayer films as well as in multilayer films (PP/HDPE/PP). The use of air cooling in addition to chill rolls noticeably increased the number of shish or nuclei

sites, and consequently the crystallization kinetic is promoted, resulting in a well oriented shish-kebab structure. This was due to preserving the oriented states for the chains; otherwise, chains relax after stretching due to their tendency to return to their initial coil state.

Sadeghi (2006) and Tabatabaei (2009) considered the influence of molecular weight and long chain branched PP on orientation of row-nucleated lamellar structure using WAXD, SAXS and FTIR. They found that molecular weight was the main resin factor that controlled the PP crystal structure. It was demonstrated that the resin with high molecular weight developed larger orientation and thicker lamellae than the resin with low molecular weight. Sadeghi (2006) realized that an initial orientation was required in order to obtain a lamellar structure. The crystalline orientation in the precursor film depended on the molecular weight of the resin and the type of film process (i.e. cast film or film blowing). It was shown that the cast film process was more efficient than film blowing for producing precursor films with the appropriate crystalline orientation. Sadeghi (2006) compared the structure and properties of the precursor films obtained from a linear PP and its blend with 2 wt% long chain branched PP (LCB-PP). The addition of a small amount of a branched component drastically affected the row-nucleated crystalline structure of the precursor film. Blending improved the orientation of both the crystalline and amorphous phases and led to the formation of much more lamellae than in the neat linear resin. Tabatabaei (2009) also reported that adding high molecular weight enhanced the orientation of both the crystalline and amorphous phases.

Somani et al. (2006) compared the oriented microstructure in isotactic polypropylene melts (PP-A and PP-B) with the same number average molecular weight but different molecular weight distribution (MWD) under shear flow. The amount of the high molecular weight species was larger in PP-B than in PP-A. Both samples were subjected to identical same shear conditions.

Their results elucidated that the shish structure formed much earlier for PP-B with a more pronounced crystal orientation and a faster crystallization kinetics. They concluded that even a small increase in the concentration of the high molecular weight chains led to a significant increase in the shish or nuclei sites formation. Seki et al. (2002) prepared a very high molecular weight polypropylene (M_w= 923.2 (kg/mol)), through the fractionation of a regular PP, and blended it with a moderate molecular weight PP. Using this approach, they showed that the addition of less than one percent of this polypropylene to a typical iPP with moderate molecular weight (M_w=186 kg/mol) significantly influenced the crystallization kinetics and resulted in a lamellar morphology.

Also, Agarwal et al. (2003) studied the shear induced crystallization in chain branched polypropylene. They investigated several polypropylenes with different branching index while their number-average molecular weights were relatively constant. But, the high molecular weight components (M_w, M_z and M_{z+1}) increased with the branching level. Thus, the highly branched species resided at the high molecular weight species of the molecular weight distribution. They studied the SAXS pattern for shear induced crystallization of a branched polypropylene and observed that equatorial and meridian maxima appeared when shear was applied to the melt. They attributed the equatorial peaks to fibrils and meridians to lamellae and also revealed that the intensity of the patterns was enhanced with increased branching (see Figure 2-6). The crystal orientation was stronger for the branched polypropylene in comparison to linear PPs. A larger crystallization rate for the branched PP was also reported in comparison to linear PPs. The higher crystallization rate in branched PPs is likely due to greater nucleation rate as a result of chain orientation.

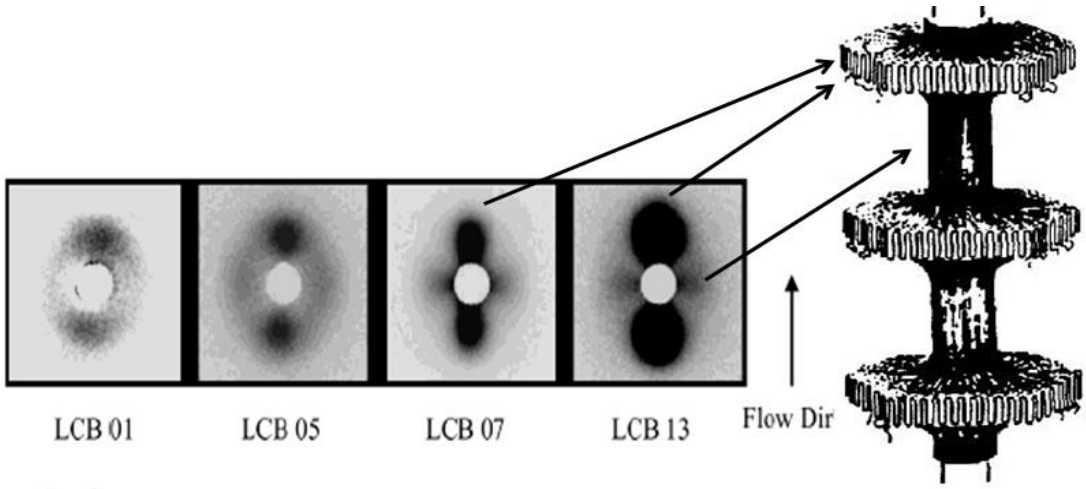

Figure 2-6: Comparison of 2D SAXS patterns of the four LCB-iPPs,: shear rate= $60s^{-1}$, t_s(shearing time) 0.25 s, T= 140 °C (Agarwal et al. 2003).

2.3 Overview of the membrane technology

2.3.1 Membrane classification

Membrane can be used as a semi-permeable barrier in order to separate particles dissolved in a fluid or components of a solution due to their chemical or physical properties when a driving force is applied (Chandavasu 2001). Polymers and polymer blends are among the best candidates for the development of the membranes due to their properties such as wide range of chemical structures, optimum physical properties and low cost. Polymeric membranes have been developed for various industrial applications such as microfiltration, ultrafiltration, reverse osmosis (RO), gas separation, and wastewater treatment (Baker 2004). Membranes are commonly classified based on the size of the separated materials as depicted in Figure 2-7.

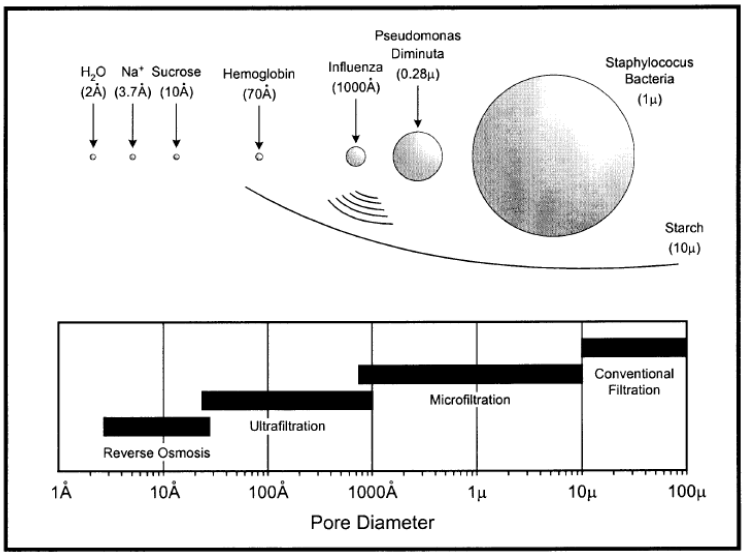

Figure 2-7: Separation processes differing in the size of the particles to be separated (Baker 2004).

Depending on the structure, polymeric membranes are divided in two categories: isotropic membranes and anisotropic membranes. Isotropic membranes contain uniform structure while anisotropic membranes have a chemically or a physically heterogeneous structure.

Isotropic membranes can also be classified in three categories as follows (Baker 2004):

Microporous membranes: this kind of membranes has a highly porous structure with randomly distributed interconnected pores. In microporous membranes, pores size varies from 0.01 to 10 μm in diameter.

Nonporous or dense membranes: this is a dense film in which permeates penetrates by diffusion under an applied driving force of a pressure, concentration, electrical potential gradient (or a combination of two or three).

Electrically charged membranes: in this type of membranes, the separation is obtained by the exclusion of the particles with same charge.

On the other hand, anisotropic membranes have a skin/core structure. The skin layer is an extremely thin surface layer supported on a much thicker core with porous structure. The skin/core structure can be formed in a single operation or separately. A schematic diagram of isotropic and anisotropic membranes is illustrated in Figure 2-8.

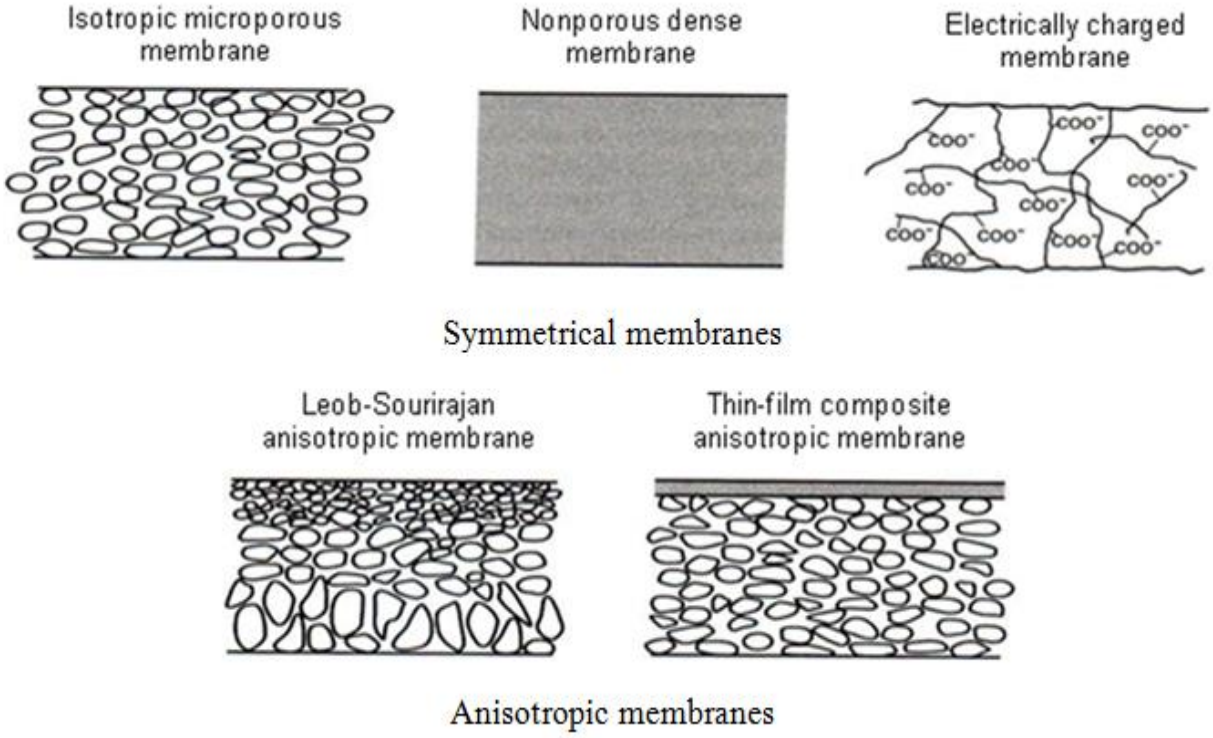

Figure 2-8: Schematic diagrams of the various polymeric membranes (Dang 2009).

2.3.2 Membrane fabrication techniques

Polymeric membranes are made through various techniques such as: phase separation, track etching, leaching, thermal precipitation, and stretching.

Phase inversion can be described as a de-mixing process whereby the initially homogeneous polymer solution is transformed in a controlled manner from a liquid to a solid state. This transformation can be accomplished in several ways, namely (a) thermally induced phase separation (TIPS); (b) controlled evaporation of solvent from three component systems; (c) precipitation from the vapour phase and (d) immersion precipitation (IP) (Liu et al. 2011). One of the main difficulties that limits the successful casting of phase inversion membranes is the lack of a predictable and systematic method in selecting solvent systems (Liu et al. 2011). The TIPS process can be applied to semi-crystalline polymers with suitable diluents; however, it is a less attractive process due to large pore sizes and the necessary post-treatments for solvents (Lin 2008).

In the track etching method, polymer films or foils are subjected to high energy particle radiation (metal ions) applied perpendicularly to the material, followed by etching in acid or an alkaline bath. Consequently, cylindrically shaped pores with uniform pore size distributions, symmetric porous structures, could be obtained. While the membrane porosity is mainly determined by the duration of radiation, the pore size is determined by the etching time and temperature (Liu et al. 2011). The membrane becomes very brittle as porosity increases. The pore size is also limited and cannot be smaller than 0.01 μm (Lin 2008). Leaching is based on extrusion of the polymeric raw material added with solid particles followed by the extraction of the solid, leading to pores formation. In thermal precipitation, cooling of a mixture of a solvent and polymer is applied to enable phase separation followed by extraction of the solvent. Stretching technique is based on the stretching of a polymer film containing a dispersed phase where upon stretching pores are created due to stress concentration at the interface of these sites (Baker 2004), or stretching a specific crystalline morphology as detailed below. In this method, a porous membrane is developed without the use of any solvent (Lin 2008).

Stretching technique: This technique is based on the drawing of a polymer film or sheet having one of the followings: filler particles (Nagō et al. 1992), droplets of an immiscible polymer component (Xanthos et al. 2002), a mixed solvent (Williams et al. 1974), beta or hexagonal unit cell crystals (Shi et al. 1989), or a stacked lamellar structure. Since the aim of this dissertation is making microporous membranes by stretching a stacked lamellar crystalline structure, introducing other stretching techniques will help the reader in understanding the importance of the process used.

In the stretching of a filler polymer film, the resin is first mixed with a filler and then melt extruded to prepare a composite film or sheet. Upon applying stretching, cracks are initiated and, subsequently, propagated at the interface of filler particles and polymer matrix. The filler can be a mineral or organic compound. The pore size, pore size distribution and porosity depend on the type of filler, its interaction with the polymer matrix, blending process, amount of filler and also film thickness. To completely remove the filler from the polymer matrix after drawing, the filler should have poor wetting ability with the polymer matrix (Yu 1995). The most important stage is the filler incorporation, which includes dispersion and distribution of the filler throughout of the matrix.

Different inorganic fillers can be used; among them, calcium carbonate and barium sulfate are particularly preferred (Aoyama et al. 1990). The important issues are the shape of the particle, the price, the whiteness, the interaction with the matrix and the availability. The average particle size of inorganic fillers according to ASTM C-721-76 should be 0.4 to 4 μm or smaller. Using filler larger than that might limit the stretchability and create a non-uniform pore distribution and, in some cases, breakdown might occur. The amount of inorganic filler to be added should be sufficient to attain the desired porosity, but it depends to some extend on the kind and particle

size of the inorganic filler. Inorganic fillers such as calcium carbonate are preferably surface treated to be hydrophobic so that the filler can repel water to reduce agglomeration of the filler. For calcium carbonate, a preferred coating is calcium stearate or steraric acid (Kundu et al. 2003). Xanthos et al. (2002) were probably the first investigators to develop microporous membranes based on stretching of immiscible polymer blends. In that study, stretching caused debonding at the interface of incompatible polymer blends of PP and PS and also a small amount of a copolymer as a compatibilizer, resulting in membrane formation. Their findings showed that the dispersion of the minor component with a narrow particle size distribution was the most important factor controlling the pores size.

The solvent stretching technique was invented by Williams et al. (1974). In this technique, a polymeric film having at least two components is immersed in a solvent and absorption of the solvent takes place in the component with lower volume fraction. Then, the film is first stretched in one or two directions while it is in contact with the solvent and then maintained in its stretched form during the removal of the solvent. The membrane development based on crystal transformation method is utilized for polymers that have different types of crystal phase, which can be transformed under specific conditions. The most common polymer of this kind is polypropylene. As mentioned before, the β crystalline form is not stable and under certain levels of stress transforms into the more stable α crystalline form. Shi et al. (1989) revealed that the β crystals transformed into a smectic state at a drawing temperature below 80 ºC, but transformed to the more stable α form at higher temperatures. Since the β crystals are less dense than α, this transformation caused volume contraction in the bulk of polymer, resulting in the creation of voids.

Costly processes and difficulties in dealing with solvent or particle contaminations as well as the presence of the nucleating agents are the main drawbacks of the methods described above.

However, besides the above stretching methods, uniaxial stretching of a stacked lamellar structure has been developed for fabricating microporous membranes. Three consecutive stages are carried out to obtain porous membranes by this technique: (1) creating a precursor film containing the desired lamellar morphology, i.e., an oriented shish-kebab structure by mechanism of shear and elongation-induced crystallization, (2) annealing the precursor film at elevated temperatures to improve the crystalline structure, and (3) stretching at low and high temperatures to create and enlarge pores, respectively, in the machine direction (MD) to create the pores by lamellae separation (Sadeghi 2006; Tabatabaei 2009) (see Figure 2-9). For instance, Figure 2-10 illustrates the structure of a PP film before and after stretching. Obviously, a large number of interconnected micro-voids are produced upon uniaxial deformation of the annealed film.

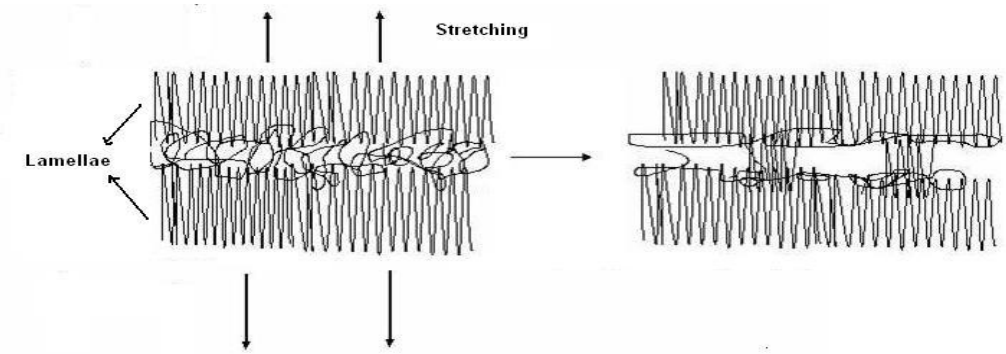

Figure 2-9: Schematic of the pore creation by stretching

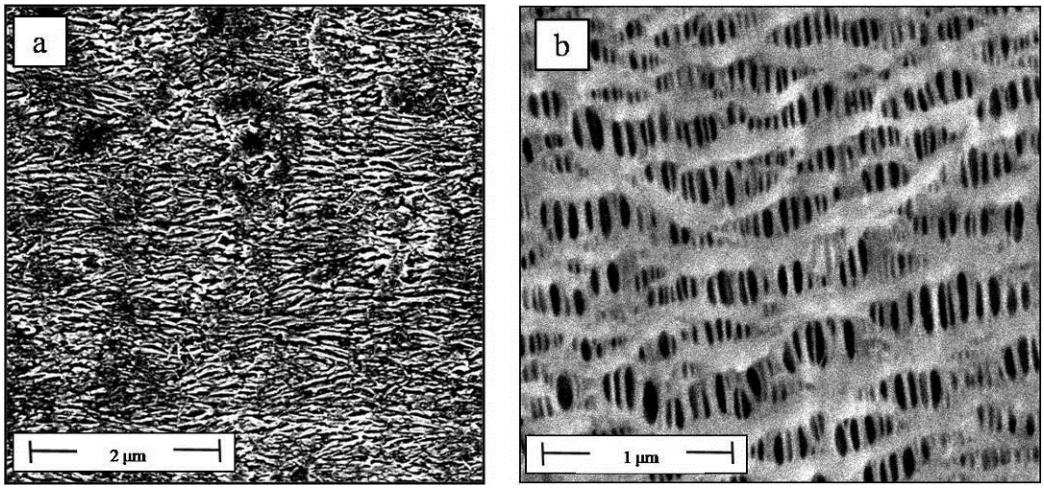

Figure 2-10: SEM micrographs of surface of a PP film a) before and b) after stretching (Tabatabaei 2009).

To produce microporous membranes by this technique, precursor films with a proper row-nucleated lamellar structure, is necessary for the beginning of the process (Sadeghi 2006; Tabatabaei 2009); the higher the crystalline alignment in the precursor, the better is expected the lamellae separation and, as a consequence, the larger the porosity and permeability of the microporous membranes. As mentioned above, in a polymer melt, upon applying a large enough shear or extensional stress, the long chains are elongated into the flow direction and serve as nucleating sites for the later lamellae crystallization. As temperature decreases, the shorter chains crystallize on the extended molecules (shish) to form a row-nucleated lamellar structure. Furthermore, as shown above, the resin characteristics and applied processing conditions are the key factors for the production of the precursor films with appropriate properties, thickness, orientation, and connection of the crystals, which in turn control the final membrane performace.

Sadeghi (2006) and Tabatabaei (2009) investigated the fabrication of polypropylene (PP) microporous membranes in a cast process. Their efforts focused on developing a lamellar

crystalline morphology appropriate for the microporous membrane formation through the control of processing conditions as well as resin characteristics. Tabatabaie (2009) examined the role of molecular weight on polypropylene membrane performance. A larger pore density, greater porosity, and more interconnectivity of the pores were observed when the level of high M_w PP increased. They also reported that microporous membranes possessing high pore density, large porosity, and high water vapor transmission rate were obtained by lamellae separation from cast films prepared using large draw ratio (DR) and air cooling. Figure 2-11 presents SEM micrographs of the surface of the fabricated membranes at different air cooling conditions. Very thick lamellae, non-uniform pores and a small amount of pores for the porous membrane obtained from the no air cooled film was observed (Figure 2-11a). However, for the membrane prepared from the cast film subjected to the air cooling flow, the number of pores noticeably increases and more uniform pore sizes and a better morphology were observed (Figure 2-11b).

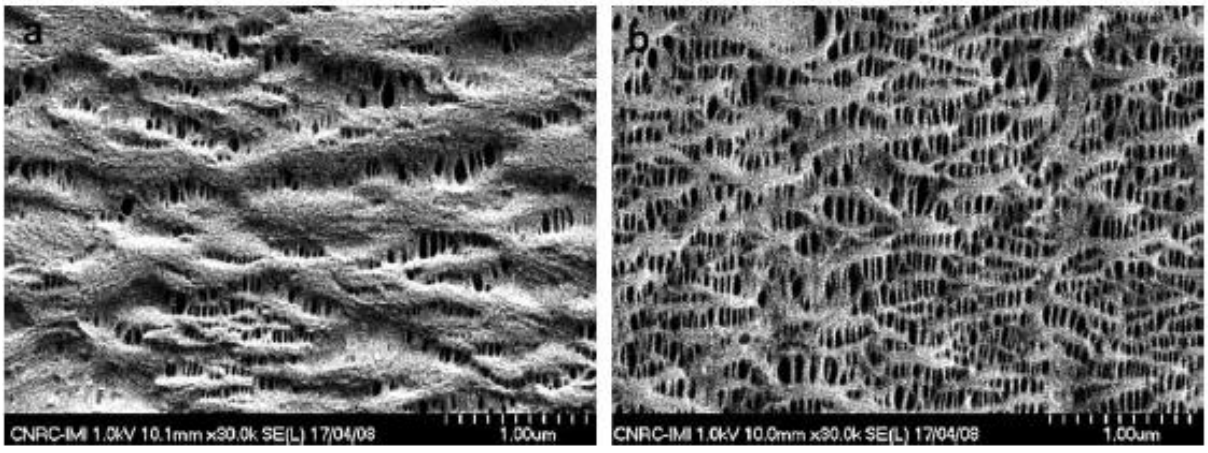

Figure 2-11: SEM micrographs of the surface of the films obtained at: (a) no air cooled film and (b) applying air cooling; cold stretching of 35%, followed by hot stretching of 55% (Tabatabaei 2009).

Sadeghi (2006) compared the structure and properties of the microporous membranes obtained from a linear PP and its blend with 2 wt% long chain branched PP (LCB-PP). An improvement in the row-nucleated crystalline structure of the film as well as superior permeability for the membrane was observed by adding a small amount of a branched component. In Figure 2-12, the surface image of the membrane obtained from the blend revealed elongated thin fibrils, more pores with somewhat smaller size than the L-PP. The blend membrane showed a porosity of 53% whereas it was 41% for the L-PP membrane.

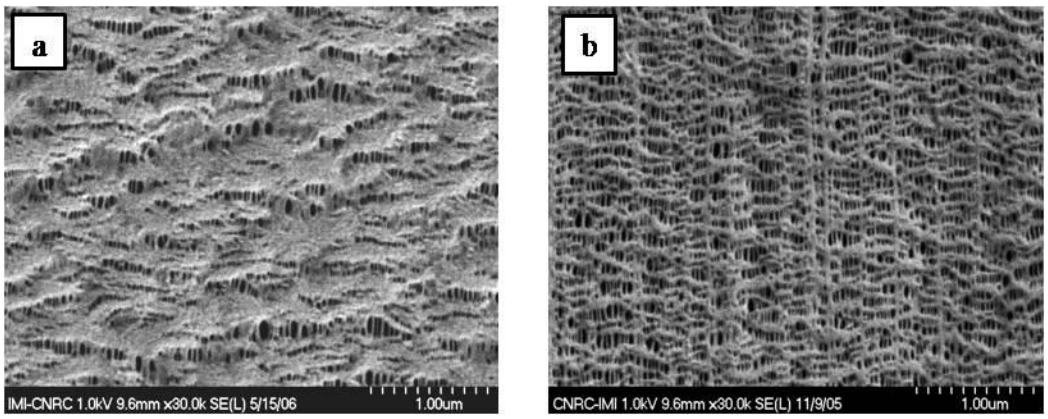

Figure 2-12: SEM micrographs of the surface of microporous membranes. (a) linear PP and (b) Blend with 2 wt% branched PP (Sadeghi 2006) .

During annealing, crystalline perfection takes place. This requires chain mobility in the crystalline phase (α relaxation) and the annealing temperature should be sufficient to activate this relaxation (Tabatabaei 2009). The influence of annealing on the microporous membrane performance was investigated in previous work of this group (Sadeghi 2006; Tabatabaei 2009). They annealed various semi-crystalline films (e.g. PE and PP) possessing stacked lamellar structure and found that crystallinity, crystalline and amorphous orientation as well as long spacing of the lamellae increased. Also, they found that annealing without extension contributed

significantly to the crystalline phase perfection. As mentioned before, during cold stretching, the pores are nucleated whereas in the subsequent hot stretching they are enlarged. Sadeghi (2006) and Tabatabaei (2009) also compared the cold and hot stretching behavior of PP films obtained from resins with distinct *Mw*.

2.4 Membrane surface modification

Despite the popularity of polypropylene as a membrane material, PP does not adhere to many substances such as water or to hydrophilic substrates because of its intrinsic hydrophobic nature. This limits its applications for wastewater treatment, desalination of sea water, electrode separators in batteries and biomedical applications (Bongiovanni et al. 1998; Hester et al. 1999; Fang et al. 2009; Xu et al. 2010). As mentioned in the introduction, hydrophobic membranes are prone to irreversible fouling when used in treating aqueous solutions containing natural organic matter, e.g., proteins, or macromolecular species. Organic matter is adsorbed onto the membrane surface or pore walls and results in the deterioration of the membrane performance (Hester et al. 1999; Fang et al. 2009; Li et al. 2009). The cause for the fouling is the lack of hydrogen bonding interactions between the hydrophobic membrane and water in the boundary layer. By contrast, membranes with a hydrophilic surface are able to form hydrogen bonds with the surrounding water molecules (Li et al. 2013). Despite this drawback, hydrophobic materials have higher mechanical and chemical stability than hydrophilic materials (Hester et al. 1999; Meier-Haack et al. 2004). Thus, the ideal membrane would combine the superior bulk properties of hydrophobic materials with the surface chemistry of hydrophilic materials (Hester et al. 1999; Datla 2008).

Several strategies have been carried out to improve the hydrophilicity of the membrane surface, i.e., increasing the amount of surface polar groups and maximizing hydration.

2.4.1 Surface coating (thin film composites)

Surface coating is the simplest way to improve the hydrophilicity of hydrophobic membranes by forming a thin functional hydrophilic layer on the surface (Liu et al. 2011; Nady et al. 2011). However, the instability of the coated layer, which could be washed away along aggressive cleaning procedures and particularly by changes in solution pH, is the main problem of this method. This could be due to the relatively weak interaction between the modified polymers and the membrane surface (Hester et al. 1999; Liu et al. 2011; Nady et al. 2011). Also, coating typically resulted in changes of the membrane pore size distribution and, consequently, permeability reduction (Hester et al. 1999; Fang et al. 2009; Liu et al. 2011).

2.4.2 Surface grafting

Surface grafting is one of the most promising methods to modify the membrane surface through covalent bonding interaction between the grafted chains and the surfaces of membrane. Covalent attachment of grafted chains on the membrane surface avoids their delamination and offers a long-term chemical stability of grafted chains in contrast with physical surface coating (Liu et al. 2011; Nady et al. 2011). But, grafting typically changes the membrane pore size distribution (Hester et al. 1999). Therefore, even if the modified membranes are less prone to fouling, the permeability after modification is generally smaller than before. Also, in this method, materials are wasted due to produced undesired homo-polymers (Fang et al. 2009). Surface grafting can be achieved by a variety of means. The choice for a specific grafting technique depends on the chemical structure of the membrane and the desired characteristics after surface modification (Hester et al. 1999; Liu et al. 2011; Nady et al. 2011):

1) Chemical initiation technique: In chemical grafting, free radicals are produced and transferred to the surface to initiate polymerization and form graft copolymers. In general, this technique is simple and cheap; but, usually it employs a harsh treatment, which leads to undesirable surface changes and contamination (Nady et al. 2011).

2) Photochemical and radiation initiation techniques: Dissociation of one or more chemical bonds into radicals is performed when a chromophore on a macromolecule absorbs light. These radicals, which are generated on the surface of the membrane, can act as initiators and react with a monomer to form a grafted copolymer. However, the irradiation of macromolecules can form free radicals on the membrane. UV irradiation and UV-assisted graft polymerization are the techniques that can selectively alter membrane surface properties without affecting the bulk polymer. UV-assisted graft polymerization modifies the membrane surface by grafting polymer chains on the surface and in the pores (Nady et al. 2011). The UV photo-grafting should be carefully used because it leads to the degradation of the pore structure and reduction of the pore size (Liu et al. 2011; Nady et al. 2011).

3) Plasma initiation technique: Plasma treatment is probably one of the most versatile membrane surface treatment techniques while it is an efficient way to anchor the functional grafted chains on the surface of membrane. The accelerated electrons from the plasma have sufficient energy to induce cleavage of the chemical bonds in the membrane structure and to form macromolecule radicals, which subsequently initiate graft copolymerization. In general, the modification with plasma treatment is fairly uniform over the whole substrate (Liu et al. 2011; Nady et al. 2011). Also, low energy of plasma causes the bulk properties of the membrane to remain unaffected. However, requirement of a vacuum system, which increases the cost of the operation, is the main disadvantage of plasma. Also, the complexity of plasma processes makes it difficult to control the

chemical composition of the surface after modification and may cause irreversible damage (Dang 2009; Liu et al. 2011; Nady et al. 2011).

2.4.3 Corona and Flame treatment

The hydrophobic surface treated with the corona discharge plasma (atmospheric plasma) exhibits a prominent increase in surface activation and as consequence it exhibits wettability properties. In this method, a high voltage of several thousand volts is applied between a grounded metal roller and knife-shaped electrodes, which are aligned in several mm intervals to the metal roller. A sample is passed through the space between these electrodes where the corona discharge is generated. The equipment setup of the corona technique is simple and cost effective. But, the variation in ambient conditions such as temperature and humidity makes these treatments inconsistent (Datla 2008). The hydrophilicity achieved by this method is also not permanent and changes with time. This could be due to: 1) induced chemical groups inter reaction, 2) diffusion of a low *Mw* oxidized material from top layer to the interior bulk, 3) new oxidation with air exposure (Kazimi et al. 2011).

Flame oxidation on the surface can be achieved by a controlled flame produced by a mixture of natural gas and air for precise treatment time (Kazimi et al. 2011). With the flame treatment, the equipment setup is simple and cost effective. But, the difficulty in controlling the chemical composition of fuel and the distance between the tip of the flame and the sample are the main drawbacks of this method (Datla 2008).

2.4.4 Blending method

Blending, i.e., a physically mixing the host polymer with a modifier, is an alternate method that can be applied at an industrial scale production to obtain a hydrophilic surface. It is a convenient

processing method than can be carried out under mild conditions; it is reliable and cost effective (Datla 2008; Paul 2009; Xu et al. 2010).

Lowering the interfacial free energy is one of the forces driving the modifier to the interface (Bongiovanni et al. 1998; Datla 2008; Rezaei Kolahchi et al. 2014). It is well known that non-polar materials such as air have lower surface free energy compared to polar materials (such as water with 70 mN/m or steel die with 1200 mN/m) (Chen et al. 2009). Consequently, if the surface is in contact with air, the hydrophobic compound will concentrate at the surface to reduce the interfacial energy of the air–polymer interface. If the surface is in contact with polar materials, the hydrophilic component will preferentially diffuse and migrate to the interface (Suk et al. 2002; Zhu et al. 2009; Zhang et al. 2010). However, weak interaction and thermodynamic incompatibility between hydrophobic and hydrophilic polymers cause the hydrophilic compound release and elution from the surface when contacted with a polar chemical solvent, like water (Datla 2008; Chen et al. 2009; Fang et al. 2009). Thus, due to their water insolubility, amphiphilic copolymers consisting of hydrophobic backbones and hydrophilic side chains are good candidates to blend with a hydrophobic matrix to develop high performance membranes. The hydrophilic chains of amphiphilic additives often migrate spontaneously to the surface while the hydrophobic tail anchors into the host polymer, due to good interaction and compatibility between the hydrophobic main chain and hydrophobic host polymer (Chen et al. 2009; Zhu et al. 2009; Zhang et al. 2010).

Hydrophilic modification using amphiphilic polymers have been reported for many semi-crystalline hydrophobic polymers. Below, we briefly review the investigations reported in literature regarding the fabrication of hydrophilic precursor films or membranes using the polymer-blend method.

Zhang et al. (2010) prepared hydrophilic high density polyethylene (HDPE) porous membranes by blending with an amphiphilic polyethylene-block-poly (ethylene glycol) copolymer through the liquid–liquid thermally induced phase separation (L–L TIPS) process. SEM micrographs of the membrane cross-sections and surfaces showed that the introduction of PE-b-PEG resulted in larger pore sizes of HDPE/PE-b-PEG blend membranes compared to that of the neat HDPE membrane. This behavior was explained by the viewpoint of droplet growth kinetics of L–L TIPS, i.e. the faster droplet growth rate and the longer droplet growth period resulted in the bigger droplet volume in HDPE/PE-b-PEG system, and thus the larger pore size in HDPE/PE-b-PEG membrane. Also, the hydrophilic PEG segments of amphiphilic PE-b-PEG enriched at the membrane surface and endowed the membranes with sufficient and stable hydrophilic properties.

Chen et al. (2009) functionalized the surface of PP by the entrapment of polypropylene-grafted-poly(ethylene glycol). At first, they synthesized a series of PP-g-PEG with different structures and then, blended them with PP to check the effect of structure of additives on the surface enrichment. Their results showed that PP-g-PEG with lower PEG contents or lower molecular weight of PP and PEG, had better selective enrichment on the surface of PP blend film. The concentration of modifier on the surface of the blend film was decreased by increasing the loading of the amphiphilic copolymer. It means that by increasing the concentration of the copolymer, the interaction among the molecules of the amphiphilic copolymer increased and, therefore, hindered the migration from the bulk to the surface.

Zhu et al. (2007; 2009) synthesized amphiphilic graft copolymers having a poly(phthalazinone ether sulfone ketone) backbone and poly(ethylene glycol) or poly-(poly(ethylene glycol) methyl ether methacrylate) side chains. These amphiphilic copolymers were used for the surface modification of poly(phthalazinone ether sulfone ketone) (PPESK) membranes by phase

inversion technique. X-ray photoelectron spectroscopy (XPS) and water contact angle analysis indicated that hydrophilic chains were excluded to the membrane surface during membrane formation and the surface hydrophilicity were significantly improved. Also, Hester et al. (2002) synthesized a polyvinylidene fluoride (PVDF)-graft-poly(oxyethylene methacrylate) (POEM) using atom transfer radical polymerization (ATRP). They showed that the hydrophilic surface modification of the PVDF filtration membranes using PVDF-g-POEM was highly effective, due to the opportunity afforded by the standard immersion precipitation process to effect surface segregation of the graft copolymer additive during membrane fabrication.

Park et al. (2006) synthesized a polysulfone-graft-poly(ethylene glycol) and used it for surface modification of polysulfone (PSf) membranes. When they added 10wt% of the additive to the polysulfone membranes prepared by immersion precipitation, porosity, wettability and resistance to protein adsorption were enhanced compared with control PSf membrane. They also believed that PSf-g-PEG modified membranes might be useful for hemodialysis, apheresis, cell encapsulation or implantable controlled release applications.

In a dissertation by Datla (2008) low molecular weight modifiers, nonyl phenol ethoxylate and stearyl alcohol ethoxylates, were employed to impart hydrophilicity to a PP. Depending on the structure of the hydrophobic main chain of the amphiphilic copolymer, nonyl phenol ethoxylate was pushed out of the bulk to the surface. They explained that behavior by the solubility parameter. In general, the lower the difference in the solubility parameters is, the more compatible the two components are. When the hydrophilic chain length is short (EO part in stearyl alcohol – ethoxylate (POEC18) and Nonyl phenol (NP) – ethoxylate), the structure of the hydrophobic group itself affects migration. The solubility parameter of the PP polymer, stearyl alcohol (C-18) as hydrocarbon chain and nonyl phenol chain in nonyl phenol ethoxylate are 16.8,

16.9 and 18.8 $(J/cm^3)^{1/2}$, respectively. Because of larger solubility parameter differences between the aromatic nonyl phenol hydrocarbon with PP compared to the linear C-18 chain in stearyl alcohol ethoxylate additives, the bulky nonyl phenol is pushed out of the bulk to the surface while hydrophilic EO chain segments lie beneath the surface. Consequently, when amphiphilic polymer has a low value of the hydrophilic chain, the incompatibility between the hydrophobic chain and PP drives the hydrophobic chain to the surface instead of the hydrophilic group. So it is better to use host polymer-based amphiphilic polymers, i.e., PP- based amphiphilic polymers, for modifying the PP.

2.4.5 Combination of modification techniques

Combination of two or three modification techniques is complex in terms of cost effectiveness, but could lead to multi-functional membranes. It is expected that membrane properties can be tuned for specific applications through this method.

Hydrophilic compounds, such as TiO_2 nanoparticles and bovine serum albumin (BSA) can graft with the functional groups on the surface.

Grafting TiO_2 nanoparticles on a surface having COOH groups might be explained by two different mechanisms. One scheme might be that TiO_2 can bind with two oxygen atoms of carboxylate groups by a bidentate coordination to Ti^{4+} cations. The other scheme might be the formation of H-bonding between carbonyl groups and the hydroxyl groups of TiO_2 (Kim et al. 2003; Li et al. 2009) (see Figure 2-13). This reaction was confirmed by several experimental and theoretical investigations, i.e. using density functional theory (DFT) cluster calculations.(Persson et al. 2006; Capecchi et al. 2007). However, only few examples are found for the hydrophilic modification of hydrophobic membranes using TiO_2 nanoparticle grafting as combination of two modification techniques. Li et al. (2009) prepared TiO_2 nanoparticles grafted membranes based

on ultrahigh molecular weight poly(styrene-alt-maleic anhydride)/poly(vinylidene fluoride) (SMA/PVDF) blend membranes. They prepared SMA/PVDF blend membranes by the phase inversion method and then, immersed it in the TiO_2 nanoparticle solution. The TiO_2 nanoparticle was prepared by the controlled hydrolysis of titanium tetraisopropoxide. They showed that the amount of TiO_2 particles on the surface was grown with the increase of COOH groups. Their results showed that, in comparison to PVDF/SMA blend membrane, the permeability and anti-fouling ability of TiO_2 self-assembly membranes were significantly improved. Xu et al. (2013) deposited TiO_2 on porous polypropylene membranes using the atomic layer deposition technique. To generate active groups on the surface, they applied a plasma activation step to the PP membranes before TiO_2 deposition. Their results showed that grafting TiO_2 on the surface significantly improved the hydrophilicity and consecuntly the resistance to protein fouling.

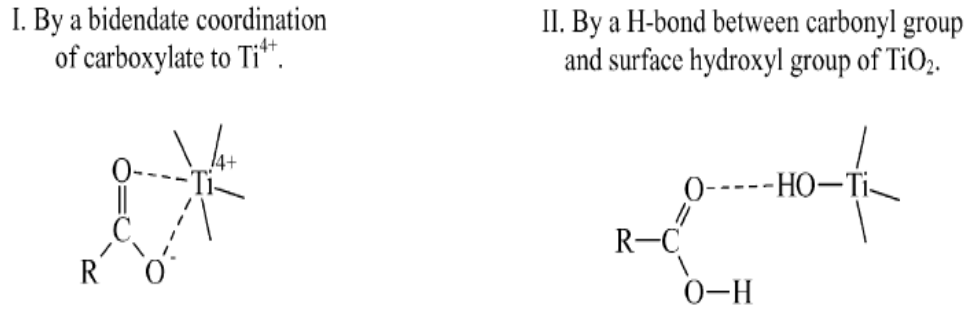

Figure 2-13:Mechanism of self-assembly of TiO2 nanoparticles (Kim et al. 2003; Li et al. 2009).

Bovine serum albumin (BSA) is a protein, which is often used to evaluate the protein-resistant characteristics of the prepared membranes. BSA can be used to improve the hydrophilicity of the membrane surface due to its high surface energy (39.5 mN/m). It has been reported that BSA could be grafted on the surface of the membranes by coupling the amino groups of the protein and COOH groups of the surface (Fang et al. 2009) (see Figure 2-14). Fang et al. (2009) modified polyethersulfone (PES) membrane by grafting BSA on the surface of PES/poly(acrylonitrile-co-

acrylic acid) blend membrane. PES/poly(acrylonitrile-co-acrylic acid) blend membranes were prepared by a phase inversion technique. After grafting BSA on the membrane surface, protein and platelet adsorption is decreased, so, the water contact angles were decreased, and meanwhile, the water flux was significantly increased. All these results suggested that the hydrophilicity and blood compatibility of the modified PES membranes were improved.

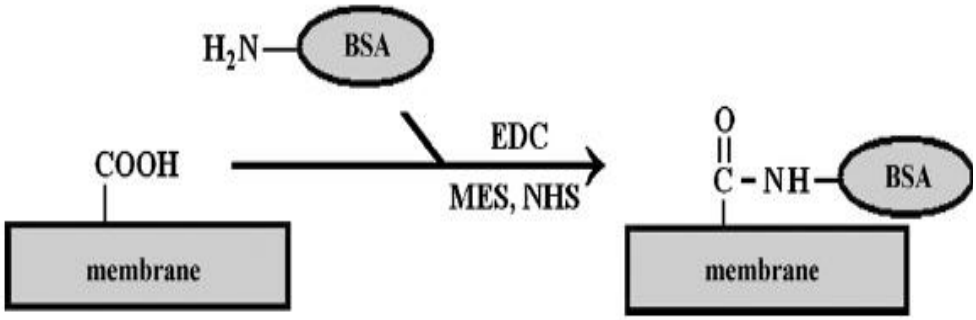

Figure 2-14:The process of grafting BSA (Fang et al. 2009).

2.4.6 Summary

Many efforts have been made to improve the hydrophilic properties of hydrophobic materials. However, some inherent drawbacks of these methods have been recognized. One promising approach, which has attracted considerable attention, is the blending method. The literature review showed quite a few studies on the hydrophilic modification of hydrophobic membranes using amphiphilic polymers. However, in all the previous studies, the membranes were prepared from phase separation techniques. It has been also observed that the crystalline structure of the precursor films are influenced by blending with low molecular weight polymers, which consequently affect the formation of the microporous membranes. Also, few studies have been conducted on the development of hydrophilic microporous membranes through grafting other

hydrophilic polymer with the hydrophilic groups on the surface. However, in all those reports, TiO_2 grafting aimed at the modification of as received hydrophobic membranes after plasma treatments or blend membranes prepared by phase separation techniques. To our knowledge, no study has been performed on the hydrophilic microporous polypropylene membranes fabricated by extrusion followed by stretching through blending with amphiphilic modifiers, and grafting TiO_2 nanoparticles on its surface. In addition, few studies reported the effect of annealing and stretching conditions on the crystalline structure and membrane performance. However, little attention has been paid to the annealing of flow-oriented polymers and stretching of the precursor films, especially to the mechanisms of the microstructural changes during each individual step.

These issues will be considered in this study; the polymer blend method will be employed and its impact of the blending on the crystalline structure and, consequently, on the final pore structure will be investigated. Also, increasing the hydrophilic properties through grafting other hydrophilic polymers with amphiphilic modifiers on the surface will be studied. In addition, a detailed investigation will be performed to evaluate the influence of annealing and stretching conditions on the crystalline structure and the subsequent membrane properties. Understanding these mechanisms is important to prepare membranes with optimal performances.

CHAPTER 3 OBJECTIVES

In view of the industrial importance of hydrophilic microporous membranes, and considering the various drawbacks of previous approaches to improve hydrophilic properties of PP films or membranes, the main objective of this study is:

"To improve the hydrophilic properties of polypropylene microporous membranes prepared through cast extrusion followed by stretching via controlling the crystalline morphology"

To meet this objective, different commercial maleic anhydride or acrylic acid grafted polypropylene (PP-g-MA and PP-g-AA) were melt blended with PP using cast film extrusion and the effects of modifiers loading on the crystalline structure and membrane performance were investigated.

Subsequently, blend film containing a sufficient content of modifier are immersed in titanium dioxide (TiO_2) suspensions and the hydrophilicity of the modified PP membranes as well as pore structure were studied.

Finally, to control the microporous membrane fabrication, each individual stages of the stretching technique in terms of the effective involved parameters are examined. The changes in the crystalline structure and membrane performance were investigated in details to optimize annealing and stretching conditions.

CHAPTER 4 ORGANIZATION OF THE ARTICLES

Chapters 5 to 8 give the main results of this thesis and corresponding scientific findings. Each of these chapters consists of an article. The following is a brief description of each chapter and the link between them:

In Chapter 5, the effects of blending commercial amphiphilic modifiers (PP-g-MA and PP-g-AA) on the hydrophilicity and crystalline structure of PP based microporous membranes, produced by cast film extrusion followed by stretching, are investigated. It is found that the optimum concentration of modifier to achieve membranes having good hydrophilic characteristics, with enough polar groups on the surface and causing a minimal change in the crystalline structure compared to the neat PP film is 2wt %. Chapter 6 presents the results on the fabrication of hydrophilic microporous membranes through grafting TiO_2 with COOH groups of the PP/PP-g-AA blend. Various tests are carried out to describe the grafting and stability of TiO_2 and COOH groups on the surface. Compared to PP and PP/PP-g-AA blend films, the water contact angle decreases by a factor of 2.5 after grafting TiO_2 onto the surface of the precursor films, meanwhile the water vapor permeability of the microporous membranes prepared from those films increases by a factor of 1.5. Chapter 7 discusses in details the effects of annealing conditions on the crystalline structure, morphology, and mechanical properties of the cast films and microporous membranes for blend of PP containing 2wt% PP-g-AA. SAXS and DSC tests have been carried out to elucidate and confirm the formation of secondary lamellae after annealing. These results allow us to illustrate key crystalline structure changes during annealing and the impact on the mechanical properties of the precursor film and membrane with the objective of establishing the structure-properties relationships after annealing. The relationships between tensile properties and the crystalline structure are also discussed. Two characteristics is distinguished in the

annealed samples: 1) presence of the double yield point and 2) a linear dependence of second yield stress with the lamellae thickness. In Chapter 8, a detailed investigation is performed to evaluate the pore structure as a function of stretching and its impact on the membrane performance. In addition, the separate effects of cold and hot stretching steps on the pore structure of the membrane are examined. The cold stretching step is found to be the important step to promote interconnection between the pores. Furthermore, the optimum stretch ratio for the cold stretching step is found to be below the strain corresponding to the second yield point of the polymer; beyond that strain, a reduction in the permeability is observed.

In Chapter 9 a general discussion regarding the most important factors affecting the hydrophilic microporous membranes fabrication is presented. Chapter 10 summarizes the most important conclusions of this thesis and gives recommendations for the future work.

CHAPTER 5 - ARTICLE 1:

DEVELOPMENT OF POLYPROPYLENE MICROPOROUS HYDROPHILIC MEMBRANES BY BLENDING WITH PP -G- MA AND PP -G- AA

Amir Saffar [a], Pierre J. Carreau [a], Abdellah Ajji [a], Musa R. Kamal [b]

[a] *Research Center for High Performance Polymer and Composite Systems (CREPEC), Chemical Engineering Department, Polytechnique Montreal, PO Box 6079, Stn Centre-Ville, Montreal, Quebec, Canada, H3C 3A7.*

[b] *CREPEC, Department of Chemical Engineering, McGill University, 3610 University Street, Montreal, Quebec, Canada, H3A 2B2.*

Published in *Journal of Membrane Science,* 462 (2014) 50–61.

Abstract

Cast films based on polypropylene (PP) blended with commercial maleic anhydride or acrylic acid grafted polypropylene (PP-g-MA and PP-g-AA) at different weight ratios were prepared by melt extrusion. These films were used to produce hydrophilic microporous membranes. The membranes were prepared by annealing at elevated temperatures followed by cold and hot stretching, respectively. DSC, FTIR and SAXS analyses showed that the addition of the modifiers changed the crystalline lamellar structure and, consequently, the membrane morphology. Membrane morphology observations using SEM showed smaller pore size and lower number of pores as the modifier content increased. Porosity and pore dimensions of the microporous membranes were also measured using mercury porosimetry and their results confirmed SEM observations. Oxygen content of the precursor film surface was analyzed using XPS. Water vapor permeability was increased significantly at low concentrations of the modifiers, compared to the neat PP. This was attributed to the presence of sufficient concentration of polar groups on the surface with a minimal change in the crystalline structure. Finally, the tensile properties of the precursor films in the machine directions (MD) as well as the puncture resistance of the precursors and the membranes in the normal direction (ND) were evaluated.

Keywords

Polypropylene blends, Hydrophilicity, Crystalline lamellar morphology, Membranes by stretching, Water vapor permeability.

5.1 Introduction

Semi-crystalline polypropylene (isotactic PP) is one of the most commonly used polymers today in a variety of applications due to its outstanding properties, such as low cost, easy processing, good mechanical properties, chemical stability and non-toxicity [1, 2]. Membranes are usually made from a solution/phase separation process. In recent studies, a process to prepare PP porous membranes using a dry process was developed by combining the specific crystalline morphology development in polymer films containing a row-nucleated lamellar structure, followed by annealing and stretching [2-6]. Despite its popularity as a membrane material, PP is difficult to adhere to many substances such as water or to hydrophilic substrates because of its intrinsic hydrophobic nature. This limits its application in wastewater treatment, desalination of sea water, electrode separators in batteries and biomedical applications [1, 7-9].

Hydrophobic membranes are prone to fouling when used in treating aqueous solutions containing natural organic matter, e.g., proteins, platelets, oil droplets or macromolecular species. Organic matter is easily adsorbed onto the membrane surface or pore walls, which results in the deterioration of the membrane performance, leading to lower permeability and shorter membrane life time. Subsequently, replacement and maintenance costs of the membrane modules are increased [7, 8, 10]. Membrane fouling can be divided into reversible and irreversible fouling. Reversible fouling caused by reversible organic matter adsorption, which occurs in a hydrophilic surface, can be fully or partly removed by hydraulic cleaning, e.g., backwashing and cross flushing. Irreversible fouling is caused by irreversible organic matter adsorption on the hydrophobic surface and can only be eliminated by chemical or biochemical cleaning [11, 12]. The cause for irreversible fouling is the lack of hydrogen bonding interactions between the hydrophobic membrane and water in the boundary layer, which leads to the spontaneous process

of the repulsion of the water molecules away from the surface. By contrast, membranes with a hydrophilic surface are able to form hydrogen bonds with the surrounding water molecules [13]. It is difficult for hydrophobic solutes to approach the water boundary and break the orderly structure due to the energy required to remove the water boundary and expose the membrane surface [11, 12]. Furthermore, the presence of a spontaneous and permanent wettable surface is a basic requirement for a battery separators to accommodate the aqueous electrolyte solution and prevent solvent leakage, which often causes the deterioration of the life of a battery [14, 15]. Accordingly, increasing the hydrophilicity of the membrane surface is the general approach used to prevent irreversible membrane fouling and, as well, to improve the surface properties, such as adhesion and printability [9, 12].

Despite this drawback, hydrophobic materials have higher mechanical and chemical stability than hydrophilic materials, which are used in membrane applications [8, 11]. Thus, the ideal membrane would combine the superior bulk properties of hydrophobic materials with the surface chemistry of hydrophilic materials [8, 16].

Different strategies have been carried out to improve the membrane surface, i.e., increasing the amount of surface polar groups and maximizing hydration. Basically, these methods include plasma treatment, blending with hydrophilic materials, radical grafting reactions, chemical coating and so on [7, 16, 17]. However, some inherent drawbacks of these methods have been recognized, such as: (a) in surface grafting polymerization, materials are wasted due to produced undesired homopolymers; (b) the adsorbed or coated polymers may not remain on the surface permanently, due to the weak adhesion force between the modified polymers and the substrate; (c) many of these surface modification methods are complicated and require additional steps in the membrane preparation, thus increased costs [7]. Thus, blending,

i.e., a physically mixing the host polymer with a modifier, can be applied to an industrial scale production to obtain a hydrophilic surface. It is a convenient processing carried out under mild conditions, it does not require pre-treatment or post-treatment procedures, and it is reliable and cost effective [1, 16, 17]. However, weak interaction and thermodynamic incompatibility between hydrophobic and hydrophilic polymers cause the hydrophilic compound release and elution from the surface when contacted with a polar chemical solvent, like water [7, 16, 18]. Thus, due to their water insolubility, amphiphilic copolymers consisting of hydrophobic backbones and hydrophilic side chains are good candidates to blend with PP for developing performing membranes. The hydrophilic chains of amphiphilic additives often migrate spontaneously to the surface while the hydrophobic tail anchors into the host polymer, due to good interaction and compatibility between the hydrophobic main chain and hydrophobic host polymer [12, 18, 19]. As a whole, amphiphilic polymers include triblock, comb and branch polymers [12]. However, only few examples are found for hydrophilic modification of hydrophobic membranes using amphiphilic polymers. Perhaps, this is because of the small number of amphiphilic additives with a hydrophobic segment that has good compatibility with the matrix. For instance, Zhang et al. [12] prepared hydrophilic high density polyethylene (HDPE) porous membranes by blending with an amphiphilic polyethylene-block-poly (ethylene glycol) copolymer. Chen et al. [18] functionalized the surface of PP by the entrapment of polypropylene-grafted-poly(ethylene glycol). Xu et al. [1] synthesized a polypropylene-block-poly(vinylpyrrolidone) copolymer through the esterification of dicarboxyl-terminated polypropylene with monohydroxyl-terminated poly(vinylpyrrolidone) and used it as a modifier to improve the surface hydrophilicity of the PP. Zhu et al. [19, 20] used poly(phthalazinone ether sulfone ketone) (PPESK)-graft-poly-(poly(ethylene glycol) methyl ether methacrylate) copolymer for the surface modification of PPESK membranes. Hester et al.[21] synthesized

polyvinylidene fluoride (PVDF)-graft-poly(oxyethylene methacrylate) (POEM) for the surface modification of PVDF filtration membranes to render them wettable and fouling-resistant. Park et al. [22] synthesized a polysulfone-graft-poly(ethylene glycol) and used it for surface modification of polysulfone membranes. Delta et al. [16] employed low molecular weight modifiers, nonyl phenol ethoxylate and stearyl alcohol ethoxylates, to impart hydrophilicity to a PP.

All the above reports aimed at the modification of hydrophobic precursor films or hydrophobic membranes prepared by phase separation techniques. To our knowledge, no work has been published regarding microporous polypropylene membranes fabricated through blending with modifiers and cast film processed followed by stretching. In the preparation of membranes by extrusion followed by stretching, the crystalline structure of the precursor films is the key factor as the first step for the formation of the microporous membranes [2]. The crystalline orientation factor of the polypropylene film is decreased by blending with low molecular weight polymers [2]. Therefore, it is important to choose good amphiphilic polymers for blending with PP to generate the desired lamellar morphology in order to achieve a good membrane. In fact, the crystalline orientation factor should be high enough (more than 0.3) in order to obtain a row-nucleated morphology suitable for porous membrane formation [23].

The only commercial amphiphilic polymers available in the market, which are based on PP, are maleic anhydride and acrylic acid grafted polypropylene (PP-g-MA and PP-g-AA). PP-g-MA has been used for various purposes, such as coupling agents for chemically bonding reinforcement of the PP matrix and an adhesive layer in multilayered coextruded laminates. The hydrophilicity and the adhesion of PP films to polar polymers are substantially improved by introducing MA polar groups to the PP chains. The surface energy and the polar components of the PP-g-MA copolymer increase significantly with the grafted MA concentration in the

copolymer [17, 24]. PP-g-AA is a chemically modified polyolefin that has good adhesion to aluminum and stainless substrates. It has been also used to increase the wettability of PP. The grafting degree of AA with PP is larger than that of MA due to the higher polymerizability of AA [25-27].

In this work, the effects of blending amphiphilic modifiers on the hydrophilicity and crystalline structure of the PP based microporous membranes, produced by cast film extrusion followed by stretching, were investigated. A series of blends with various types and concentrations of commercial PP-g-MA and PP-g-AA were prepared and the surface and bulk properties of the precursor films and membranes were characterized.

5.2 Experimental

5.2.1 Materials

Two commercial linear high and low molecular weight PPs (MFR values of 0.8 g/10 min under ASTM conditions of 230 ºC and 2.16 kg and 2.8 g/10 min) were selected as the matrix polymers for the microporous membranes; both PPs were supplied by ExxonMobil Company. As modifiers, two types of commercial amphiphilic polymers consisting of hydrophobic backbones (polypropylene) and hydrophilic side chains, i.e., PP-g-MA and PP-g-AA were used. Five grades of PP-g-MA having different molecular weights and maleic anhydride contents were selected and purchased from different companies as follows: Bynel 50E571 and 50E739 from DuPont Company, Orevac 18750 and CA100 from Arkema Company and Epolene E-43 from Westlake Chemical Corporation. In the case of PP-g-AA, two resins from Chemtura corporation with the same acrylic acid content, different MFRs (20 and 40 g/10 min), were used. The main

characteristics of the resins are shown in Table 1.1. The melting point, T_m, and the crystallization temperature, T_c, of the resins were obtained using differential scanning calorimetry.

5.2.2 Film preparation

Precursor films from blends of PP and modifiers at different weight ratios were prepared using a 45 mm diameter Killion single screw extruder with a slit die of 0.7 mm opening. The temperature profile along the barrel was: 165/195/210/215 °C and the die temperature was 220 °C. For film cooling, an air knife was applied right at the exit of the die to supply air to the film surface. The extrusion was carried out using a screw speed of 12.5 rpm and a draw-down ratio (ratio of the roll speed to the die exit velocity) was set at 25 to produce precursor films having a thickness of around 30 μm. The distance between the die exit to the nip cast roll was around 15 cm and the cast roll temperature was constant at 50 °C.

5.2.3 Rheological characterization

Dynamic rheological measurements were performed using a Rheometric Scientific Anton-Paar MCR 301 stress controlled rheometer with parallel plate geometry of diameter of 25 mm and gap of 1 mm. The measurements were carried out at 190 ºC and nitrogen atmosphere was used to avoid thermal degradation. Molded discs of 1.2 mm thick and 25mm in diameter were prepared from the blends using a hydraulic press at 190 ºC. Time sweep tests were first performed at a frequency of 0.628 rad/s for 1 h in order to check for any degradation. The complex viscosity and storage modulus were determined in the linear viscoelastic regime (the strain amplitude was set at 10 %) in the frequency range from 0.0628 to 628 rad/s (0.01 to 100 Hz).

Table 5-1: Main characteristics of the neat materials.

Resin Code	Supplier	MFR (g/10 min) (230 ºC-2.16 kg)	Nomenclature	T_m (°C)	T_c (°C)
Polypropylene PP5341E1	Exxon Mobil	0.8	PP0.8	161	115
Polypropylene PP4712E1	Exxon Mobil	2.8	PP2.8	160	114
PP-g-MA (Bynel®50E571)	DuPont	3.5	PPMA3.5	150	105
PP-g-MA (Bynel®50E739)	DuPont	6	PPMA6	141	102
PP-g-MA (Orevac®18750)	Arkema	35	PPMA35	109&160	97&112
PP-g-MA (Orevac®CA100)	Arkema	150	PPMA150	159	113
PP-g-MA (Epolene® E-43)	Westlake Chemical	M_w =9100 g/mol	PPMA-E43	152	107
PP-g-AA (Polybond®1002)	Chemtura	20	PPAA20	161	123
PP-g-AA (Polybond®1001)	Chemtura	40	PPAA40	161	123

5.2.4 Membrane preparation

For membrane fabrication, precursor films with thickness, width and length of 30 μm, 8 cm, and 4 cm, respectively, were used as follows [2]: At first, the films were annealed at 120 °C for 30 min and then the annealed samples were cold and hot stretched up to 35% of the initial length at room temperature and 60% at 120 °C, respectively. Both annealing and stretching were performed using an Instron machine equipped with an environmental chamber. A drawing speed of 50 mm/min was applied during the cold and hot stretching steps.

5.2.5 Film and membrane characterization

5.2.5.1 Fourier transform infrared spectroscopy (FTIR)

For FTIR measurements, a Perkin Elmer infrared spectrometer with a spectral resolution of 4 cm^{-1} and a scanning speed of 32 kHz, was used. The data were collected in the range from 4000 to 600 cm^{-1}. The surface composition of the samples was investigated using attenuated total reflectance (ATR) mode.

The crystalline and amorphous orientation, based on the difference of the absorption of the plane-polarized radiation, was measured using a vibration in parallel and perpendicular to the stretching machine direction (MD) in the transmission-FTIR mode. The Herman orientation function was calculated according to:

$$f = \frac{D-1}{D+2} \qquad (5\text{-}1)$$

where D is the dichroic ratio and defined as the ratio of parallel and perpendicular absorbencies of the specific vibration used to MD. For PP, absorption at the wavelength of 972 cm^{-1} is due to the contribution of the crystalline and amorphous phases while absorption at the wavelength of

998 cm^{-1} is attributed to the crystalline phase only. From the 972 cm^{-1} absorption, the average orientation function, f_{av}, is obtained while from the other, the crystalline orientation function, f_c, can be determined. So, the amorphous orientation function, f_{am}, can be calculated according to:

$$f_{av} = X_c f_c + (1 - X_c) f_{am} \quad (5\text{-}2)$$

where X_c is the degree of the crystallinity.

5.2.5.2 X-ray Photoelectron Spectroscopy (XPS)

XPS provides quantitative analysis of the atomic composition of a surface by detecting the characteristic binding energies associated with each element. XPS measurements were conducted on a VG ESCALAB 3 MKII spectrometer with Mg-Kα ray source. Survey scans of 100 eV pass energy were used to identify initially all components. The surface elemental stoichiometry was obtained from the ratios of peak areas corrected with the Wagner sensitivity factors and Shirley background subtraction.

5.2.5.3 X-Ray diffraction (XRD)

XRD is a non-destructive technique that reveals detailed information about the chemical composition and crystallographic structure of the natural and manufactured materials.

Wide angle X-ray diffraction (WAXD) measurement was performed using a Bruker D8 Discover equipped with a Hi-STAR two-dimensional area detector. The generator was set up at 40 kV and 40mA. A Cu source was used (Kα energy of 8.04 keV and wavelength of 1.542 Å) with a graphite monochromator. The detector was fixed at 9.95 cm distance from the sample. To get the maximum diffraction intensity several layers of the film were stacked together to obtain the total thickness of about 2 mm.

Small angle X-ray scattering (SAXS) measurements were performed in order to study the crystalline structure and estimate the long period distance between the lamellae. The SAXS patterns were collected via a Bruker AXS Nanostar system. The instrument is equipped with a Microfocus Copper Anode at 45 kV / 0.65 mA. The MONTAL OPTICS and a VANTEC 2000 2D detector were located at 107.2 mm distance from the samples. The distance was calibrated with a Silver Behenate standard prior to the measurements while four layers of the film were stacked together.

5.2.5.4 Differential Scanning Calorimetry (DSC)

Thermal properties of the specimens were analyzed using a TA instrument differential scanning calorimeter (DSC) Q 1000. Samples were heated from 50 to 220 ºC at a heating rate of 10 °C/min.

5.2.5.5 Mercury intrusion porosimetry (MIP)

The porosity and pore dimensions of the membranes were evaluated using an AutoPore IV 9500 mercury intrusion porosimeter developed by Micromeritics Instrument Corporation.

5.2.5.6 Morphology

In order to observe the microporous membranes surfaces, a field emission scanning electron microscope (FE-SEM-Hitachi S4700) was employed.

5.2.5.7 Water vapor transmission rate (WVTR)

The permeability to water vapor was measured via a MOCON PERMATRAN-W Model 101K at room temperature. The equipment is composed of three chambers. An upper chamber, which is separated from the center chamber by two porous films, contains liquid water. The center chamber is separated from the lower one by the test film. Water vapor diffuses from the first film

to fill the space between the films and is swept away by N_2 gas to a relative humidity (RH) sensor.

5.2.5.8 Tensile properties

Tensile tests were performed on the films using an Instron 3365 at room temperature according to ASTM D638. The tensile specimens having rectangular geometry of 25 mm wide and 50 mm long were stretched at a cross-head speed of 50 mm/min.

5.2.5.9 Puncture resistance

Puncture tests were performed via a 250N load cell of the Instron machine used for the tensile tests. A needle of 3.2 mm radius was used to pierce the samples at a speed of 25 mm/min. The procedure used was based on ASTM F1306. The film was held tight in the clamping device with a central hole of 34.9 mm. The displacement of the film was recorded against the force (N) and the maximum force was reported as the puncture strength.

5.2.5.10 Dynamic mechanical analyses (DMA)

The storage modulus at room temperature was measured using a TA dynamic mechanical analyzer (TA Instruments, DMA 2980). The measurements were carried out in the linear zone at 1 Hz, using the dual cantilever clamp mode by bending procedure. The oscillation amplitude was 30 µm and the static force was 1 N.

5.3 Results and discussion

5.3.1 Characterization of the neat materials

The complex viscosities as functions of frequency for the neat polymers are presented in Figure 5-1. The behavior of all the neat polymers is typical of polymer melts except PPMA150 that exhibits an anomalous behavior, probably due to some structural transition. The zero-shear viscosities of the polymers are consistent with their MFRs, as reported in Table 5.1. As the molecular weight increases, the polymer exhibits more shear thinning, and, the transition from the Newtonian plateau to the power-law region occurs at lower frequencies [2, 6]. It can be seen that the PP0.8 possesses the largest viscosity compared to the other polymers.

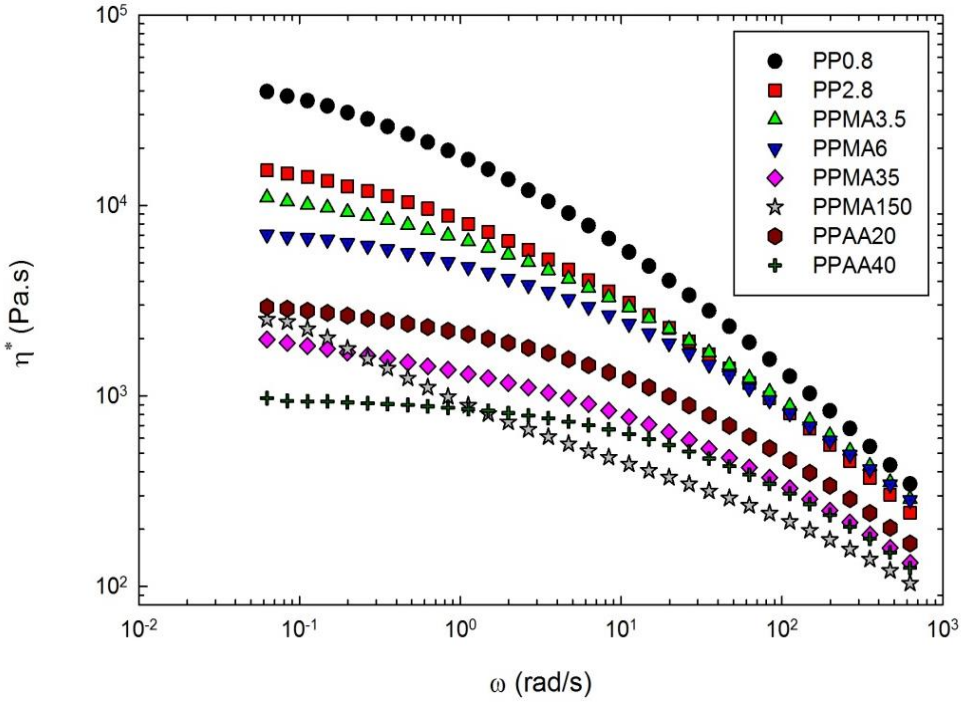

Figure 5-1: Complex viscosity as a function of angular frequency for the neat polymers; T = 190ºC.

ATR-FTIR spectroscopy can help in the identification/quantification of the various groups contained in polymers. Figure 5-2a illustrates the presence of maleic anhydride groups at different positions on the polypropylene chain (located at 1850, 1784, 1772 and 1740 cm^{-1}) [10, 24, 25] and acrylic acid groups (located at 1710 cm^{-1}) [25, 26] of the neat modifiers. In addition to peaks associated with maleic anhydride, PPMA150 and PPMA-E43 exhibit peaks of acrylic acid around 1710 cm^{-1}. This can be due to the hydrolysis of maleic anhydride groups. The succinic anhydride rings can undergo hydrolytic processes, i.e., surface transformation of $(CO)_2O$- to $(COOH)_2$, which can occur both in humid air and liquid water [9, 10]. Traces of ethylene groups in PPMAs, except PPMA-E43, were identified in ATR-FTIR test. Despite the fact that polypropylene and polyethylene are similar, these two polymers are thermodynamically immiscible [28]. Thus, presence of ethylene groups could reduce compatibility and even miscibility between the PP matrix and modifiers [29, 30]. Absorption at wavenumbers of 720 and 730 cm^{-1} is related to the presence of ethylene groups in the polymers (Figure 5-2b) [6, 31].

The DSC results support the ATR-FTIR results regarding the presence of ethylene groups in PP -g- MAs (see Figure 5-3). They demonstrate the occurrence of two melting and cooling peaks in PPMA35, one attributed to PP groups and another one attributed to ethylene groups, which supports the presence of block ethylene groups in the polymers [6, 31]. It has been reported that the presence of ethylene groups in random arrangement for other PPMAs tends to suppress and flatten the peaks of the melting curves [32]. It is known that the presence of a co-monomer would disrupt the crystallization behavior, resulting in a reduction of the crystallization rate and lowering of the melting point [30, 33]. Thus, upon cooling of samples from the melt state, the crystallization rate becomes slower and the crystallization temperature shifts to lower values [34]. However, in the case of PPAAs, the functionalization does not change the melting

temperature and actually raises the crystallization temperature of the polymer. The grafted AA monomer acts as a nucleation agent, which enhances the crystallization capability [27].

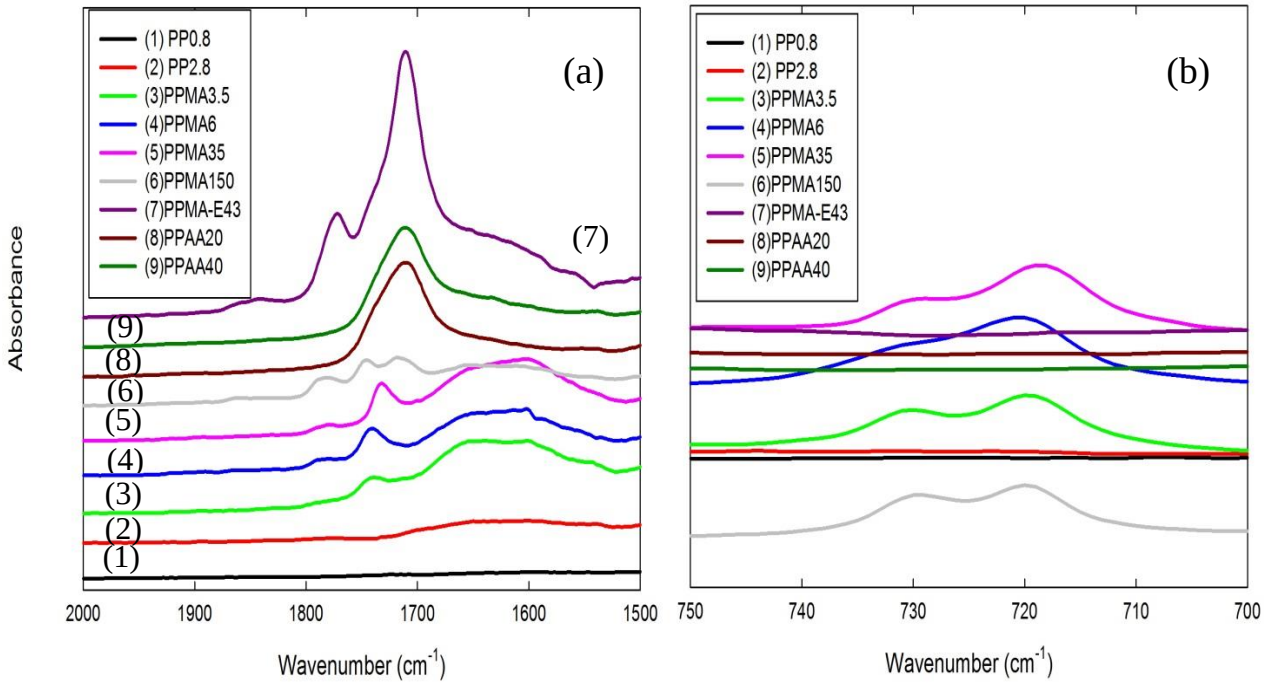

Figure 5-2: ATR FTIR spectra of the neat polymers; (a) maleic anhydride and acrylic acid groups, (b) ethylene groups.

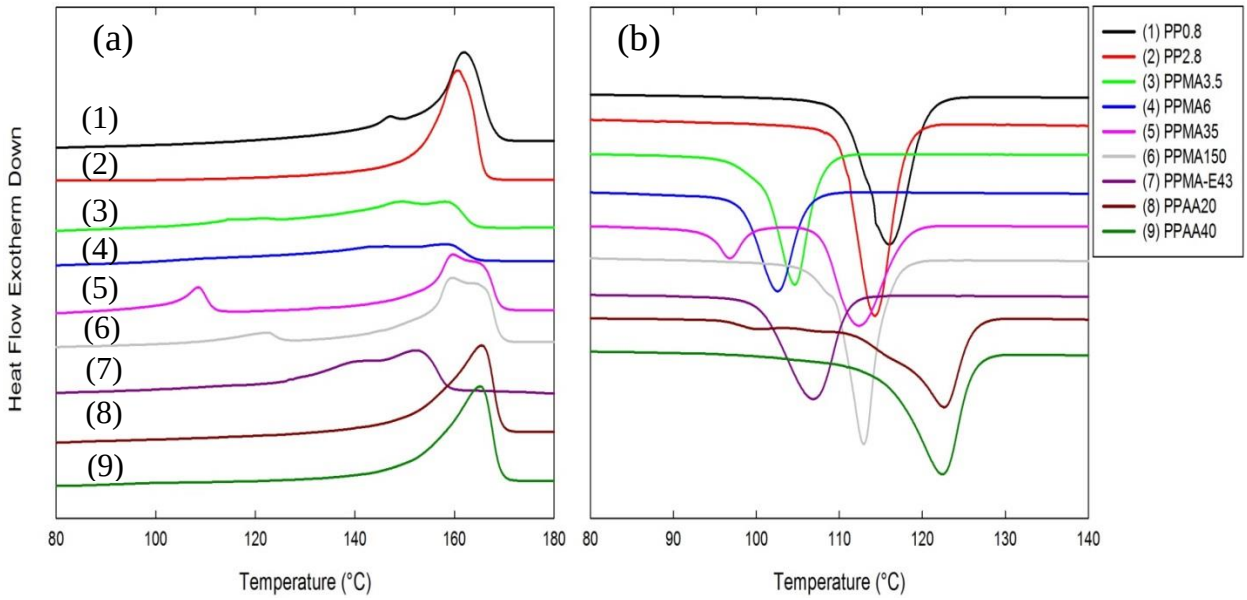

Figure 5-3: DSC thermograms of the neat polymers: (a) second heating and (b) cooling.

5.3.2 Effect of blending 2wt% of modifiers with PP0.8

The effects of blending 2wt% of the different modifiers with PP0.8 were first examined using DSC and the results are reported in Figure 5-4. The lowering of crystallinity for the blends is understandable in light of the low molecular weight modifiers that act as defects in the crystals due to the presence of incompatible groups with the PP matrix [17]. Furthermore, the presence of ethylene component in the PPMAs adds to disturbing the crystalline structure and causes the crystallinity of the PP/PPMA blends to be lower than that of the PP/PPAA blends [25, 29]. Among the PPMAs, the least crystallinity was found in PPMA35 blend, which could be due to the presence of block ethylene groups in the modifier (as pointed out earlier) [30].

The effects of annealing and stretching (microporous membranes) on the crystallinity of PP0.8 and its blends were examined and compared to the crystallinity of the precursor films (not presented here). Due to chain rearrangements at temperatures close to the melting point of the

samples, annealing increased the crystalline content for all the precursor films of the blends, but the crystallinity of all annealed samples were practically the same. A slight change in crystallinity was detected after stretching, which was also observed in previous work performed by this group [2].

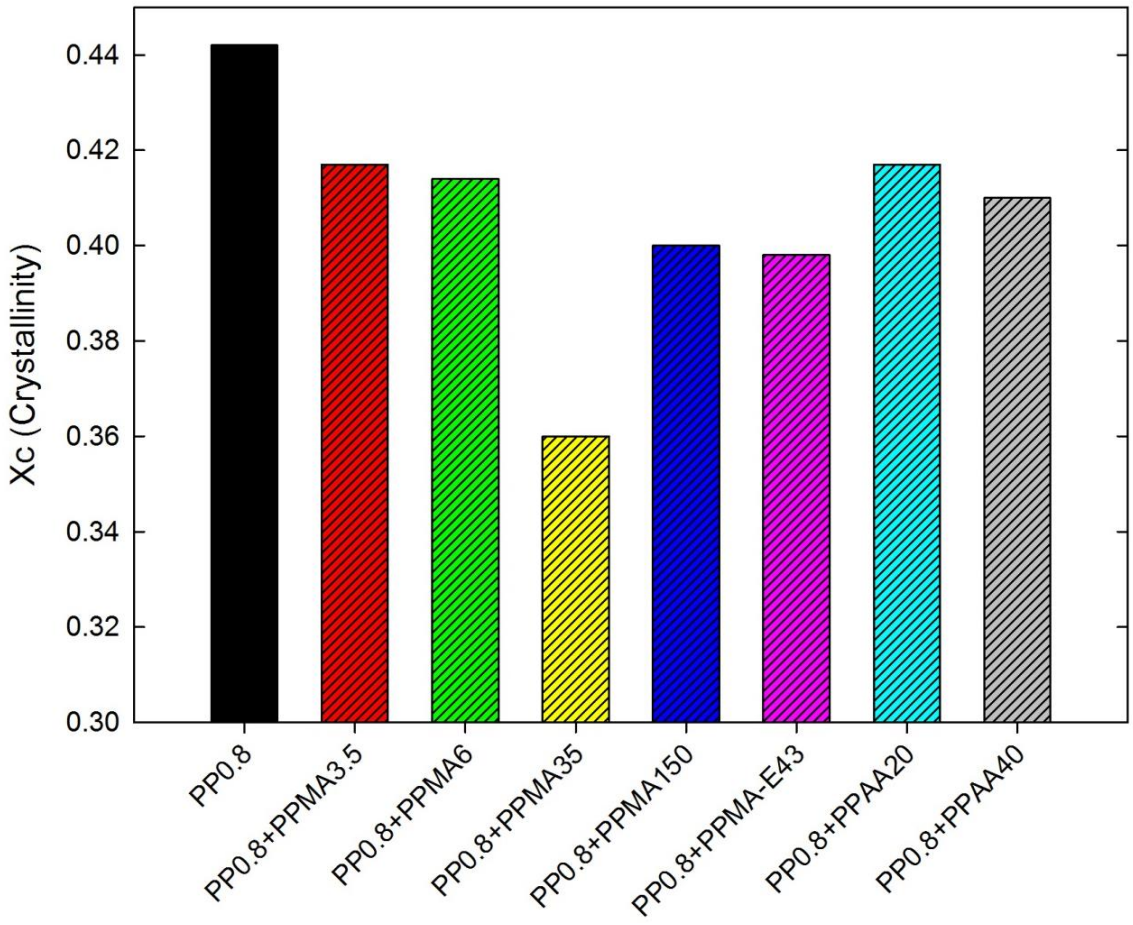

Figure 5-4: Crystallinity of the precursor films of PP0.8 and its blends with different modifiers (2wt%).

Figure 5-5 presents the Herman orientation functions of the crystalline and amorphous phases for the precursor and annealed films of all the blends. It shows that adding PPMA-E43 lowers the orientation of both the crystalline and amorphous phases, due to the lower molecular

weight [2]. In addition, in comparison with the non-annealed films, a significant improvement in the orientation was found for the annealed specimens. Annealing provides the possibility for the lamellae to be rearranged in the machine direction and enhances the crystalline orientation. However, rearrangement in the crystalline orientation could affect the tie chains as well, because they are the zones connecting lamellae. Thus, the improvement in the amorphous phase orientation might be due to a slight movement of the molecules in the amorphous phase and the formation of some new organized regions [2, 3].

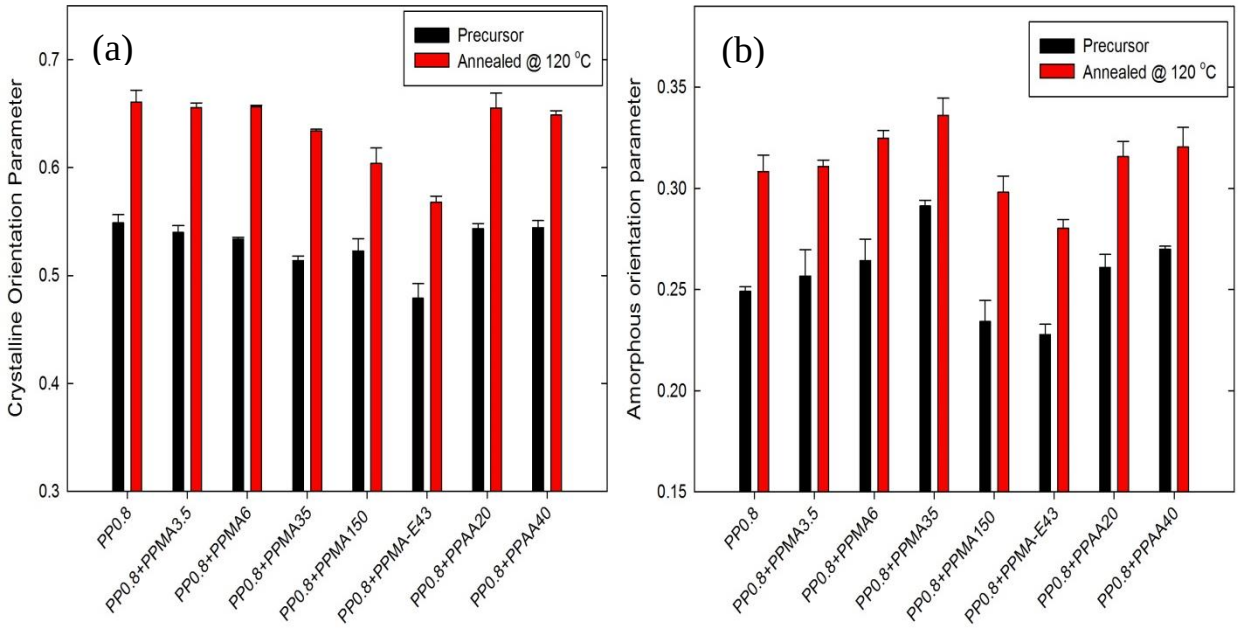

Figure 5-5: (a) Crystalline and (b) amorphous orientation parameters (obtained from FTIR) of precursor films of PP0.8 and its blends with different modifiers (2wt%). Annealing was performed at 120 °C for 30 min.

The presence of polar groups in the precursor film and membrane surface, which enhances the surface energy and the hydrophilicity of polymers [15, 35], is supported by the

appearance of maleic anhydride and acrylic acid groups in the ATR-FTIR spectrum (results not shown). Figure 5-6 presents the results regarding the key property of the membranes, i.e., water vapor permeability.

The water vapor permeability of the membranes reflects its bulk properties and hydrophilicity of the surfaces [36]. The bulk parameters of the membrane, i.e., tortuosity and pore size. Etc, are affected by the crystallinity and crystalline orientation [2]. However, improving the hydrophilicity of the surface causes increases of the solubility of water in polymers and, consequently, increases of the permeability due to the formation of hydrogen bonds with water molecules. This hydrogen bonding thereby causes a de-structuring of the original water complexes and facilitates their transport through the membrane [13, 37].

In porous PP/modifier membranes the functional groups of the modifiers will be located on the surfaces, including pore surfaces, where they enhance the hydrophilicity. By keeping the crystalline structure the same as for the neat PP in the cases of PPAAs (see Figures. 5-4 and 5-5), the hydrophilic part of the surface and pores plays an important role in determining the water vapor permeability [7]. Consequently, for blends of PP with 2 wt% PPAAs the permeability is increased markedly compared with the neat PP. Also, the addition of PPMA35 or PPMA-E43 yields the lowest permeability, which can be attributed to the presence of ethylene groups [36] and the lower molecular weight, respectively [6].

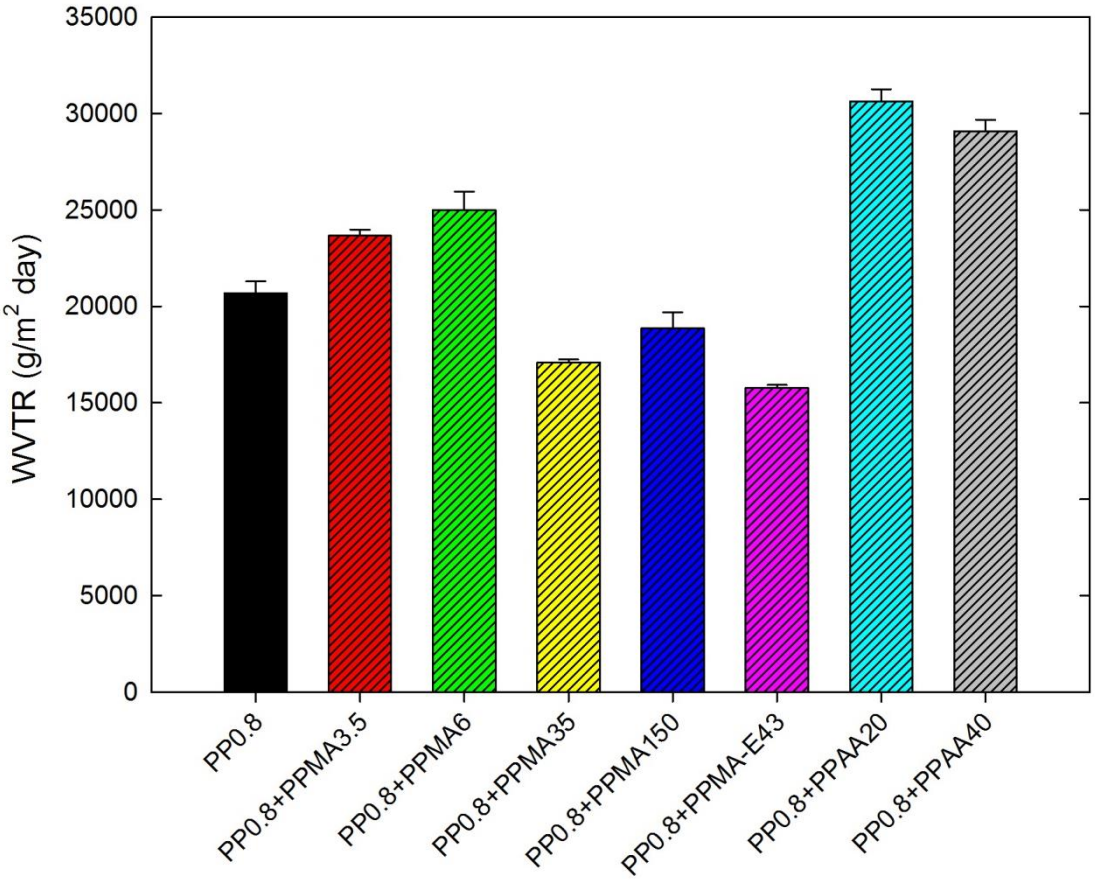

Figure 5-6: Water vapor transmission rate of the PP0.8 blends with different modifiers (2wt%).

Based on the results reported in this section, PPMA6 and PPAA20 were selected, respectively, as the best potential modifiers among the five PPMAs and two PPAAs. In the next section, different concentrations of PPMA6 and PPAA20 in PP will be investigated to determine the optimum concentration that will lead to the ideal microporous membrane (less changes in the bulk properties compared to the neat PP, while their surfaces possess hydrophilic properties).

5.3.3 Effect of blending PPMA6 and PPAA20 at different concentrations with PP0.8 and PP2.8

The measured crystalline orientation parameter and melting enthalpy value for various blends are plotted in Figure 5-7. Lower crystalline orientation and crystallinity for the blends of PPAA were expected in comparison with blends of PPMA, due to the lower molecular weight of the former [2]. However, the results showed that the crystalline orientation of the blends remained approximately the same while the crystallinity of the PPMA blends is lower compared to the PPAA blends. This could be attributed to the presence of ethylene groups in PPMA6 as already discussed before. Furthermore, in comparison with the PP2.8 matrix, a significant improvement in the crystalline orientation is observed in the PP0.8 matrix due to higher molecular weight (M_w), which increases the number of fibrils or nuclei sites [2].

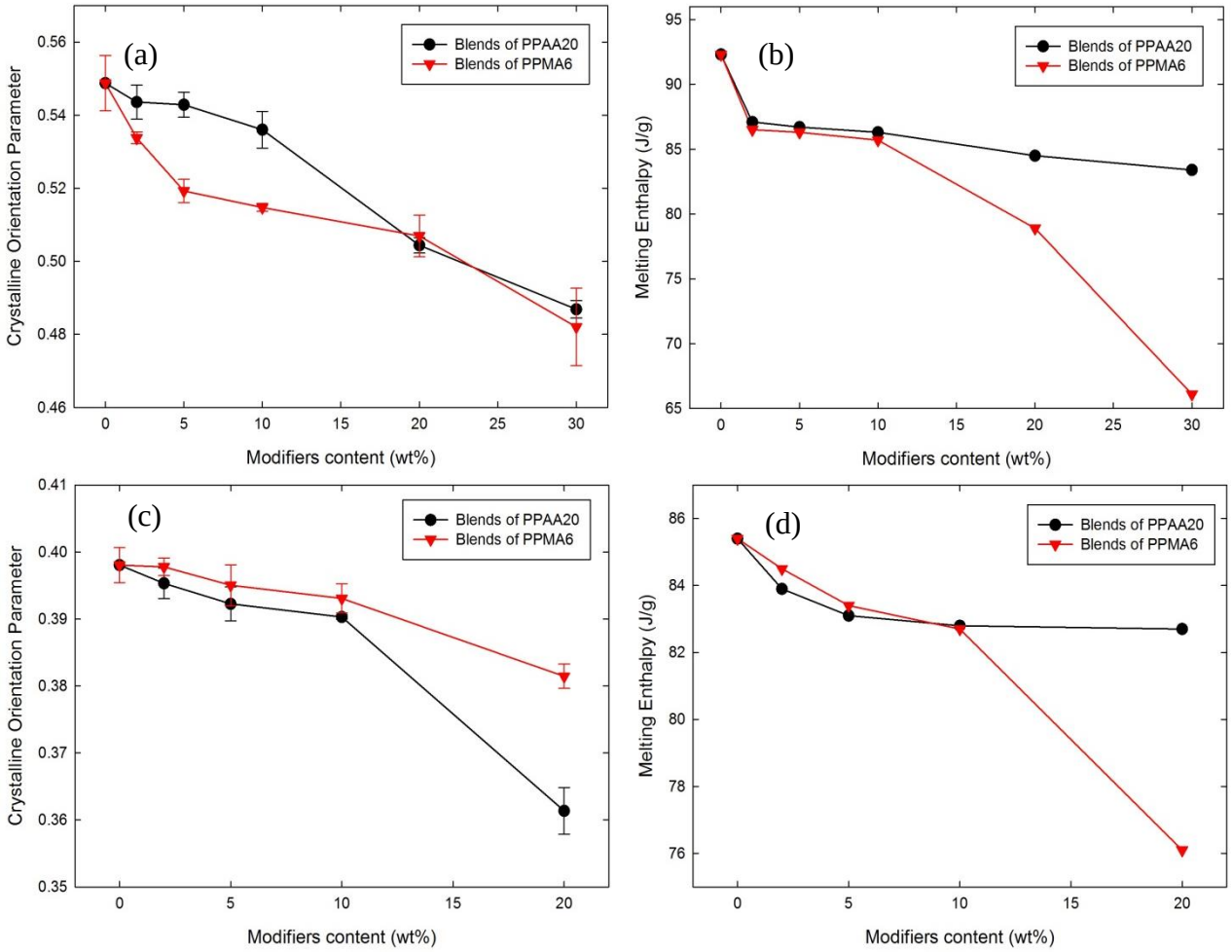

Figure 5-7: Crystalline orientation parameter (obtained from FTIR) and melting enthalpy (obtained from DSC) as a function of PPMA6 and or PPAA20 content (wt%) in (a) & (b) PP0.8 matrix, and (c) & (d) PP2.8 matrix.

The effect of M_w on the level of orientation and alignment of the crystal lamellae in the neat PPs was also considered using WAXD, as illustrated in Figure 5-8. The first and second rings of the pole figures show the patterns for the 110 and 040 crystalline planes, respectively [2, 38]. The normal to the 110 plane is the bisector of the *a* and *b* axes and 040 is along the *b*-axis of crystal unit cells [39]. More intense arcs in the equatorial zones and sharper arcs in the equatorial

zone are apparent for the PP0.8 sample, implying greater orientation for the crystal lamellae, in accordance with the FTIR data.

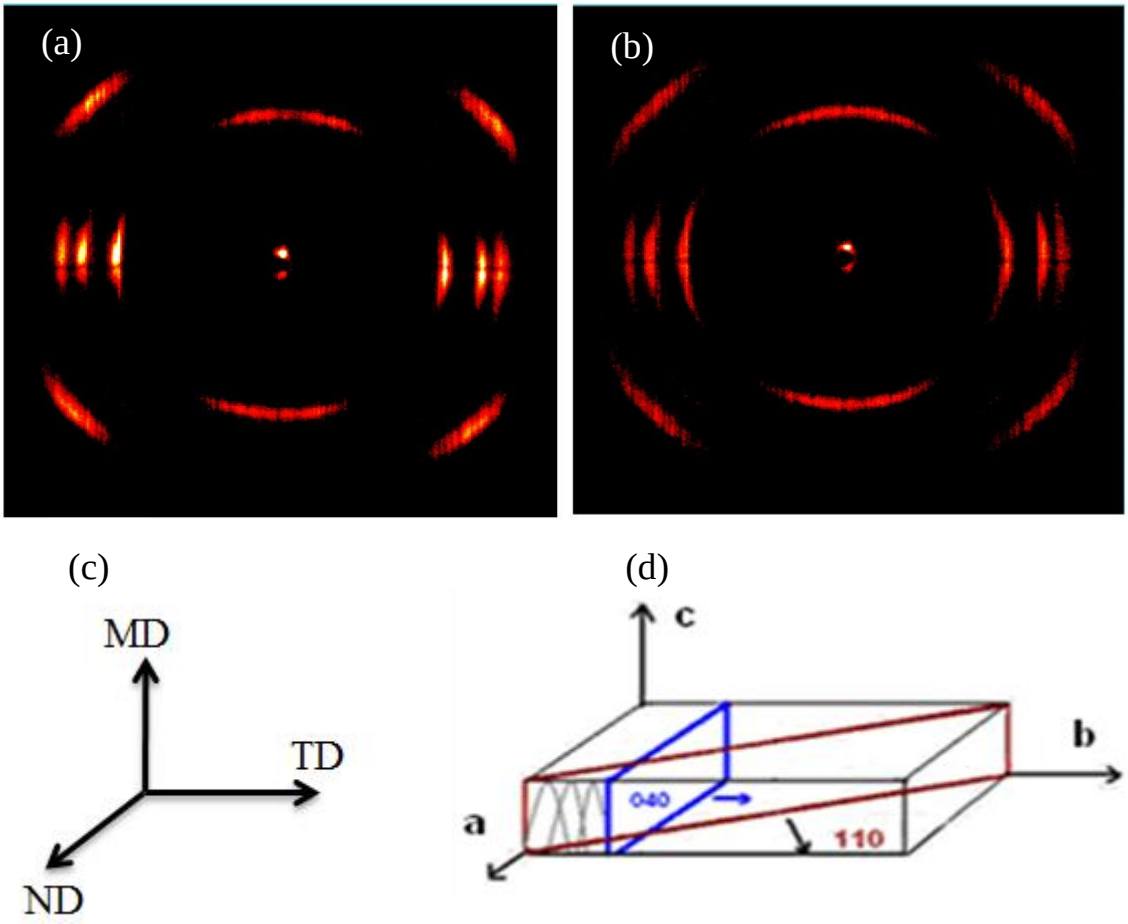

Figure 5-8: WAXD patterns of the precursor films. (a) PP0.8, (b) PP2.8, (c, d) film production axes and crystal block coordinates, respectively.

SAXS measurements were also performed to examine the role played by blending in influencing the crystalline structure. Figure 5-9 illustrates the 2D SAXS patterns for the neat PP2.8 film and the blends with PPAA20. The equatorial streak in the SAXS patterns is attributed to the formation of shishes, while the meridian maxima are attributed to lamellae or kebabs [2]. Looking at the meridian intensity, the formation of less lamellae for the blended films is obvious and by adding more PPAA20 the number of lamellae further decreases. The long period distance,

L_p, was estimated from the position of the intensity maximum ($L_p = 2\pi/q_{max}$ where q is the intensity vector=$4\pi\sin\theta/\lambda$, λ is the X-ray wavelength and 2θ is the scattering angle). It can be seen from Fig. 9d that blending shifts the peaks to higher values of q, indicating a decrease in the long spacing, thus a change in lamellae thickness [2].

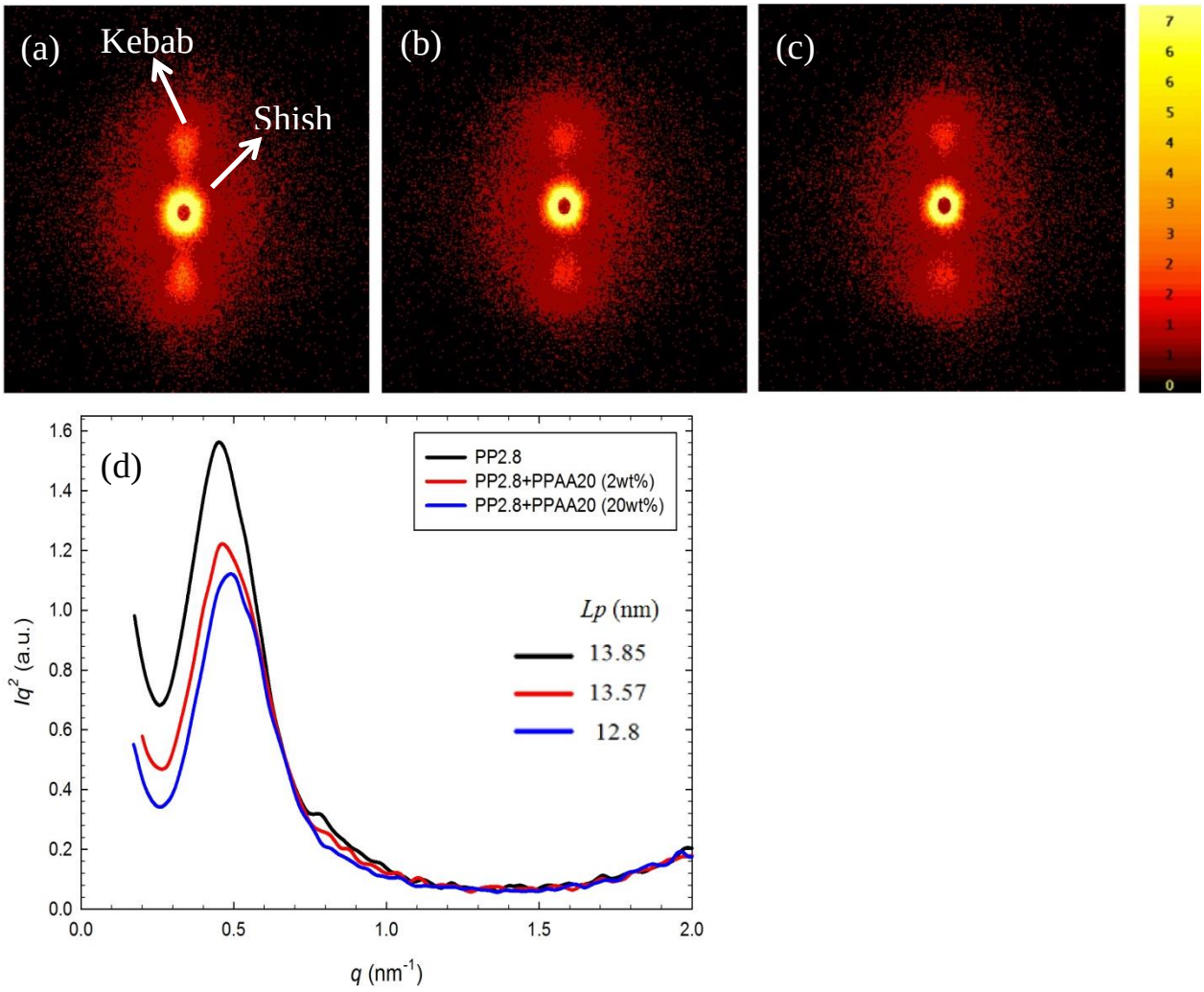

Figure 5-9: SAXS patterns of precursor films, (a) PP2.8, (b) PP2.8+PPAA20 (2wt%), (c) PP2.8+PPAA20 (20wt%) and (d) SAXS intensity profiles for precursor films for the neat PP2.8 and blends with PPAA20.

Water vapor permeability measurements were performed on the blends of PPMA6 and PPAA20 with both PPs and the results are presented in Figure 5-10. As mentioned earlier, the blends of PPMA6 showed lower values compared to the blends of PPAA20, which can be attributed to the presence of ethylene groups in PPMA6. The results reveal maximum peaks at two weight percentages (2wt%) of modifiers in PPs. This trend can be explained as follows. The hydrophilic groups on the membrane surface can increase the solubility of water and, consequently, enhance the permeability. The enhanced permeability in the low content of the modifiers may be mainly attributed to the improved surface hydrophilicity since the membranes possess a similar structure. However, by increasing the modifier content, the changes in the membrane structure (crystallinity and orientation) may be the dominating factor for the decreased permeability. As the results of Figures 5-7 and 5-9 show, blending PPAA20 or PPMA6 destroys the crystalline structure by decreasing the regularity in the chains, which consequently decrease the porosity and pore size of the membrane. On the other hand, it is clear that the presence of hydrophilic groups on the surface increases the water vapor permeability due to the formation of the hydrogen bonds with water molecules [37]. As a result, it seems that the optimum concentration for blending is about 2 wt%, for which there is enough crystalline orientation for a row-nucleated morphology suitable for the formation of porous membranes and sufficient polar groups on the surface to create hydrogen bonding as well. The water vapor permeability for the blend of PP0.8 with 1 wt% of PPMA6 was also verified and the result showed a larger permeability than that of the neat PP0.8 but smaller compared to the blend containing 2 wt% PPMA6. Incidentally, Figure 5-10 reveals that the values of water vapor permeability of the neat PP and the blend containing 20wt% PPAA20 is approximately the same; yet the neat PP exhibits a higher crystallinity and a better crystalline orientation and, consequently, greater pore sizes and

a larger number of pores in their membrane (shown below) compared to the blend. This confirms the effect of polar groups on the water vapor permeability.

Blends of the PP0.8 matrix show higher permeability compared with the PP2.8 based blends, which is due to the difference in M_w. As mentioned above, the larger M_w enhances the crystalline orientation (see Figures 5-7 and 5-8) and, consequently, raises the permeability, due to the creation of more pores, higher porosity and better interconnection between the pores [2]. However, the WVTR value increases by a factor of 1.2 or 1.5 when 2 wt% PPMA6 or PPAA20 is added to the PP0.8 matrix and by a factor of 1.8 or 2.8 when added to the PP2.8 matrix, respectively. To explain these results the mechanism of migration of modifiers during cast film processing is now discussed.

Lowering the interfacial free energy is one of the forces driving the modifier to the interface [9, 16]. It is well known that non-polar materials have lower surface free energy (like air or PP with 29 mN/m) compared to polar materials (like water with 70 mN/m or steel die with 1200 mN/m) [18]. Consequently, if the surface is in contact with air, the hydrophobic compound will concentrate at the surface to reduce the interfacial energy of the air–polymer interface. If the surface is in contact with polar materials, the hydrophilic component (like MA and AA) will preferentially diffuse and migrate to the interface [12, 19, 40]. Furthermore, lower M_w of PP2.8 compared to PP0.8 caused lower interaction and compatibility of the matrix with the PP segments of modifiers. Thus, it seems that during the process, the modifier has more opportunity to migrate to the surface when the matrix is PP2.8 compared to PP0.8 [1, 16, 18]. This might be responsible for the results observed for the water vapor permeability discussed before.

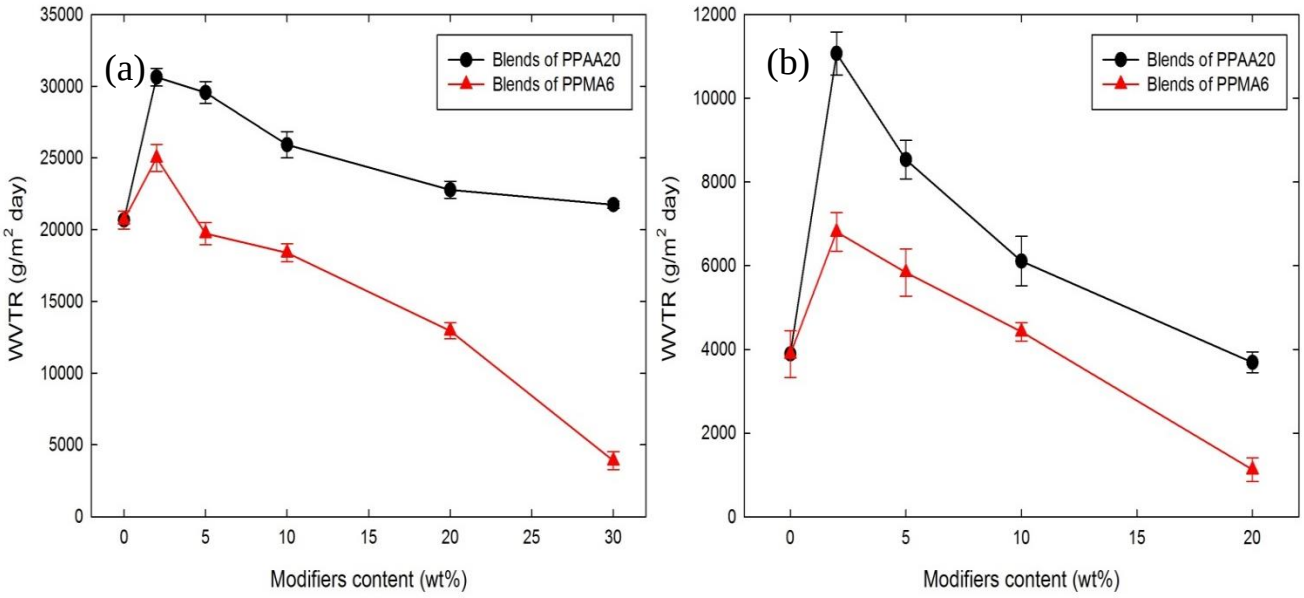

Figure 5-10: Water vapor transmission rate as a function of PPMA6 or PPAA20 content (wt%) in (a) PP0.8 and (b) PP2.8.

XPS results allow the determination of the relative content of the oxygen attributable to different groups on the film surface. Figure 5-11 presents the results of the surface analysis using XPS for the PP2.8/PPAA20 precursor films with different PPAA20 contents. Two major emission peaks can be observed at 285 eV for C1s and at 532 eV for O1s [12, 19]. The results reveal that blend modification leads to the appearance of oxygen as a result of presence of the hydrophilic groups (acrylic acid) on the surface. This supports the observed improvement in the water vapor permeability results. Since no oxygen exists in the neat PP2.8, the very low value of the oxygen on the surface of the neat PP2.8 film suggests that the surface of the PP2.8 film contains some contaminants.

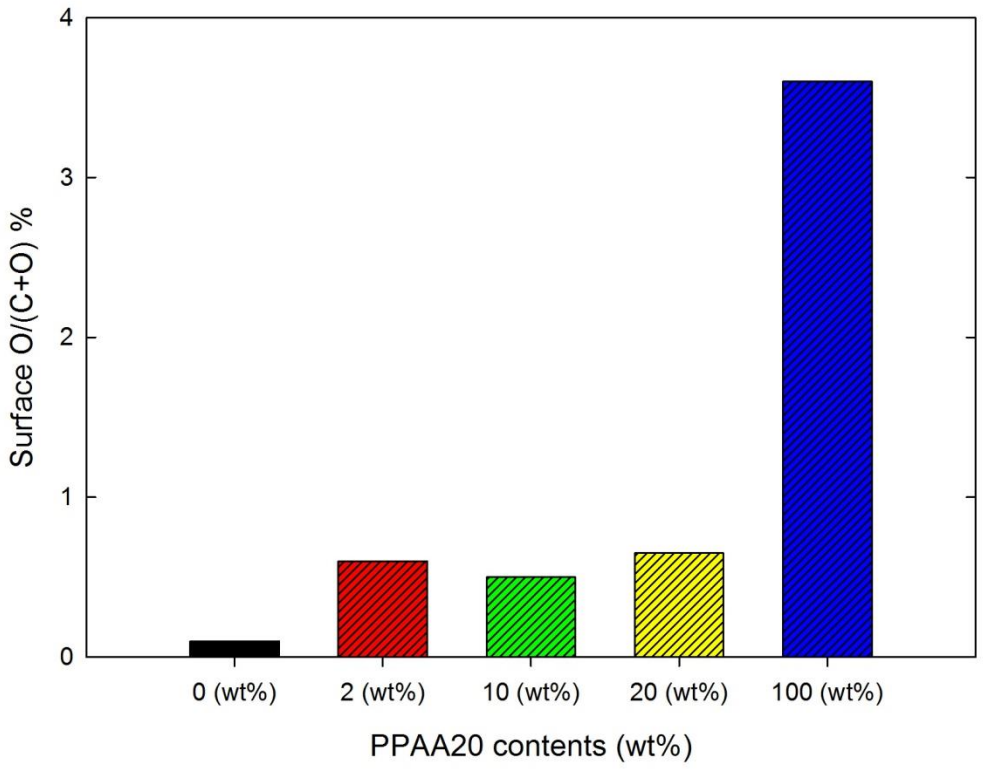

Figure 5-11: Surface O/(C+O)% for PP2.8 films modified using PPAA20 with different additive concentrations determined using XPS.

The surface morphology of the developed membranes for the neat PP2.8 and the blends with PPAA20 at different concentrations was investigated using SEM and the images are presented in Figure 5-12. It is evident that in comparison with the micrograph of the unmodified membrane (Figure 5-12a) adding a modifier causes a decrease in the size and number of pores [26], which confirms again the effect of polar groups on the water vapor permeability.

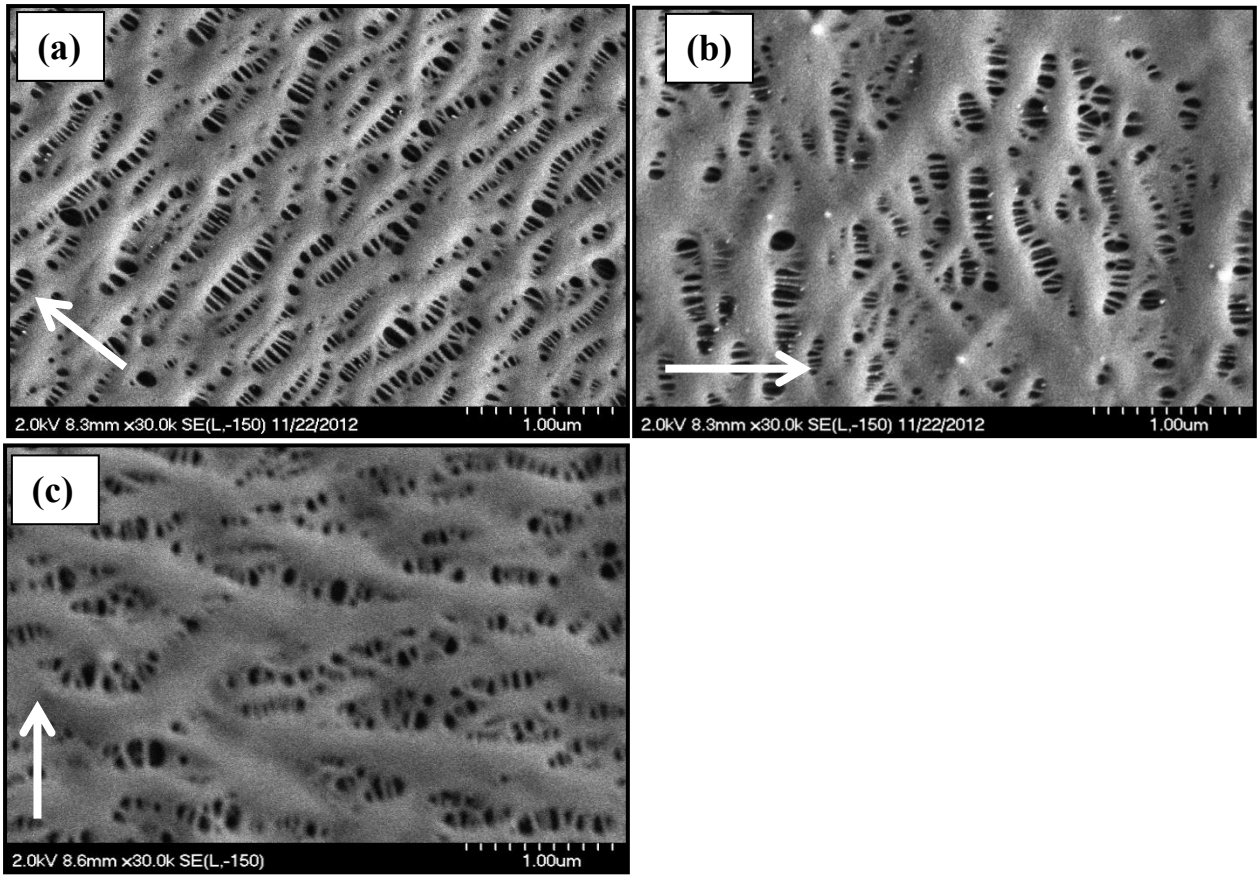

Figure 5-12: SEM micrographs of the surface of the microporous membranes, (a) PP2.8, (b) PP2.8+PPAA20 (2wt%) and (c) PP2.8+PPAA20 (20wt%); (the arrows indicate the stretching machine direction).

Results of the mercury porosimetry analysis for the microporous membranes made of the neat PP2.8 and blends with PPAA20 at different concentrations are reported in Table 5.2. It is known that the mercury intrusion volume is directly related to the pore size and porosity due to interconnected pores [3]. The results show that adding 20 wt% PPAA20 lowers the total pore area and average pore diameter, which is in agreement with the SEM results. However, the pore size distribution (not shown here) show that blending does not dramatically influence the peak positions in the pore size distribution curves and all three samples reveal peaks around 0.1 µm. Furthermore, porosity values of 25, 25.3 and 21.1% are obtained for the neat PP2.8, 2 wt% and

20 wt% blend membranes, respectively. The decreasing porosity for a blend membrane sample is attributed to the lower orientation of the crystal blocks and, consequently, more resistance to lamellae separation, which results in less pore interconnections [2, 3, 5].

Table 5-2: Results of the mercury porosimetry analysis for the microporous membranes.

	Total pore area (m^2/g)	Average pore diameter (nm)	Porosity (%)
PP2.8	20.2	85	25
PP2.8+PPAA20 (2wt%)	19.8	82	25.3
PP2.8+PPAA20 (20wt%)	15.4	62	21.1

The mechanical properties of the blend films and membranes are of great importance for practical applications. The elongation at break and Young modulus along MD for all the films based on PP2.8 were determined and are presented in Figure 5-13. The same trends were found in the blends based on PP0.8 and the data are not shown here for the sake of brevity. Small decreases in the mechanical properties are observed for the blends compared to the neat PP2.8, which are probably caused by the intrinsic mechanical properties of the modifiers and the disturbance of the PP crystalline structure [41]. The slight increases with modifier content in the elongation at break along MD, presented in Figure 5-13a for the precursor films, is possibly due to decrease in crystallinity and orientation of the amorphous and crystalline phases for these samples, as indicated in Figure 5-7. It is well known that more orientation and alignment of the

lamellae along MD result in less deformation at break [2, 6, 38]. Figure 5-13b shows that the Young modulus of the precursor films changes with increasing modifier content. For the PPAA20 modified blends, the Young modulus increases while for the PPMA6 cases it decreases. This could be due to the intrinsic properties of the two modifiers. The DMA results confirmed this behavior. The storage modulus of the neat PPAA20 was larger, while that of the PPMA6 samples was lower than that of the neat PP2.8 (results not shown).

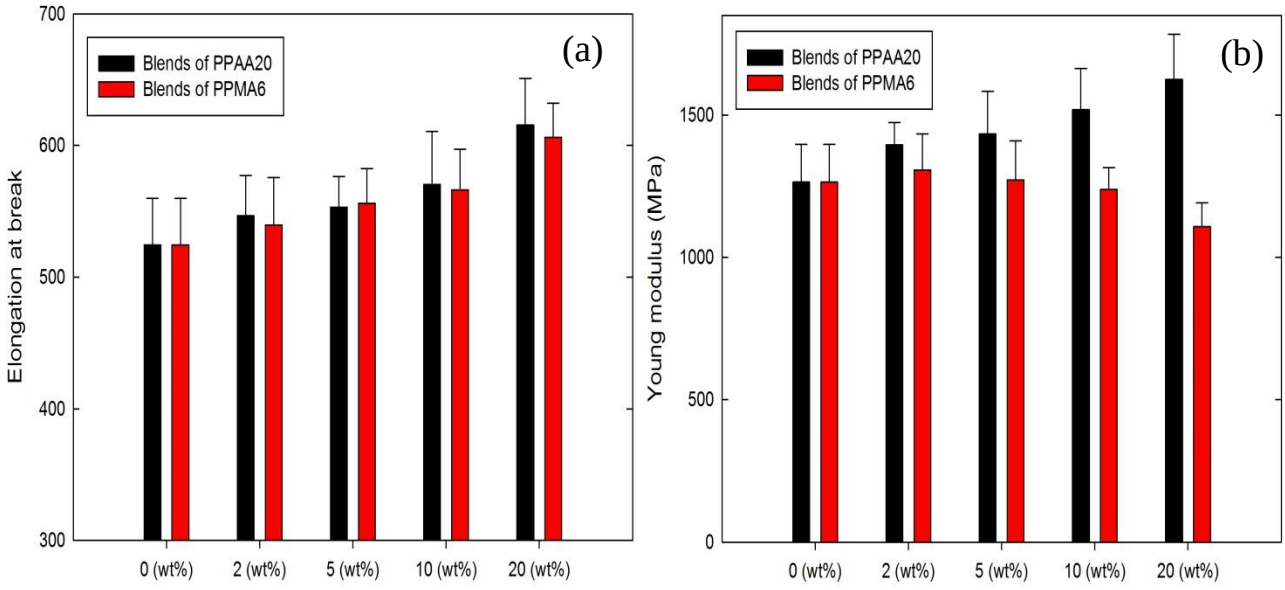

Figure 5-13: (a) Elongation at break and (b) Young modulus as functions of PPMA6 or PPAA20 content (wt%) in PP2.8 based precursor films; strain rate = 50mm/min.

Membranes are often used under pressure and their puncture resistance is important. Puncture tests were performed on circular samples having a diameter of 47 mm in order to investigate the effect of blending on the mechanical properties of the precursor films and membranes along the normal direction (ND) and the results are presented in Figure 5-14. Each point is an average of over 10 samples. As pointed out earlier (Figure 5-7), increasing PPMA6

content decreases the crystallinity as well as the alignment of the crystalline phases [2, 3]. This can explain the reduction of the puncture resistance with increasing PPMA6 content. Furthermore, as mentioned earlier, due to chain rearrangements at temperatures close to the melting point of the samples during annealing and slight changes in the crystallinity during stretching, the crystalline contents of all membranes are increased in comparison to the precursor films. This explains the slightly enhanced puncture values for the membranes compared to the precursor films.

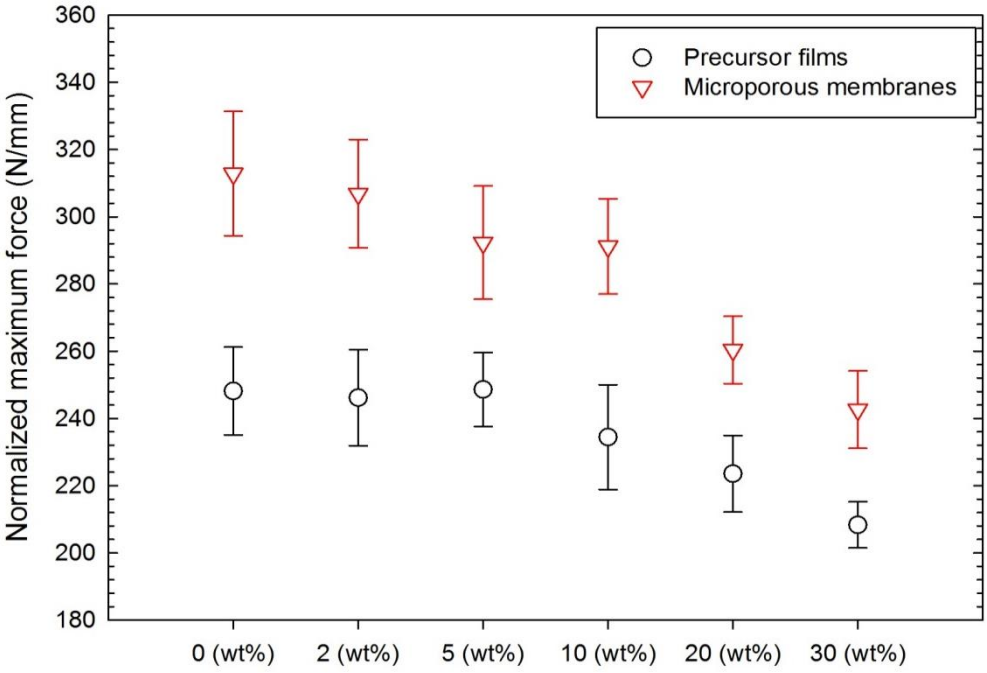

Figure 5-14: Normalized maximum force for piercing in PP0.8 based precursor films and membranes as function of PPMA6 content (wt%).

5.4 Conclusions

In this work, the structure and performance of microporous membranes made from blends of polypropylene (PP) with maleic anhydride and acrylic acid grafted PP (PP -g- MA and PP -g- AA) were investigated. Based on the ATR-FTIR and DSC results of neat modifiers, the hydrophobic segments of the PPMAs used, except PPMA-E43, are believed to be a copolymer of polypropylene and ethylene.

The results from FTIR, thermal analysis and SAXS indicated that blending of the modifiers with PP decreased the crystalline orientation and degree of the crystallinity as a result of reduction in chain regularity. By the addition of amphiphilic copolymers, PP -g- MA and PP -g- AA, the surface hydrophilicity of PP membranes was enhanced. The amphiphilic modifiers act as surface functional groups on the film surface and improve the membrane performances. The optimum concentration was found to be 2wt % modifier to achieve membranes having good hydrophilic characteristics, with enough polar groups on the surface and causing a minimal change in the crystalline structure compared to the neat PP film.

SEM micrographs of the membrane surface revealed less uniform pores and a worse distribution as the modifier content increased. This was attributed to the lower orientation of the crystal blocks and, consequently, more resistance to lamellae separation. Finally, the water vapor permeability of the membranes, which reflects the pore interconnection and hydrophilicity of the surface, was checked for the blends as well as for the neat polymers and it was consistent with SEM and XPS results.

The addition of the modifiers did not show a dramatic effect on the mechanical properties of the precursor films and membranes along MD and ND in the range of low modifier contents. Tensile

tests revealed slight reductions of the Young modulus along MD with increasing PPMA6 content, while the inverse trend was observed for PPAA20.

5.5 Acknowledgments

Financial support from NSERC Network for Innovative Plastic Materials and Manufacturing Processes (NIPMMP) is gratefully acknowledged. We are also thankful to Ms. Sylvie St-Amour and Ms. Sylvie Sauriol from FP Innovations (Paprican Division) for the use of and training on their AutoPore IV mercury intrusion porosimeter.

5.6 References

[1] M. Xu, X. Shi, H. Chen, T. Xiao, Synthesis and enrichment of a macromolecular surface modifier PP-b-PVP for polypropylene, Appl. Surf. Sci. 256 (2010) 3240-3244.

[2] S.H. Tabatabaei, P.J. Carreau, A. Ajji, Microporous membranes obtained from polypropylene blend films by stretching, J. Membr. Sci. 325 (2008) 772-782.

[3] F. Sadeghi, A. Ajji, P.J. Carreau, Analysis of microporous membranes obtained from polypropylene films by stretching, J. Membr. Sci. 292 (2007) 62-71.

[4] F. Sadeghi, A. Ajji, P.J. Carreau, Analysis of row nucleated lamellar morphology of polypropylene obtained from the cast film process: Effect of melt rheology and process conditions, Polym. Eng. Sci. 47 (2007) 1170-1178.

[5] F. Sadeghi, A. Ajji, P.J. Carreau, Microporous membranes obtained from polypropylene blends with superior permeability properties, J. Polym. Sci., Part B: Polym. Phy. 46 (2008) 148-157.

[6] S.H. Tabatabaei, P.J. Carreau, A. Ajji, Microporous membranes obtained from PP/HDPE multilayer films by stretching, J. Membr. Sci. 345 (2009) 148-159.

[7] B. Fang, Q. Ling, W. Zhao, Y. Ma, P. Bai, Q. Wei, H. Li, C. Zhao, Modification of polyethersulfone membrane by grafting bovine serum albumin on the surface of polyethersulfone/poly(acrylonitrile-co-acrylic acid) blended membrane, J. Membr. Sci. 329 (2009) 46-55.

[8] J.F. Hester, P. Banerjee, A.M. Mayes, Preparation of Protein-Resistant Surfaces on Poly(vinylidene fluoride) Membranes via Surface Segregation, Macromolecules. 32 (1999) 1643-1650.

[9] R. Bongiovanni, B. Gagnor, G. Malucelli, A. Priola, A. Pollicino, Surface properties and adhesion of maleinized polyethylene films, J. Mater. Sci. 33 (1998) 1461-1464.

[10] J.H. Li, Y.Y. Xu, L.P. Zhu, J.H. Wang, C.H. Du, Fabrication and characterization of a novel TiO2 nanoparticle self-assembly membrane with improved fouling resistance, J. Membr. Sci. 326 (2009) 659-666.

[11] J. Meier-Haack, M. Valko, K. Lunkwitz, M. Bleha, Microporous membranes from polyolefin-polyamide blend materials, Desalination. 163 (2004) 215-221.

[12] C. Zhang, Y. Bai, Y. Sun, J. Gu, Y. Xu, Preparation of hydrophilic HDPE porous membranes via thermally induced phase separation by blending of amphiphilic PE-b-PEG copolymer, J. Membr. Sci. 365 (2010) 216-224.

[13] E. Li, Z. Du, S. Yuan, Properties of a water layer on hydrophilic and hydrophobic self-assembled monolayer surfaces: A molecular dynamics study, Sci. China. Chem. 56 (2013) 773-781.

[14] N.K. Goel, Y.K. Bhardwaj, R. Manoharan, V. Kumar, K.A. Dubey, C.V. Chaudhari, S. Sabharwal, Physicochemical and electrochemical characterization of battery separator prepared by radiation induced grafting of acrylic acid onto microporous polypropylene membranes, Express. Polym. Lett. 3 (2009) 268-278.

[15] J.Y. Kim, D.Y. Lim, Surface-Modified Membrane as A Separator for Lithium-Ion Polymer Battery, Energies. 3 (2010) 866-885.

[16] V.M. Datla, Surface modification of fibers and nonwovens with melt additives, North Carolina State University, Ann Arbor, 2008, (Ph.D. thesis).

[17] S. Paul, Surface modification of polypropylene nonwovens to improve adhesion to elastomers, North Carolina State University, Ann Arbor, 2009, (Ph.D. thesis).

[18] H. Chen, X. Shi, Y. Zhu, Y. Zhang, J. Xu, Surface functionalization of polypropylene by entrapment of polypropylene-grafted-poly(ethylene glycol), J. Appl. Polym. Sci. 114 (2009) 2461-2468.

[19] L.P. Zhu, Y.Y. Xu, H.B. Dong, Z. Yi, B.K. Zhu, Amphiphilic PPESK-graft-P(PEGMA) copolymer for surface modification of PPESK membranes, Mater. Chem. Phys. 115 (2009) 223-228.

[20] L.P. Zhu, L. Xu, B.K. Zhu, Y.X. Feng, Y.Y. Xu, Preparation and characterization of improved fouling-resistant PPESK ultrafiltration membranes with amphiphilic PPESK-graft-PEG copolymers as additives, J. Membr. Sci. 294 (2007) 196-206.

[21] J.F. Hester, P. Banerjee, Y.Y. Won, A. Akthakul, M.H. Acar, A.M. Mayes, ATRP of Amphiphilic Graft Copolymers Based on PVDF and Their Use as Membrane Additives, Macromolecules. 35 (2002) 7652-7661.

[22] J.Y. Park, M.H. Acar, A. Akthakul, W. Kuhlman, A.M. Mayes, Polysulfone-graft-poly(ethylene glycol) graft copolymers for surface modification of polysulfone membranes, Biomaterials. 27 (2006) 856-865.

[23] F. Sadeghi, A. Ajji, P.J. Carreau, Study of Polypropylene Morphology Obtained from Blown and Cast Film Processes: Initial Morphology Requirements for Making Porous Membrane by Stretching, J. Plast. Film. Sheet. 21 (2005) 199-216.

[24] I. Novák, E. Borsig, L.u. Hrčková, A. Fiedlerová, A. Kleinová, V. Pollák, Study of surface and adhesive properties of polypropylene grafted by maleic anhydride, Polym. Eng. Sci. 47 (2007) 1207-1212.

[25] C.H. Jung, J.H. Choi, Y.M. Lim, J.P. Jeun, S.J. An, P.H. Kang, Y.C. Nho, Preparation of Polypropylene Compatibilizer by Radiation Grafting and Its Effect on PP/Nylon 6 Blend, Macromol. Symp. 249-250 (2007) 573-579.

[26] Z. Xu, J. Wang, L. Shen, D. Men, Y. Xu, Microporous polypropylene hollow fiber membrane: Part I. Surface modification by the graft polymerization of acrylic acid, J. Membr. Sci. 196 (2002) 221-229.

[27] S.G. Flores-Gallardo, S. Sánchez-Valdes, L.F.R. De Valle, Polypropylene/polypropylene-grafted acrylic acid blends for multilayer films: Preparation and characterization, J. Appl. Polym. Sci. 79 (2001) 1497-1505.

[28] J. Song, A. Bringuier, S. Kobayashi, A.M. Baker, C.W. Macosko, Adhesion between polyethylenes and different types of polypropylenes, Polym. J. 44 (2012) 939–945.

[29] A. Colbeaux, F. Fenouillot, J.F. Gerard, M. Taha, H. Wautier, Compatibilization of a polyolefin blend through covalent and ionic coupling of grafted polypropylene and polyethylene. II. Morphology, J. Appl. Polym. Sci. 93 (2004) 2237-2244.

[30] F. Sadeghi, S.H. Tabatabaei, A. Ajji, P.J. Carreau, Properties of uniaxially stretched polypropylene films: effect of drawing temperature and random copolymer content, Can. J. Chem. Eng. 88 (2010) 1091-1098.

[31] A. Karami, Polymer Blend De-mixing and Morphology Development During Tube Flow, University of Toronto, Toronto, 1999 (Ph.D. thesis).

[32] S. Laihonen, U.W. Gedde, P.E. Werner, J. Martinez-Salazar, Crystallization kinetics and morphology of poly(propylene-stat-ethylene) fractions, Polymer. 38 (1997) 361-369.

[33] F. Sadeghi, A. Ajji, Rheological, physical, and thermal characterization of single-site catalyst based polyethylenes for seal layer applications, Polym. Eng. Sci. 52 (2012) 1089-1098.

[34] F.M. Mirabella, Correlation of the melting behavior and copolymer composition distribution of Ziegler–Natta-catalyst and single-site-catalyst polyethylene copolymers, J. Polym. Sci., Part B: Polym. Phy. 39 (2001) 2800-2818.

[35] D.H. Garg, W. Lenk, S. Berwald, K. Lunkwitz, F. Simon, K.J. Eichhorn, Hydrophilization of microporous polypropylene Celgard® membranes by the chemical modification technique, J. Appl. Polym. Sci. 60 (1996) 2087-2104.

[36] S.J. Metz, Water vapor and gas transport through polymeric membranes, University of Twente, Enschede, 2003 (Ph.D. thesis).

[37] M.M. Deshmukh, N.V. Sastry, S.R. Gadre, Molecular interpretation of water structuring and destructuring effects: Hydration of alkanediols, J. Chem. Phys. 121 (2004) 12402-12410.

[38] S.H. Tabatabaei, P.J. Carreau, A. Ajji, Effect of processing on the crystalline orientation, morphology, and mechanical properties of polypropylene cast films and microporous membrane formation, Polymer. 50 (2009) 4228-4240.

[39] S.H. Tabatabaei, P.J. Carreau, A. Ajji, Structure and properties of MDO stretched polypropylene, Polymer. 50 (2009) 3981-3989.

[40] D.E. Suk, G. Chowdhury, T. Matsuura, R.M. Narbaitz, P. Santerre, G. Pleizier, Y. Deslandes, Study on the Kinetics of Surface Migration of Surface Modifying Macromolecules in Membrane Preparation, Macromolecules. 35 (2002) 3017-3021.

[41] X. Ma, Y. Su, Q. Sun, Y. Wang, Z. Jiang, Preparation of protein-adsorption-resistant polyethersulfone ultrafiltration membranes through surface segregation of amphiphilic comb copolymer, J. Membr. Sci. 292 (2007) 116-124.

CHAPTER 6 - ARTICLE 2:

HYDROPHILIC MODIFICATION OF POLYPROPYLENE MICROPOROUS MEMBRANES BY GRAFTING TIO2 NANOPARTICLES WITH ACRYLIC ACID GROUPS ON THE SURFACE.

Amir Saffar[1], Pierre J. Carreau[1], Musa R. Kamal[2], Abdellah Ajji[1]

1) Research Center for High Performance Polymer and Composite Systems (CREPEC), Chemical Engineering Department, Polytechnique Montreal, PO Box 6079, Stn Centre-Ville, Montreal, Quebec, Canada, H3C 3A7.

2) CREPEC, Department of Chemical Engineering, McGill University, 3610 University Street, Montreal, Quebec, Canada, H3A 2B2.

This work was submitted to *The Journal of Physical Chemistry B*

Abstract

Hydrophilic microporous membranes were prepared based on polypropylene (PP) cast films blended with a commercial acrylic acid grafted polypropylene (PP-g-AA) via melt extrusion followed by grafting titanium dioxide (TiO_2) nanoparticles on its surface, annealing and stretching. Different techniques such as ATR-FTIR, SEM, water contact angle and water vapor permeability measurements were used to investigate the effect of grafting TiO_2 nanoparticles on membrane performance. ATR-FTIR analyses showed that the hydrophilic segments of an amphiphilic modifier (PP-g-AA) acted as surface functional groups on the precursor film surface. The results indicated that the presence of the modifier was very important for grafting TiO_2 nanoparticles on the precursor film surface. Compared to PP and PP/PP-g-AA blend films, the water contact angle decreased by a factor of 2.5 after grafting TiO_2 onto the surface of the precursor films, meanwhile the water vapor permeability of the microporous membranes prepared from those films increased by a factor of 1.5. All these results indicated that the hydrophilicity of the modified PP membranes was improved. Membrane morphology observations using SEM showed approximately the same pore structure before and after TiO_2 grafting.

Keywords

Polypropylene blends, Surface functional groups, TiO_2 nanoparticles, Hydrophilicity, Membranes by stretching.

6.1 Introduction

Semi-crystalline polypropylene (isotactic PP) is one of the most commonly used polymers today in a variety of applications due to its outstanding properties such as low cost, easy processing, good mechanical properties, chemical stability and non-toxicity [1, 2]. However, because of its intrinsic hydrophobicity, hydrophilic substances such as water or hydrophilic substrates will not adhere to the surface of PP. This limits its applications as membranes for wastewater treatment, desalination of sea water, electrode separators in batteries and biomedical areas [1, 3-5].

One of the main obstacles in membranes applications is fouling, which is markedly influenced by the surface properties of the membranes [6-8]. Organic matter is easily adsorbed onto the membrane surface or pore walls, which results in the deterioration of the membrane performance. Thus, membrane fouling leads to shorter membrane life time and, subsequently, an increase in the operation costs for the replacement and maintenance of membrane modules [3, 4, 6]. Membrane fouling can be divided into reversible and irreversible fouling. Reversible fouling occurs in a hydrophilic surface, which can be fully or partly eliminated by hydraulic cleaning, e.g., backwashing and cross flushing. Irreversible fouling is caused by irreversible organic matter adsorption on the hydrophobic surface and can only be removed by chemical or biochemical cleaning [9, 10]. The reason for irreversible fouling is the lack of hydrogen bonding interactions between the hydrophobic membrane and water in the boundary layer, which leads to the repulsion of the water molecules away from the surface. By contrast, membranes with a hydrophilic surface can form hydrogen bonds with the surrounding water molecules and produce a water boundary on the surface [11]. Accordingly, increasing the hydrophilicity of the

membrane surface is a potential fouling mitigation method and can also improve surface properties such as adhesion [5, 10].

Despite the fouling effects, hydrophobic materials have higher mechanical and chemical stability than hydrophilic materials [4, 9]. Thus, an ideal membrane would combine the superior bulk properties of hydrophobic materials with the surface chemistry of hydrophilic materials [4, 12].

Different strategies have been used to increase the amount of surface polar groups and improve the membrane surface. Basically, these methods include plasma treatment, blending with hydrophilic materials, radical grafting reactions, chemical coatings and so on [3, 12, 13]. In order to avoid some inherent drawbacks of these methods [14], blending the host polymer with a hydrophilic modifier can be applied at an industrial scale to obtain a hydrophilic surface [1, 12, 13]. However, thermodynamic incompatibility between hydrophobic and hydrophilic polymers causes the release of the hydrophilic compound and elution from the surface when contacted with a polar chemical solvent [3, 12, 15]. Thus, amphiphilic copolymers consisting of hydrophobic backbones and hydrophilic side chains are good candidates to blend with PP for developing performing membranes. The hydrophobic part of the amphiphilic additive will anchor onto the host polymer, due to good interactions between both hydrophobic chains [10, 15, 16].

Membranes are usually made from a solution/phase separation process. Recently, a different process was developed to prepare PP porous membranes from the melt by combining the development of a specific crystalline morphology in polymer films, i.e., an aligned row-nucleated lamellar structure, followed by annealing and stretching [2, 17, 18]. In this method, the crystalline structure of the precursor films is the key factor for the formation of microporous membranes [2]. The crystalline orientation factor of the precursor films is lowered by blending

with low molecular weight polymers [2]. Therefore, it is important to choose the right amphiphilic polymer to blend with PP and generate the desired lamellar morphology. In fact, the crystalline orientation factor should be high enough (more than 0.3) in order to obtain the row-nucleated morphology suitable for porous membrane formation [19].

In our previous work [14], acrylic acid grafted polypropylene (PP-g-AA) was blended at different concentrations with PP to develop microporous hydrophilic membranes. The optimum concentration to achieve membranes having hydrophilic characteristics, with enough polar groups on the surface and a minimal change in the crystalline structure compared to the neat PP, was found to be 2wt % of the modifiers. However, the hydrophilicity of these blend membranes was not high enough for practical applications. The polar groups of the modifiers can act as surface functional groups on the precursor film surface for grafting with other hydrophilic groups.

Titanium dioxide (TiO_2) nanoparticles can be used for further hydrophilic modification because of its super hydrophilicity, chemical resistance to acids and bases as well as its commercial availability and low cost [6, 20, 21]. Furthermore, TiO_2 nanoparticles are widely used for environmental applications such as water purification, wastewater treatment and air purification [8, 22]. These useful applications could be attributed to its photo-catalytic effects that decompose organic chemicals and kill bacteria under ultraviolet (UV) radiation [6, 8].

There are two main approaches to prepare polymer/TiO_2 nanoparticles composite membranes: blending the nanoparticles with a polymer or dipping the prepared polymer film in a suspension of TiO_2 nanoparticles and fabricate the hydrophilic membrane via grafting [22, 23].

As mentioned above, the crystalline structure of the precursor film is affected by blending with low molecular weight polymers. Furthermore, several studies showed that preparing polymer/TiO_2 nanoparticles composite membranes via blending results in noticeable changes in

the crystalline structure and, subsequently, in the pores structure of the membranes [22-24]. On the other hand, the immersion method leads to grafting TiO_2 nanoparticles with the functional groups on the surface without affecting the crystalline structure of PP.

Grafting TiO_2 nanoparticles on a surface having COOH groups might be explained by two different mechanisms. One scheme might be that TiO_2 can bind with two oxygen atoms of carboxylate groups by a bidentate coordination to Ti^{4+} cations. The other scheme might be the formation of H-bonding between carboxylic acid and the hydroxyl groups of TiO_2 [6, 8, 25]. This reaction was confirmed by several experimental and theoretical investigations, i.e. using density functional theory (DFT) cluster calculations [26, 27]. However, only few examples are found for the hydrophilic modification of hydrophobic membranes using TiO_2 nanoparticle grafting. Kim et al.[8] produced a hybrid thin film composite membrane by grafting TiO_2 nanoparticles through interaction with the COOH functional groups of an aromatic polyamide thin film layer. Li et al. [6] prepared TiO_2 nanoparticles grafted membranes based on ultrahigh molecular weight poly(styrene-alt-maleic anhydride)/poly(vinylidene fluoride) (SMA/PVDF) blend membranes. Bae et al. [7] fabricated composite membranes by grafting TiO_2 nanoparticles and sulfonic acid groups residing on commercial polyethersulfone membranes. Xu et al. [28] deposited TiO_2 on porous polypropylene membranes using the atomic layer deposition technique. To generate active groups on the surface, they applied a plasma activation step to the PP membranes before TiO_2 deposition.

All the above reports for TiO_2 grafting aimed at the modification of as received hydrophobic membranes after plasma treatments or blend membranes prepared by phase separation techniques. To our knowledge, no study has been performed on microporous

polypropylene membranes fabricated by extrusion followed by stretching through blending with amphiphilic modifiers, and grafting TiO_2 nanoparticles on its surface.

In this study the effects of grafted TiO_2 nanoparticles on the hydrophilicity of the PP/PP-g-AA blend microporous membranes, produced by cast film extrusion followed by stretching, were investigated. Various tests were carried out to describe the grafting between TiO_2 and COOH groups. Furthermore, the stability of grafted TiO_2 nanoparticles on the surface of microporous membrane (after annealing and stretching) was investigated.

6.2 Experimental

6.2.1 Materials

A commercial linear polypropylene (PP4712E1) and amphiphilic polymer consisting of a PP hydrophobic backbone and an acrylic acid grafted PP (PP-g-AA Polybond®1002) were selected. Their MFR values are of 2.8 g/10 min under ASTM conditions of 230 ºC and 2.16 kg and 20 g/10 min, respectively.). The PP4712E1 was supplied by ExxonMobil Company and the PP-g-AA was purchased from Chemtura Corporation. The main characteristics of these two resins are shown in Table 6.1. The melting point, T_m, and crystallization temperature, T_c, of the resins were obtained using differential scanning calorimetry (DSC).

Titanium dioxide nanoparticles (AEROXIDE TiO_2 P25), in powder form, were obtained from Evonik Industries. According to the manufacturer, P25 has a density of 4.26 g/mL with a nano crystalline structure of anatase:rutile (79:21 wt%). The primary mean particle size of commercial TiO_2 nanoparticles is about 21 nm [23, 28].

Table 6-1: Main characteristic of the neat materials.

Resin Code	Supplier	MFR (g/10 min)	T_m (°C)	T_c (°C)
Polypropylene (PP4712E1)	Exxon Mobil	2.8	160	114
PP-g-AA (Polybond®1002)	Chemtura	20	161	123

6.2.2 Film preparation

Precursor films from the neat PP and a blend of PP containing 2wt% PP-g-AA were prepared using a 45 mm diameter Killion single screw extruder equipped with a slit die of 0.7 mm opening. The temperature profile along the barrel was: 165/195/210/215 °C and the die temperature was 220 °C. For film cooling, an air knife was applied right at the exit of the die to supply air to the film surface. The extrusion was carried out using a screw speed of 12.5 rpm and a draw-down ratio (ratio of the roll speed to the die exit velocity) was set at 25 to produce precursor films having a thickness of around 30 μm. The distance between die exit to the nip cast roll was around 15 cm and the cast roll temperature was constant at 50 °C.

6.2.3 Preparation of TiO_2 grafted precursor film

TiO_2 suspensions were prepared by adding TiO_2 nanoparticles to deionized water (0.1 g/L). The suspensions were stirred for 45 min with ultrasonic vibrations to avoid agglomeration of particles

before usage. Finally, the precursor films were immersed in the TiO_2 nanoparticle suspension by continuous shaking for 1 day at room temperature. To remove non grafted particles, the precursor films were dipped in deionized water and stirred for 3 h with ultrasonic vibrations. Then, these precursor films were washed with deionized water at least three times and dried at room temperature.

This method led to the preparation of hydrophilic surfaces without the problems as associated to the use of a toxic solvent, high temperature, costly fabrication and complex process control.

6.2.4 Membrane preparation

The dry-stretching method was used to prepare the microporous membranes as follows [14]:

The precursor films, before and after immersion in the TiO_2 nanoparticle suspension, with a thickness, width and length of 30 μm, 8 cm, and 4 cm, respectively, were first annealed at 120 °C for 30 min. Then, the annealed samples were cold and hot stretched up to 35% of the initial length at room temperature and 60% at 120 °C, respectively. Both annealing and stretching were performed using an Instron machine (ElectroPlus ^{TM} E3000) equipped with an environmental chamber. A drawing speed of 50 mm/min was applied during the cold and hot stretching steps.

6.2.5 Film and membrane characterization

6.2.5.1 Fourier transform infrared spectroscopy (FTIR)

The surface composition of the samples was investigated using attenuated total reflectance (ATR) mode of Fourier transform infrared spectroscopy (FTIR). The measurements were performed using a Perkin Elmer infrared spectrometer with a spectral resolution of 4 cm^{-1} and a scanning speed of 32 kHz. The data were collected in the range from 4000 to 600 cm^{-1}.

6.2.5.2 X-ray Photoelectron spectroscopy (XPS)

XPS provides quantitative analysis of a surface by detecting the characteristic binding energies associated with each element. XPS measurements were conducted on a VG ESCALAB 3 MKII spectrometer with Mg-Kα ray source. Survey scans of 100 eV pass energy were used to identify initially all components followed by a high resolution individual scans using pass energy of 20 eV. The surface elemental stoichiometry was obtained from the ratios of peak areas corrected with the Wagner sensitivity factors and Shirley background subtraction.

6.2.5.3 Thermogravimetric analyses (TGA)

In order to determine the content of TiO_2 nanoparticles grafted on the membrane surface, thermogravimetric analysis (TGA) was conducted using a TGAQ500 from TA Instruments. For these tests, samples were weighted (typical weights of 5-10 mg) and heated from room temperature to 800 °C with a heating rate of 10 °C/min under an air atmosphere.

6.2.5.4 Contact angle

The hydrophilicity of the precursor film surface was characterized by water contact angle measurements performed using a video contact angle system (VCA Optima, AST Products, Inc.) at room temperature. A drop of 1.5 µL distilled water was carefully poured on the airside surface of the precursor films and the contact angles were then determined semi-manually from the droplet images. The average of at least 8 measurements was reported.

6.2.5.5 Water vapor transmission rate (WVTR)

The permeability to water vapor was measured via a MOCON PERMATRAN-W Model 101K at room temperature. The equipment is composed of three chambers. An upper chamber, which is separated from the center chamber by two porous films, contains liquid water. The center

chamber is separated from the lower one by the test film. Water vapor diffuses from the first film to fill the space between the films and is swept away by N_2 gas to a relative humidity (RH) sensor.

6.2.5.6 Morphology

The microporous membranes surfaces were observed by scanning electron microscopy (SEM). The samples were firstly coated with a gold-palladium alloy and electron micrographs were then taken using a Hitachi (S4700) microscope operated at 2 kV accelerating voltage. Also, the composition of the samples surface was determined by energy dispersive X-ray spectroscopy (EDS). The test was carried out using a JEOL JSM-840A detector at an accelerating voltage of 15 kV.

6.3 Results and discussion

6.3.1 Surface characterization of the precursor films

ATR-FTIR spectroscopy was used to investigate the binding mode of TiO_2 nanoparticles with the blend films, i.e., PP+PP-g-AA (2 wt%). The ATR-FTIR spectra for the neat materials and ungrafted and TiO_2 grafted blend films, i.e., blend films before and after immersion in the TiO_2 suspension, respectively, are shown in Figure 6-1. The peak associated with acrylic acid groups in the blend samples can be observed around 1710 cm^{-1} [30, 31]. As mentioned before, TiO_2 can adsorb on the surface of polymers via grafting with COOH groups according to various probable schemes [6, 27, 32]. One scheme might be that two oxygen atoms of ionic COOH species bind with the same or two different Ti^{4+} cations by a bidentate coordination. Another scheme might be the formation H-bonding between carboxylic acid and the hydroxyl groups at the surface of TiO_2 nanoparticles [25, 27].

Compared to the neat polymer and ungrafted blend sample, the observed spectral change for the TiO_2 grafted blend sample is the appearance of double peaks at wavenumbers of 1542 and 1578 cm^{-1}, in the carboxylate region (COO^-) [33-35]. This corresponds to deprotonated carboxyl groups. These peaks could be the result of the formation of chemical bonds between TiO_2 and carboxylate groups through bidentate binding modes [36]. Strong bonds of TiO_2 nanoparticles with COOH groups prevent its washing and removal from the surface.

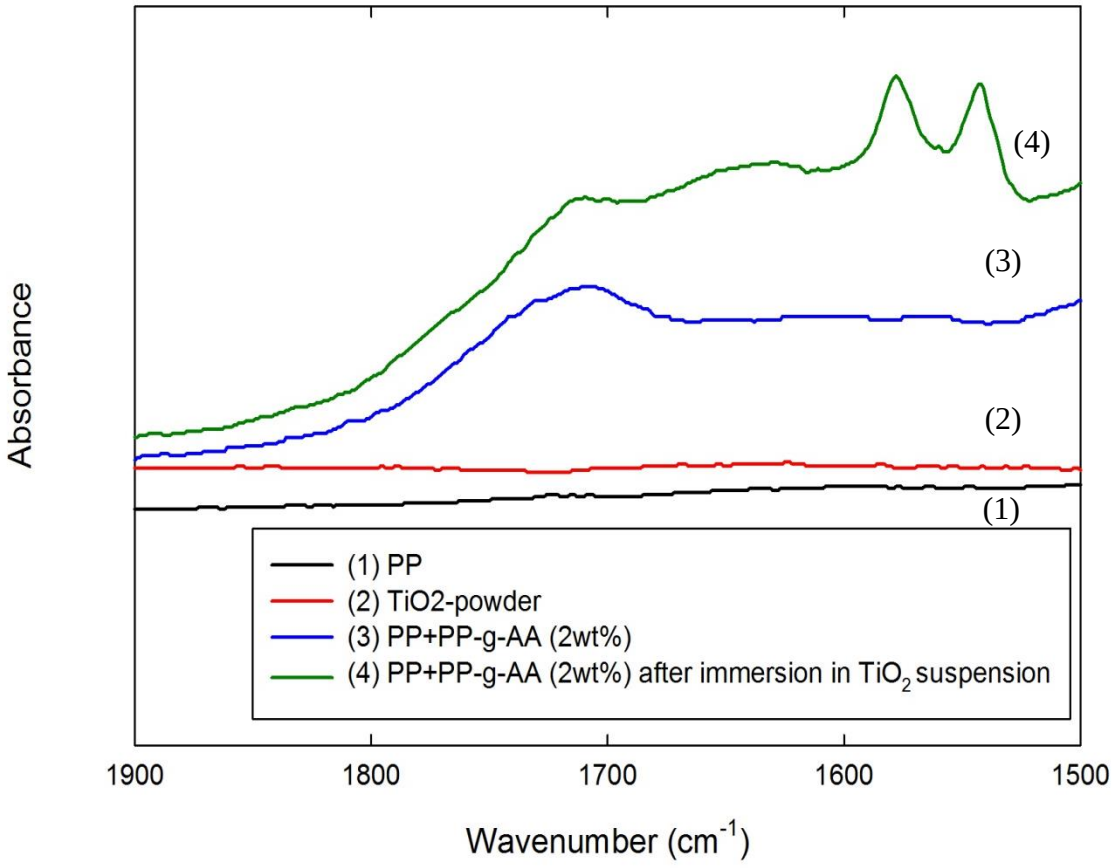

Figure 6-1: ATR-FTIR spectra of the neat materials and the precursor films of the blend sample before and after immersion in theTiO_2 nanoparticle suspension.

XPS is a powerful technique to characterize and identify the chemical species of a surface based on the specific binding energy measured for a particular type of photoelectrons [37]. The fully scanned spectra results, i.e. survey spectra, (results not shown here) show the presence of the O1s and C1s elements on the surface of the ungrafted blend sample, while the surface of the TiO_2 grafted blend sample contains Ti2p, in addition to those peaks. This result confirms the presence of titanium dioxide (TiO_2) nanoparticle on the surface of the TiO_2 grafted blend sample.

The high resolution XPS spectra of Ti2p and O1s of the pure TiO_2 powder are displayed in Figure 6-2a and 6-2b. The $Ti2p_{1/2}$ and $Ti2p_{3/2}$ spin-orbital splitting photoelectrons for the pure TiO_2 powder are located at binding energies of 465.1 and 459.3 eV, respectively, as seen in Figure 6-2a. The difference between the binding energies of the $Ti2p_{1/2}$ and $Ti2p_{3/2}$ is 5.8 eV, suggesting the existence of a Ti^{4+} oxidation state [8, 38, 39]. Also, the wide and asymmetric O1s spectrum for the neat TiO_2 powder indicates that it contains more than one component (see Figure 6-2b). The spectrum can be fitted into two peaks including crystal lattice oxygen (Ti-O) at a binding energy of 530.6 eV and surface hydroxyl groups (Ti-OH) at a binding energy of 531.6 eV [38, 39].

The high resolution XPS spectra of C1s and O1s for the blend sample are also presented in Figures 6-2c and 6-2d. Figure 6-2c shows that the C1s core level spectrum of the blend sample contains two peak components, with binding energy at 285.1 eV and 288.8 eV. The peak at 285.1 eV can be attributed to C-H or C-C bonds in the main chain, while the peak at 288.8 eV corresponds to the O-C=O species (carboxylic carbon) [40, 41]. Also, the peaks in the spectra correspond to the oxygen atoms having different binding energies in the chemical structure. The oxygen of the carbonyl bonds (C=O) has a lower binding energy than the single-bonded oxygen

(C-O) [42]. So, this spectrum could be decomposed into two peaks: C=O centered at 532 eV and C–OH centered at 533.5 eV [42, 43].

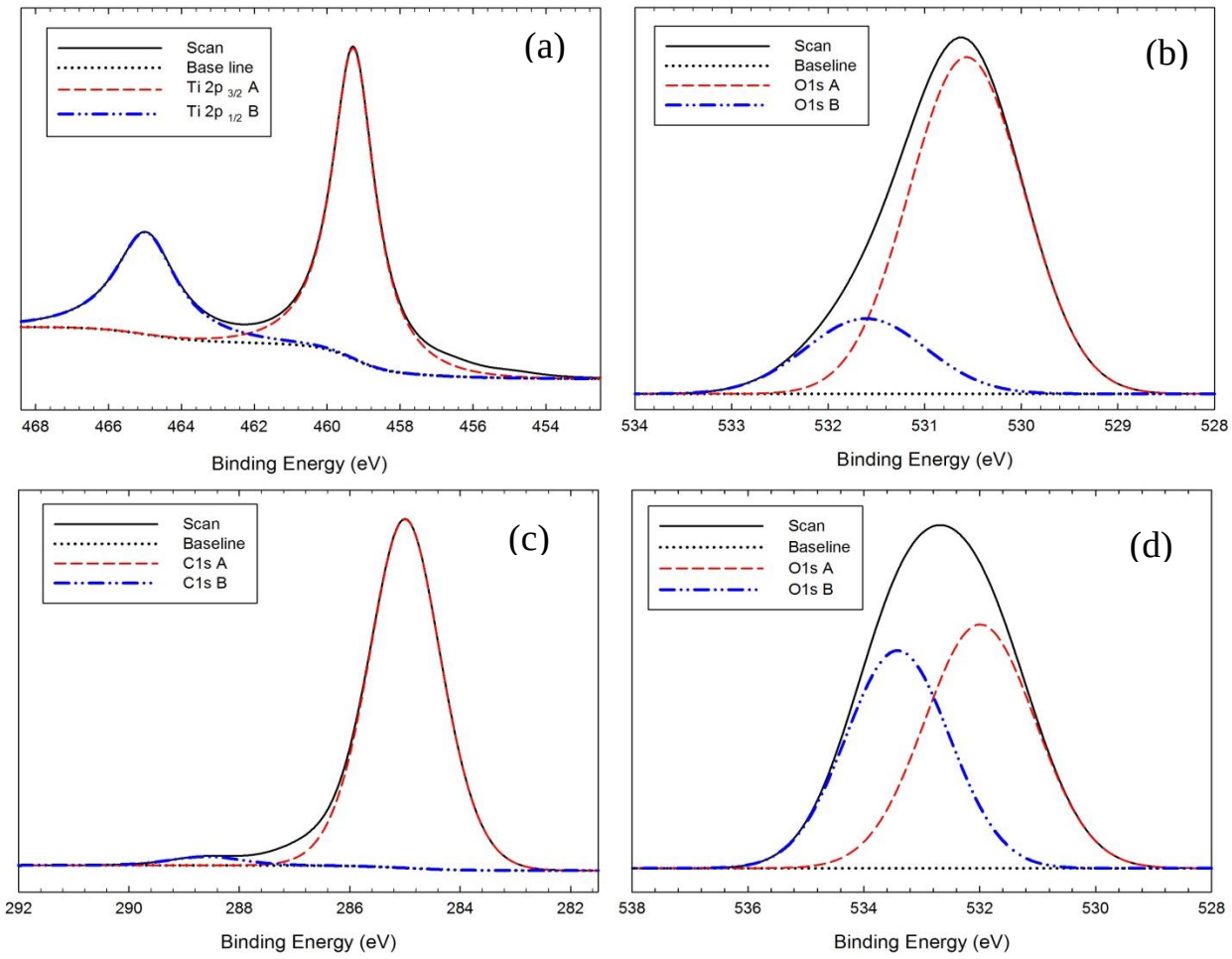

Figure 6-2: High-resolution XPS spectra of (a) the Ti2p peaks of the TiO2 powder, (b) the O1s peaks of the TiO2 powder, (c) the C1s peaks of the blend sample and (c) the O1s peaks of the blend sample.

Surface hydrophilicity is one of most important properties of microporous membranes [6]. The most convenient way to assess hydrophilic/hydrophobic properties of a surface is water contact angle measurements [3], which has a reverse dependence on hydrophilicity [20]. This

parameter was obtained by estimating the tangent to a water drop surface at its intersection with the film surface [44]. However, the water contact angle of the precursor films were characterized instead of the microporous membranes to avoid the capillary effects due to the three-dimensional tiny voids [6]. Also, these measurements were done during one minute to avoid evaporation effect of the water droplets.

Figure 6-3 reports the water contact angles of the precursor film of the blend sample before and after immersion in the TiO_2 suspension. It can be observed that the blend sample before grafting possesses a relatively high contact angle of 90°. However, grafting TiO_2 nanoparticles on the surface lowers significantly the water contact angle (decrease by a factor of 2.5). These results imply that the grafting of TiO_2 nanoparticles on the surface imparts an excellent hydrophilicity to the precursor films [21, 22, 45]. The decrease of the water contact angle can be explained by the presence of many Ti-OH groups on the TiO_2 nanoparticles at the surface. The hydroxylic Ti-OH structure interacts well with water through van der Waals forces and hydrogen bonding [23, 45, 46]. It can also be seen that the water contact angles of the samples remain almost constant during the contact time.

Based on the results reported in this section, it can be concluded that the grafting of TiO_2 nanoparticles is a simple and powerful method for surface modification of polymeric membranes.

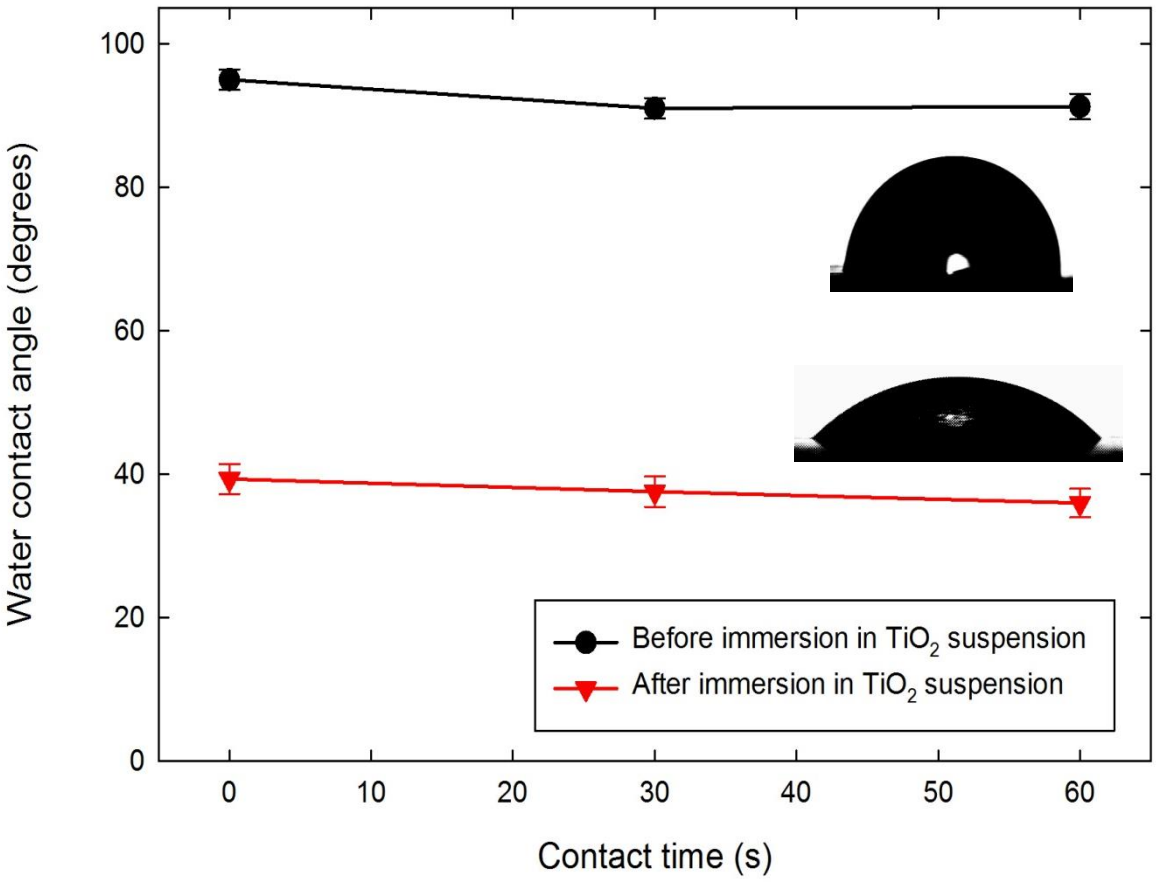

Figure 6-3: Water contact angles of the blend sample (precursor films of PP+PP-g-AA (2wt%)) before and after immersion in TiO2 suspension; The insets exhibit images of the water droplets.

6.3.2 Characterization of the microporous membranes

Polar groups on the precursor film surface enhance the surface energy and the hydrophilicity of polymers [34, 47]. This is supported by the presence of acrylic acid groups and TiO_2 nanoparticles confirmed by ATR-FTIR, XPS and water contact angle results (Figures 6-1 to 6-3).

To examine the content of TiO_2 grafted on the membrane surface, thermogravimetric analysis (TGA) test was done on the membrane of the blend sample before and after immersion in the TiO_2 suspension. The TGA results of Figure 6-4 shows that the residue of the modified

TiO_2 blend membrane is around 3 wt%; while the ungrafted membrane does not leave any char residue at 800 °C.

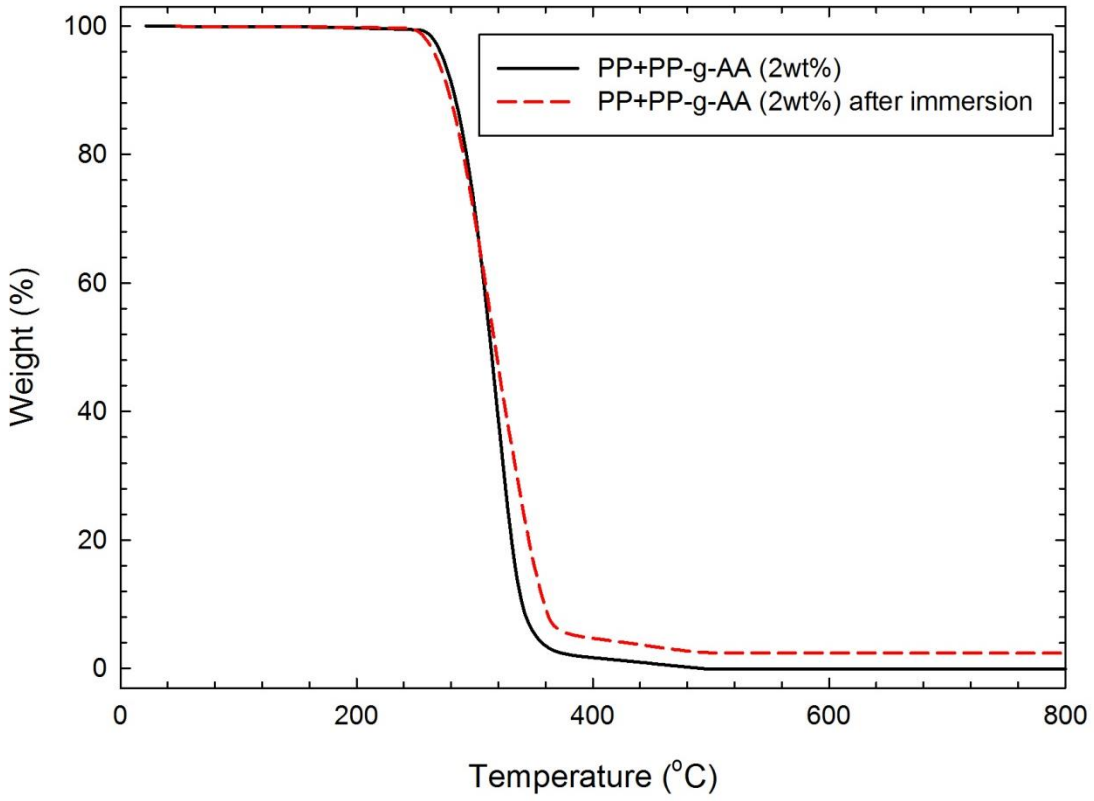

Figure 6-4: TGA curves of the blend sample (microporous membrane of PP+PP-g-AA (2wt%)) before and after immersion in the TiO2 suspension under an air atmosphere.

Figure 6-5 presents results regarding the key property of the membranes, i.e., water vapor permeability. It is well known that several factors including bulk properties and hydrophilicity of the surfaces affect the water vapor permeation property of membranes [22]. For dry-stretch prepared microporous membranes, the bulk parameters, i.e., tortuosity and pore size. etc, are affected by the crystallinity and crystalline orientation [2]. However, improving hydrophilicity of the surface will cause an increase of the solubility of water in the polymers and, consequently, increases of the permeability due to the formation of hydrogen bonds with water molecules. This

hydrogen bonding thereby causes a de-structuring of the original water complexes and facilitates their transport through the membrane [11, 48].

As mentioned earlier, in the porous PP/PP-g-AA membranes, the functional (polar) groups of the modifier will be located preferentially at the surfaces, including pore surfaces, because the hydrophobic chains of amphiphilic additives tail will anchor onto the host polymer. By keeping the crystalline structure (membrane structure) the same as for the neat PP [14], the hydrophilic part of the surface and pores plays an important role on the water vapor permeability [3]. Consequently, for blends of PP with 2 wt% PP-g-AA, the permeability increased markedly compared to the neat PP [14]. Since TiO_2 has higher affinity to water than that acrylic groups and PP (see Figure 6-3), the modified TiO_2 blend membrane exhibits the highest water vapor permeability (1.5 times larger than ungrafted blend membrane), as can be observed in Figure 6-7 [22, 23, 28]. Then, it can be seen that grafting TiO_2 nanoparticles on the precursor film surface of the membrane could influence its performance without affecting the bulk properties.

Incidentally, Figure 6-5 reveals that immersing neat PP precursor films in the TiO_2 suspension does not yield any noticeable permeability changes compared to the original unmodified PP films. This indicates that TiO_2 does not graft and attach to this precursor film surface during the preparation process in the absence of PP-g-AA. This also confirms that the presence of anchor groups on the surface (COOH groups) plays an important role in the treatment method.

As mentioned earlier, the precursor films of the blend samples were first immersed in TiO_2 suspension and then were used for preparing microporous membranes. To investigate the stability of this TiO_2 grafting during preparation of microporous membranes, ungrafted blend microporous membranes were immersed in theTiO_2 suspension. Slight changes and decreases were observed

in the WVTR data, compared to the membranes prepared from TiO_2 grafted blend films (data not shown here). This suggests that nanoparticles are relatively stable on the surface of the microporous membrane, since they are not dislodged by high temperature and stretching during the preparation of microporous membranes.

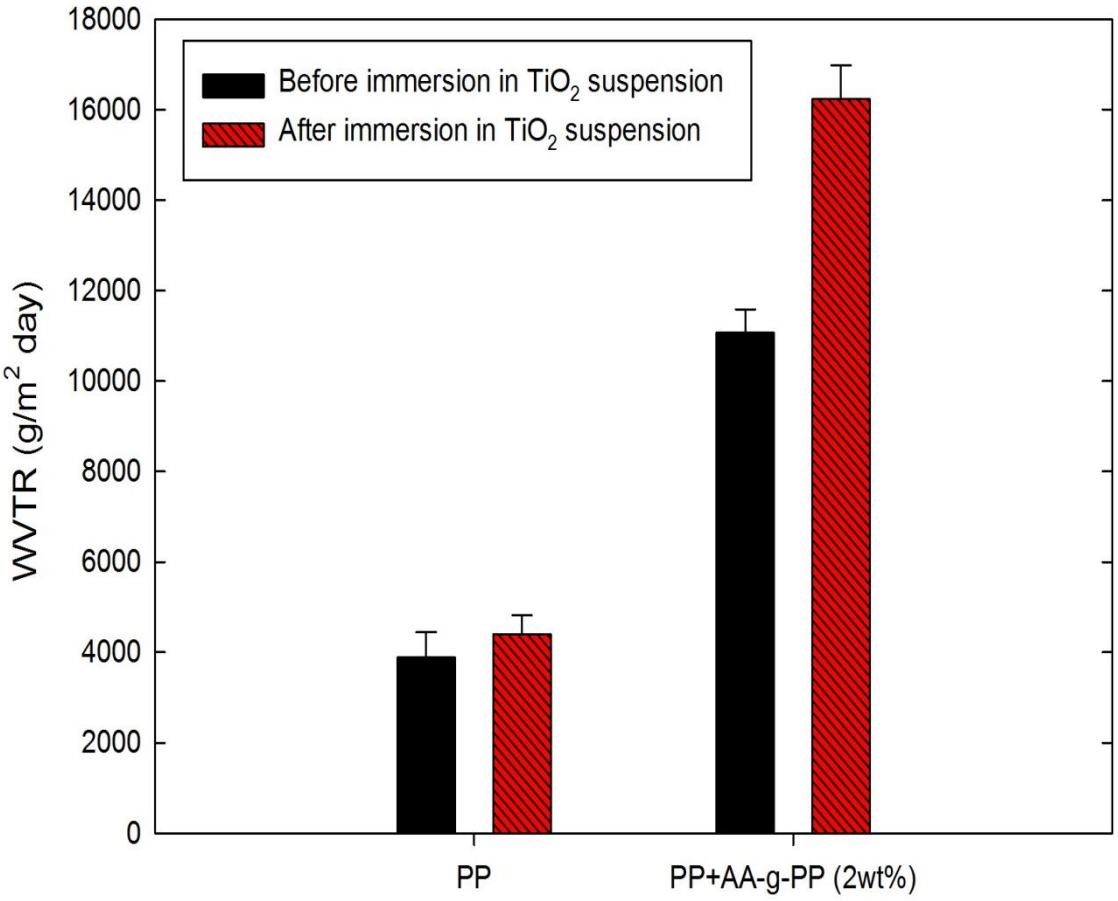

Figure 6-5: Water vapor transmission rate (WVTR) of the neat PP and blend microporous membranes, before and after immersion in TiO2 suspension.

The EDS results support the permeability results regarding the stability of the TiO_2 on the surface during the preparation of microporous membranes (see Figure 6-6a). The chemical compositions show the characteristic X-ray energy of titanium, oxygen and carbon level as follow: titanium Kα = 4.51 keV and Kβ = 4.93 keV, oxygen Kα = 0.52 keV, and carbon Kα =

0.27 keV [7]. They demonstrate the presence of the Ti and O groups with approximately the same ratio for the grafted blend precursor film and microporous membrane, respectively. Furthermore, Figure 6-6b shows the EDS spectrum of the TiO_2 powder. A comparison of the titanium to oxygen ratio of the TiO_2 powder and the grafted blend samples (Ti/O = 4.5 to 0.65, respectively) suggests that some of the Ti atoms are bonded to hydroxyl (OH) groups from water during immersion (Ti-OH) [39, 49]. This indicates the formation of the hydrogen bonding between TiO_2 nanoparticles and COOH groups, in addition to the binding form of a bidentate mode (see Figure 6-1). Consequently, it is concluded that the TiO_2 nanoparticles are linked and grafted to the acrylic acid yielding a stable hydrophilic microporous membrane.

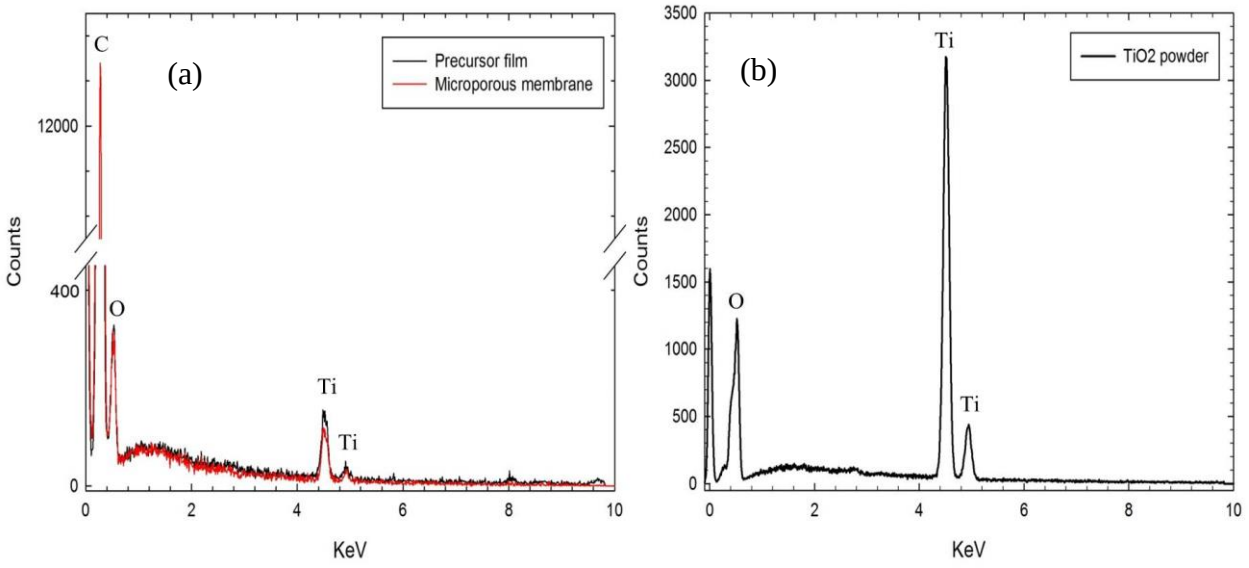

Figure 6-6: EDS spectra of (a) the blend precursor film and microporous membrane, after immersion in the TiO2 suspension and (b) TiO2 powder.

The surface morphology of the developed membranes from the blend sample before and after immersion in TiO_2 suspension was investigated using SEM. As shown in Figure 6-7, the surface of ungrafted and TiO_2 grafted blend membranes have a similar pore structure. Compared with the

ungrafted blend membrane, both sides of TiO_2 grafted membrane surface are covered with TiO_2 nanoparticles. The SEM image also shows that TiO_2 nanoparticles on the membrane surface have the form of snowflakes of different sizes, probably as a result of their agglomeration.

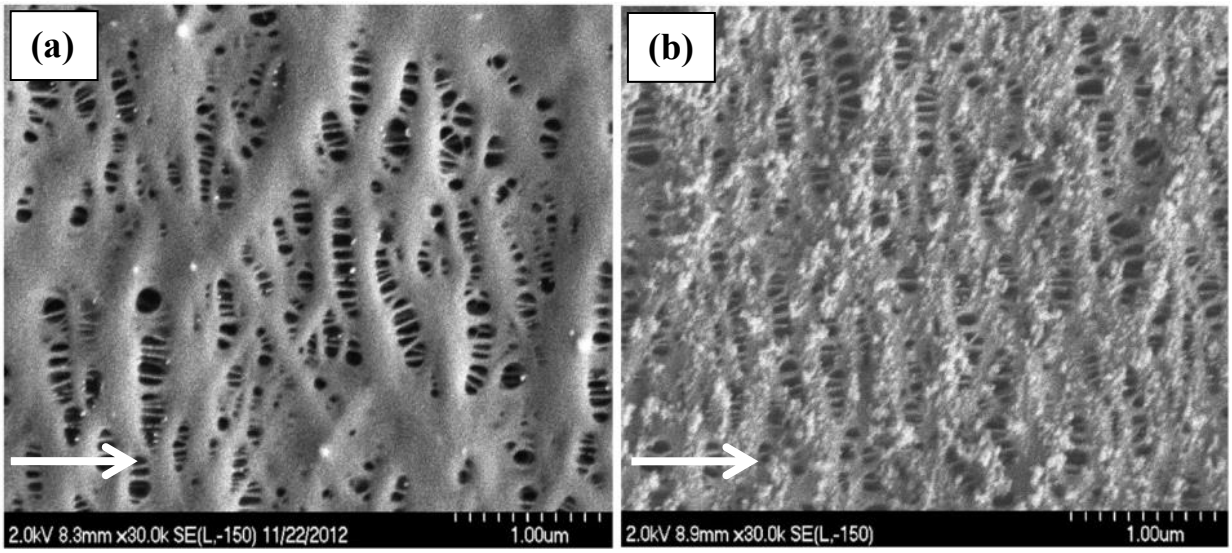

Figure 6-7: SEM micrographs of the surface of the blend microporous membranes, (a) before and (b) after immersion in the TiO2 suspension; (the arrows indicate the stretching machine direction).

6.4 Conclusions

TiO_2 grafted precursor films and their membranes from blends of polypropylene (PP) with acrylic acid grafted PP (PP-g-AA) were prepared and their structural characteristics and performances were investigated. Our findings can be summarized as follows:

The hydrophilic segments of the amphiphilic modifier (PP-g-AA) blended with PP acted as surface functional groups on the precursor film surface.

ATR-FTIR and EDS results confirmed that TiO_2 nanoparticles were successfully grafted on the surfaces of the precursor films through bidentate coordination between Ti^{4+} cations

and COOH groups as well as the formation of hydrogen bonding between the carboxylic acid and TiO_2 nanoparticles.

After TiO_2 modification, the water contact angle of the precursor films was significantly lowered and the water vapor permeability of the membranes was increased by a factor of 1.5. This resulted from extraordinary hydrophilicity in contrast with the neat PP and PP/PP-g-AA blend precursor films and membranes.

Good agreement with the water vapor permeability data, SEM and EDS results was observed.

SEM micrographs of the surface of ungrafted and TiO_2 grafted blend membranes showed similar pores structure. This result indicated that grafting TiO_2 nanoparticles did not have a dramatic effect on the pore structure of the membranes surface.

6.5 Acknowledgments

Financial support from NSERC Network for Innovative Plastic Materials and Manufacturing Processes (NIPMMP) is gratefully acknowledged.

6.6 References

1. Xu M, Shi X, Chen H, and Xiao T. Applied Surface Science 2010;256(10):3240-3244.
2. Tabatabaei SH, Carreau PJ, and Ajji A. Journal of Membrane Science 2008;325(2):772-782.
3. Fang B, Ling Q, Zhao W, Ma Y, Bai P, Wei Q, Li H, and Zhao C. Journal of Membrane Science 2009;329(1–2):46-55.
4. Hester JF, Banerjee P, and Mayes AM. Macromolecules 1999;32(5):1643-1650.
5. Bongiovanni R, Gagnor B, Malucelli G, Priola A, and Pollicino A. Journal of Materials Science 1998;33(6):1461-1464.
6. Li JH, Xu YY, Zhu L-P, Wang JH, and Du CH. Journal of Membrane Science 2009;326(2):659-666.
7. Bae TH and Tak TM. Journal of Membrane Science 2005;266(1–2):1-5.
8. Kim SH, Kwak SY, Sohn BH, and Park TH. Journal of Membrane Science 2003;211(1):157-165.
9. Meier-Haack J, Valko M, Lunkwitz K, and Bleha M. Desalination 2004;163(1–3):215-221.
10. Zhang C, Bai Y, Sun Y, Gu J, and Xu Y. Journal of Membrane Science 2010;365(1–2):216-224.
11. Li E, Du Z, and Yuan S. Science China Chemistry 2013;56(6):773-781.
12. Datla VM. Surface modification of fibers and nonwovens with melt additives. vol. Ph.D. Ann Arbor: North Carolina State University, 2008. pp. 259.
13. Paul S. Surface modification of polypropylene nonwovens to improve adhesion to elastomers. vol. Ph.D. Ann Arbor: North Carolina State University, 2009. pp. 189.
14. Saffar A, Carreau PJ, Ajji A, and Kamal MR. Journal of Membrane Science 2014;462(0):50-61.
15. Chen H, Shi X, Zhu Y, Zhang Y, and Xu J. Journal of Applied Polymer Science 2009;114(4):2461-2468.
16. Zhu L-P, Xu Y-Y, Dong H-B, Yi Z, and Zhu B-K. Materials Chemistry and Physics 2009;115(1):223-228.
17. Sadeghi F, Ajji A, and Carreau PJ. Journal of Membrane Science 2007;292(1–2):62-71.
18. Sadeghi F, Ajji A, and Carreau PJ. Polymer Engineering & Science 2007;47(7):1170-1178.
19. Sadeghi F, Ajji A, and Carreau PJ. Journal of Plastic Film and Sheeting 2005;21(3):199-216.
20. Rahimpour A, Madaeni SS, Taheri AH, and Mansourpanah Y. Journal of Membrane Science 2008;313(1–2):158-169.

21. Wang Q, Wang X, Wang Z, Huang J, and Wang Y. Journal of Membrane Science 2013;442(0):57-64.

22. Li JF, Xu ZL, Yang H, Yu LY, and Liu M. Applied Surface Science 2009;255(9):4725-4732.

23. Razmjou A, Mansouri J, and Chen V. Journal of Membrane Science 2011;378(1–2):73-84.

24. Wu G, Gan S, Cui L, and Xu Y. Applied Surface Science 2008;254(21):7080-7086.

25. Qu Q, Geng H, Peng R, Cui Q, Gu X, Li F, and Wang M. Langmuir 2010;26(12):9539-9546.

26. Persson P, Lundqvist MJ, Ernstorfer R, Goddard WA, and Willig F. J Chem Theory Comput 2006;2(2):441-451.

27. Capecchi G, Faga M, Martra G, Coluccia S, Iozzi M, and Cossi M. Research on Chemical Intermediates 2007;33(3-5):269-284.

28. Xu Q, Yang J, Dai J, Yang Y, Chen X, and Wang Y. Journal of Membrane Science 2013;448(0):215-222.

29. Zohrevand A, Ajji A, and Mighri F. Polymer Engineering & Science 2013:n/a-n/a.

30. Xu Z, Wang J, Shen L, Men D, and Xu Y. Journal of Membrane Science 2002;196(2):221-229.

31. Jung CH, Choi JH, Lim YM, Jeun JP, An SJ, Kang PH, and Nho YC. Macromolecular Symposia 2007;249-250(1):573-579.

32. Diebold U. Surface Science Reports 2003;48(5–8):53-229.

33. Zhang LM and Dai GC. eXPRESS Polymer Letters 2007;1(9):608-615.

34. Garg DH, Lenk W, Berwald S, Lunkwitz K, Simon F, and Eichhorn KJ. Journal of Applied Polymer Science 1996;60(12):2087-2104.

35. Gumusderelioglu M and Topal IU. Radiation Physics and Chemistry 2005;73(5):272-279.

36. Thyagarajan S, Liu A, Famoyin OA, Lamberto M, and Galoppini E. Tetrahedron 2007;63(32):7550-7559.

37. He Q, Yuan T, Zhang X, Luo Z, Haldolaarachchige N, Sun L, Young DP, Wei S, and Guo Z. Macromolecules 2013;46(6):2357-2368.

38. Su C, Liu L, Zhang M, Zhang Y, and Shao C. CrystEngComm 2012;14(11):3989-3999.

39. Erdem B, Hunsicker RA, Simmons GW, Sudol ED, Dimonie VL, and El-Aasser MS. Langmuir 2001;17(9):2664-2669.

40. Zhu LP, Yi Z, Liu F, Wei XZ, Zhu BK, and Xu YY. European Polymer Journal 2008;44(6):1907-1914.

41. Cheng Z and Teoh SH. Biomaterials 2004;25(11):1991-2001.

42. Li D and Niu L. Science in China Series E: Technological Science 2002;45(6):666-670.

43. Xu Q, Yang Y, Yang J, Wang X, Wang Z, and Wang Y. Journal of Membrane Science 2013;443(0):62-68.

44. Chang WY, Fang TH, Chiu ZW, Hsiao YJ, and Ji LW. Microporous and Mesoporous Materials 2011;145(1–3):87-92.

45. Luo ML, Tang W, Zhao JQ, and Pu CS. Journal of Materials Processing Technology 2006;172(3):431-436.

46. Bae TH and Tak TM. Journal of Membrane Science 2005;249(1–2):1-8.

47. Kim JY and Lim DY. Energies 2010;3(4):866-885.

48. Deshmukh MM, Sastry NV, and Gadre SR. Journal of Chemical Physics 2004;121(24):12402-12410.

49. Murcia JJ, Hidalgo MC, Navío JA, Araña J, and Doña-Rodríguez JM. Applied Catalysis B: Environmental 2014;150–151(0):107-115.

CHAPTER 7 - ARTICLE 3:

THE IMPACT OF NEW CRYSTALLINE LAMELLAE FORMATION DURING ANNEALING ON THE PROPERTIES OF POLYPROPYLENE BASED FILMS AND MEMBRANES

Amir Saffar[1], Abdellah Ajji[1], Pierre J. Carreau[1] and Musa R. Kamal[2]

1) Research Center for High Performance Polymer and Composite Systems (CREPEC), Chemical Engineering Department, Polytechnique Montreal, PO Box 6079, Stn Centre-Ville, Montreal, Quebec, Canada, H3C 3A7.

2) CREPEC, Department of Chemical Engineering, McGill University, 3610 University Street, Montreal, Quebec, Canada, H3A 2B2.

Published in *Polymer*, 55 (2014) 3156–3167.

Abstract

Cast films, based on polypropylene (PP), were prepared via melt extrusion and, then, annealed below the melting temperature. The effect of annealing conditions on the properties of the films and the microporous membranes formed by stretching was investigated. It is shown that annealing is an effective method to improve the physical properties of semi-crystalline polymers by promoting chain rearrangement and creating secondary lamellae in the amorphous region. DSC results for annealed samples revealed the appearance of a shoulder endothermic peak and a new peak in the correlation function from the SAXS patterns was observed. The annealed films exhibited double yield points in the tensile deformation curves. A direct linear relationship was found between the strength of the second yield point and the fraction of the lamellae. From mercury porosimetry and SEM images of the membranes larger pore sizes and porosity were observed as the annealing time and temperature increased.

Keywords

Polypropylene based films, Crystalline lamellar morphology, Annealing, Mechanical properties, Membranes by stretching.

7.1 Introduction

Polypropylene (PP) is a semi-crystalline polymer, which is one of the most commonly used polymers to produce porous membranes for various applications, due to its outstanding properties, such as low cost, easy processing, good mechanical properties, chemical stability and non-toxicity [1-3].

Polymeric membranes are usually made using three different commercially available techniques: solution casting followed by phase separation, particle stretching and dry-stretching (extrusion followed by stretching) [2, 4-8]. Processing cost and solvent or particle contaminations are the main drawbacks of the solution and particle stretching techniques. The dry-stretch process is based on the stretching of a polymer film or sheet containing beta unit cell crystals [6-8] or a row-nucleated lamellar structure (lamellae separation) [2, 9-11]. Membrane development based on the crystal transformation method is utilized for polymers that exhibit different types of crystalline phases and can be transformed under specific processing conditions. Polypropylene is the most common of such polymers. It is known that the β crystalline form of PP is not stable and, under certain levels of stress, it transforms into the more stable α crystalline form. Since the β crystals are less dense than the α form [12], this transformation causes a volume contraction in the bulk of polymer, resulting in the creation of voids [6]. One of the main drawbacks of this method relates to the presence of the nucleating agents that are used to obtain β crystals. The main disadvantages of the β nucleating agents are physical or chemical instability, intense color (brown, pink, yellow, gray) and poor reproducibility [13]. Another shortcoming of this method is the relative difficulty in obtaining uniform pore size, compared to the lamellae separation method [7, 8, 14].

The uniaxial stretching a polymer film containing a row-nucleated lamellar structure (lamellae separation) was developed 30 years ago for some semi-crystalline polymers. It involves extrusion, annealing and stretching. However, most of the detailed information-processing remains proprietary to the companies and is not available to the scientific community. To obtain a good porous membrane, three consecutive stages are carried out: (1) creating a precursor film containing the desired lamellar morphology, i.e., an oriented shish-kebab structure, (2) annealing

the precursor film at elevated temperatures to improve the crystalline structure, and (3) stretching at room temperature to create the pores by lamellar separation and then, stretching at a high temperature to enlarge them [2, 9-11, 15].

The orientation and arrangement of the crystal lamellae are the key factors in controlling the properties of the precursor film and, consequently, the properties of the porous membrane [2, 15, 16]. The first step for controlling the crystalline orientation and generating the desired lamellar morphology, is the selection of the right materials and the use of suitable processing conditions. This has drawn considerable interest over the past decades [2, 11, 16, 17]. The second step is annealing to change the structure and properties of semi-crystalline polymers via healing of the defects and diminishing residual stress and strain [18]. To our knowledge, little attention has been paid to the annealing of flow-oriented polymers, especially to the mechanisms of the microstructural changes during annealing. Annealing is thought to be an effective method to improve the crystalline structure by thickening the lamellae and re-arranging the molecular chains in the amorphous phase. These modifications cause significant changes in the physical properties of the precursor film and of the microporous membrane [2, 15, 19, 20]. It should be noted that the annealing effect is expected to be different for PP with an isotropic structure from that for PP with an oriented structure (e.g. shish-kebabs). In the former structure, annealing only permits a fine adjustment of the crystalline structure such as chain rearrangement in the interphase of the crystalline and amorphous phases. However, in the latter, the oriented shishes may provide nucleating sites for the lateral growth of new (secondary) kebabs [19]. Moreover, the mechanisms of microstructural changes of crystalline structure during annealing process are still under debate in the literature [15, 19, 21].

In our previous work [14] acrylic acid grafted polypropylene (PP-g-AA) at different concentrations was blended with PP to develop microporous hydrophilic membranes. The optimum concentration was found to be 2wt % PP-g-AA to achieve membranes having good hydrophilic characteristics, with enough polar groups on the surface and a minimal change in the crystalline structure compared to the neat PP. Following our previous investigations [2, 9, 11, 14, 17] a detailed investigation was performed to evaluate the influence of annealing conditions on the crystalline structure and the subsequent membrane properties for this blend (PP containing 2wt% PP-g-AA). In addition, various tests have been carried out to elucidate and confirm the formation of secondary lamellae after annealing. These results allow us to illustrate key crystalline structure changes during annealing and the impact on the mechanical properties of the precursor film and membrane with the objective of establishing the structure-properties relationships after annealing.

7.2 Experimental

7.2.1 Materials

A commercial linear polypropylene (PP) and a commercial amphiphilic polymer consisting of a hydrophobic backbone (polypropylene) and acrylic acid as hydrophilic side chains (PP-g-AA) (MFR values of 2.8 g/10 min under ASTM conditions of 230 ºC and 2.16 kg and 20 g/10 min, respectively) were selected. The PP was supplied by ExxonMobil Company and the PP-g-AA was purchased from Chemtura Corporation. The main characteristics of the resins are reported in Table 7.1. The melting point, T_m, and the crystallization temperature, T_c, of the resins were obtained using differential scanning calorimetry (DSC).

Table 7-1: Main characteristics of the neat materials.

Resin Code	Supplier	MFR (g/10 min) (230 ºC-2.16 kg)	T_m (°C)	T_c (°C)
PP (4712E1)	Exxon Mobil	2.8	160	114
PP-g-AA (Polybond®1002)	Chemtura	20	161	123

7.2.2 Film preparation

Precursor films from a blend of PP containing 2wt% PP-g-AA were prepared using a 45 mm diameter Killion single screw extruder equipped with a slit die of 0.7 mm opening. The temperature profile along the barrel was: 165/195/210/215 °C and the die temperature was 220 °C. For film cooling, an air knife was used right at the exit of the die to supply air to the film surface. The extrusion was carried out using a screw speed of 12.5 rpm and a draw-down ratio (ratio of the roll speed to the die exit velocity) was set at 25 to produce precursor films having a thickness of around 30 μm. The distance between the die exit and the nip cast rolls was around 15 cm and the cast rolls temperature was constant at 50 °C.

7.2.3 Membrane preparation

The dry-stretching method was used to prepare the microporous membranes as follows [14]:

The precursor film with a thickness, width and length of 30 μm, 8 cm, and 4 cm, respectively, was first annealed at different temperatures between 80 to 140 ºC, for various times, i.e. 2, 5, 10, 20, 30 and 60 min. For comparison, a non-annealed specimen was used as a reference. Then, the

annealed and non-annealed samples were cold and hot stretched up to 35% of the initial length at room temperature and 60% at 120 °C, respectively. Both annealing and stretching were performed using an Instron machine (ElectroPlus ^{TM} E3000) equipped with an environmental chamber. A drawing speed of 50 mm/min was applied during the cold and hot stretching steps.

7.2.4 Characterization

A brief explanation of the methods and techniques used to characterize the precursor films and its microporous membranes are described below.

7.2.4.1 Fourier transform infrared spectroscopy (FTIR)

For FTIR measurements, a Perkin Elmer infrared spectrometer with a spectral resolution of 4 cm^{-1} and a scanning rate of 32 kHz, was used. The data were collected in the range from 4000 to 600 cm^{-1}. The crystalline orientation, based on the difference in absorption of the plane-polarized radiation, was measured using a polarized radiation in parallel and perpendicular to the stretching machine direction (MD) in the transmission-FTIR mode. The Herman's orientation function was calculated according to [2]:

$$f = \frac{D-1}{D+2} \tag{7-1}$$

where D is the dichroic ratio and defined as the ratio of absorbencies parallel and perpendicular to MD at the specific vibration used. For PP, absorption at the wavelength of 998 cm^{-1} is attributed to the crystalline phase only and can be used for obtaining the crystalline orientation function, f_c.

7.2.4.2 Small angle X-ray scattering (SAXS)

SAXS is a well-developed method to study the crystalline structure in semi-crystalline polymers [10]. The SAXS patterns were collected via a Bruker AXS Nanostar system. The instrument is equipped with a microfocus copper anode at 45 kV / 0.65 mA. The MONTAL OPTICS and a VANTEC 2000 2D detector were located at 107.2 mm distance from the samples. The distance was calibrated with a silver behenate standard prior to the measurements, while four layers of the film were stacked together.

7.2.4.3 Differential scanning calorimetry (DSC)

Thermal properties of the specimens were analyzed using a TA Instruments differential scanning calorimeter (DSC) Q 1000. Samples were heated from 50 to 220 ºC at a heating rate of 10 °C/min.

7.2.4.4 Mercury intrusion porosimetry (MIP)

The porosity and pore distributions of the membranes were evaluated using an AutoPore IV 9500 mercury intrusion porosimeter developed by Micromeritics Instrument Corporation.

7.2.4.5 Morphology

In order to observe the microporous membranes surfaces, a field emission scanning electron microscope (FE-SEM-Hitachi S4700) was employed.

7.2.4.6 Water vapor transmission rate (WVTR)

The permeability to water vapor was measured via a MOCON PERMATRAN-W Model 101K at room temperature. The equipment is composed of three chambers. An upper chamber, which is separated from the center chamber by two porous films, contains liquid water. The center chamber is separated from the lower one by the test film. The water vapor diffuses from the first

film to fill the space between the films, i.e., the standard guard film and test film, and is swept away by N_2 gas to a relative humidity (RH) sensor.

7.2.4.7 Tensile properties

Tensile tests were performed on the precursor films using an Instron universal tensile machine (Model 3365) with 500 N load-cell at room temperature. The tensile specimens having a rectangular geometry of 25 mm wide and 50 mm long were stretched at a cross-head speed of 50 mm/min.

7.2.4.8 Puncture resistance

Puncture tests were performed using a 250N load cell of the Instron machine (ElectroPlus ™ E3000) used for the tensile tests. A needle of 3.2 mm radius was used to pierce the samples at a speed of 25 mm/min. The procedure used was based on ASTM F1306. The film was held tight in the clamping device with a central hole of 34.9 mm. The displacement of the film along the normal direction (ND) was recorded against the force (N) and the maximum force was reported as the puncture strength.

7.2.4.9 Tear resistance

The tear resistances of the precursor films, having a square geometry (127×127 mm), were measured using the Pro-Tear (Thwing Albert Instrument) testing machine based on ASTM D1922. According to this standard, the work required for tearing is measured by the loss of energy of an encoder, which records the angular position of the pendulum during the tearing operation.

7.3 Results and discussion

SAXS, DSC, FTIR and mechanical properties provide information on the effect of annealing on the crystalline structure. We first present experimental data regarding the precursor films. They clearly demonstrate the effect of the quiescent annealing process in the absence of stress on the crystalline structure. Subsequently, the correlation between tensile and SAXS data are discussed. Finally, morphological micrographs, porosity and water vapor permeability illustrating the influence of the annealing process on microporous membrane performances obtained from the precursor films are discussed.

7.3.1 Effect of annealing temperature on the crystalline structure and mechanical properties of precursor films

Temperature is probably the most important factor in the annealing process [17]. The extruded films were annealed at different temperatures, from 80 to 140 °C, which are all below the melting temperature of the precursor film. It is known that the onset of mobility in the crystalline structure, or α relaxation, for polypropylene occurs below 100 °C [2, 18, 22]. The effect of temperature on annealing was evaluated via SAXS, which is a powerful technique for examining formed nanostructures, whether in the melt, solution or crystal state [23]. Figure 7-1 illustrates the 2D SAXS patterns as well as the Lorentz corrected intensity profile and SAXS correlation functions for the precursor films (shish-kebab structure) and after annealing at different temperatures for 30 min. The equatorial streak in the SAXS patterns (Figures 7-1a-d) is attributed to the formation of shishes aligned in MD, while the meridian maxima are attributed to lamellae or kebabs perpendicular to MD [2, 10]. Looking at the meridian intensity, the formation of more lamellae for the annealed films is obvious. Increasing the annealing temperature increases further

the number of lamellae [19]. This may originate from secondary kebabs formation as well as primary kebabs thickening (discussed below).

The long period distance, L_p, is the thickness of the crystalline lamellae plus amorphous interlayer in an ideal two-phase system, in addition to the diffuse interface in a non-ideal two-phase system. The long period distance, which is almost periodically repeated, was estimated from the position of the intensity maximum according to Bragg's law ($L_p = 2\pi/q_{max}$ where q is the intensity vector$=4\pi\sin\theta/\lambda$, λ is the X-ray wavelength and 2θ is the scattering angle) [2, 18, 24]. It can be seen from Figure 7-1e that annealing shifts the peaks to lower values, indicating an increase in the long spacing, thus a change in the thickness distribution of the lamellae and amorphous regions [18, 25, 26]. The value of L_p for the annealed film at 140 °C is much larger than that for the non-annealed film (L_p = 17.67 nm compared to 13.57 nm). The formation of secondary lamellae in the amorphous region probably causes shrinkage in the size of the amorphous region [18, 27].

SAXS is also extensively used to identify morphologies from the sequence of Bragg reflections observed and the positions of the peaks in the structure [23]. The location of the observed reflections in the SAXS data, i.e., nq in which n =1, 2, 3, in Figure 7-1e, indicates that our system has a lamellar structure [23, 26]. Also, the intensity of the Bragg peaks at nq decreases smoothly as n increases.

More importantly, in order to gain a better insight regarding the structural changes caused by annealing, the one-dimensional (1D) correlation function method can be used. The correlation function, $\gamma(z)$, is a powerful tool in revealing the morphological parameters of the crystalline-amorphous two-phase systems and is obtained from indirect Fourier transformation of the scattering function [28-30]:

$$\gamma(z) = \frac{\int_0^\infty q^2 I(q)\cos(qz)dq}{\int_0^\infty q^2 I(q)dq} \tag{7-2}$$

where *z* represents the distance in real space, normal to the lamellae (nm) and *I(q)* is the experimental scattering function. The approximate distance between the crystalline lamellae can be obtained from the position of the maxima in the SAXS correlation function curves that describe the distribution of the lamellae and amorphous thickness [27-29]. Figure 7-1f is a plot of the SAXS correlation functions for various annealing temperatures. It can be seen that the lamellae morphology of the precursor films has a wide distribution of lamellar thicknesses. Increasing the annealing temperature yields noticeable changes in the SAXS correlation function plots. These features can be used for capturing the differences between annealed and non-annealed crystalline morphologies as illustrated in Figure 7-2. The captured information from this figure is summarized as follows.

As mentioned above, the long period can be determined from the Bragg spacing (L_p). The long period can also be estimated from twice of the position point of the minimum (L_{min}) or from the position of the maximum in the correlation function curves (L_{max}) (see Figure 7-2) [31, 32]. L_{min} represents the distance between the center of crystals and the adjacent amorphous region, while L_{max} represents the distance between the centers of two adjacent crystals. For an ideal two phase model, $L_p=L_{max}=L_{min}$ but, for most polymers, the thickness distribution of the crystals and amorphous regions are not the same and are usually broad, which results in $L_p \neq L_{max} \neq L_{min}$ [32, 33]. Similar to L_p, the size of L_{min} and L_{max} increase with the annealing temperature. At the low annealing temperature L_{max} is larger than L_{min} and by increasing the annealing temperature, both parameters reach the same value. This is caused by the different distribution thicknesses of

lamellae and amorphous regions, which will become the same with increasing annealing temperature [32, 33].

As pointed out earlier, some researchers [18, 29, 31] proposed a three-phase model instead of the traditional two-phase model for the crystalline structure. They suggested that an interphase region might exist in the structure between the crystalline and amorphous regions of semi-crystalline polymers. In the traditional ideal two-phase model, the initial region of the correlation function curve is expected to be a straight line. In our cases, a curvature near the origin is present for both the non-annealed and annealed samples, which could be due to the presence of a diffuse interface [28, 29, 31]. However, the thickness of the interphase region was found to be around 0.2 nm (L_d in Fig. 2) [34], which is negligible in comparison with the thickness of the crystal lamellae. Therefore, our systems can be simplified to a two-phase system and it can be considered as alternating crystalline and amorphous domains having variable dimensions.

The approximate distances between the center of crystalline lamellae are shown in Figure 7-2 [23, 27]. Exact calculations to find lamellar and amorphous thicknesses are not possible in this system, because of the complicated correlation functions obtained. Furthermore, the distortions in the curves reveal the variation (non-uniformity) in the thicknesses of the lamellae and amorphous regions. Also, a new peak begins to appear upon annealing, which corresponds to the formation of secondary lamellae [26-28]. The maximum peak of the non-annealed sample is symmetric and unlike that in the annealed sample, which is asymmetric. This reveals a variation in the long period distance for the annealed samples [24, 28]. Furthermore, the variation in the slope of the initial region, $\gamma'(z=0)$, in both the non-annealed and annealed samples is caused by the presence of a thickness distribution of the crystalline lamellar and amorphous interlayers [28, 31].

An approximate size for one of the crystalline lamellae, L_c, can be evaluated from the intersection of the straight line in the origin region with the baseline at the minimum of the correlation function, as shown graphically in Figure 7-2 [25, 26]. The increasing L_c values suggest thickening of the primary crystalline lamellae after annealing.

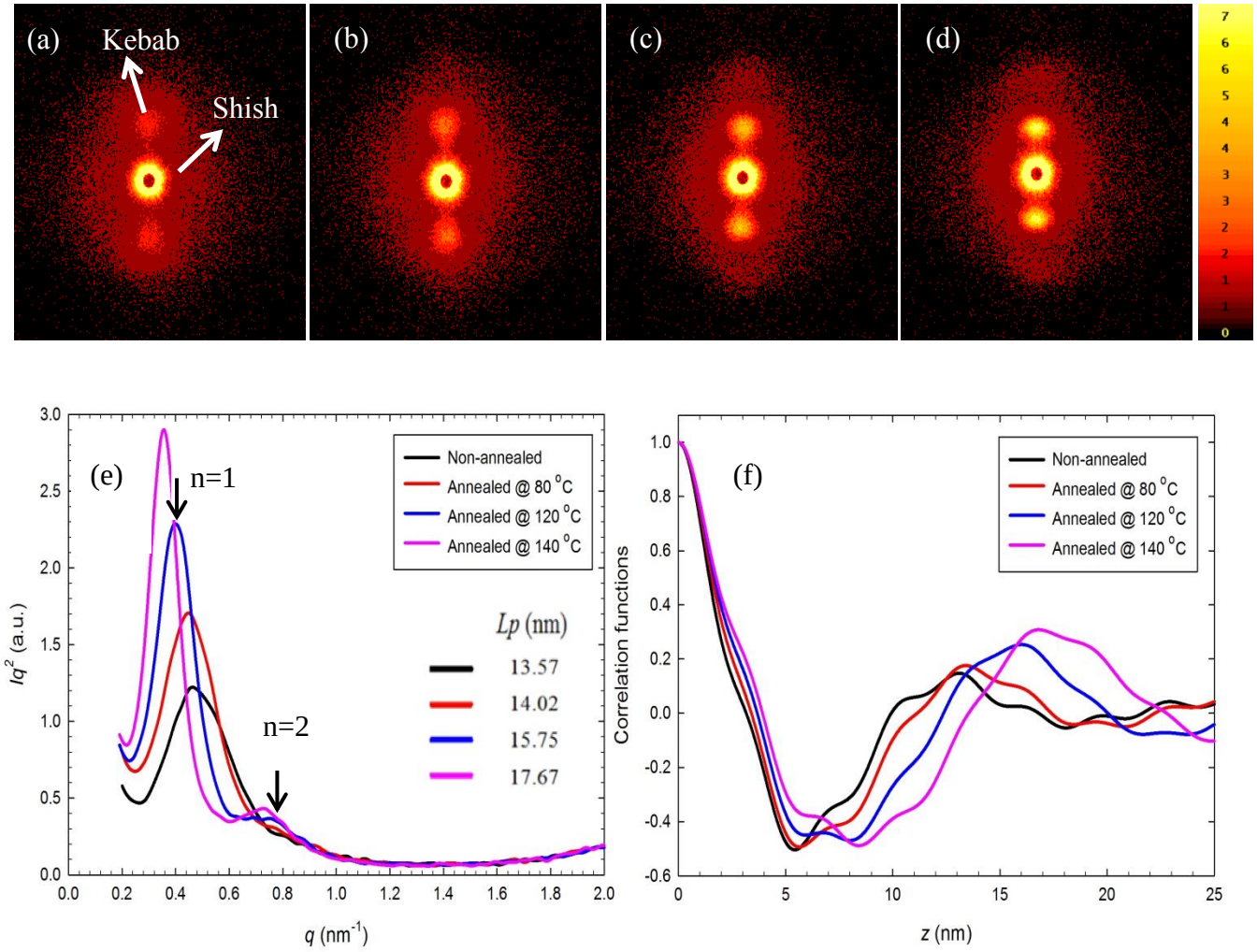

Figure 7-1: SAXS patterns of precursor films, (a) non-annealed, (b) annealed at 80 °C, (c) annealed at 120 °C, (d) annealed at 140 °C and (e) SAXS intensity profiles and (f) SAXS correlation functions for non-annealed and annealed samples at different annealing temperatures (t=30 min).

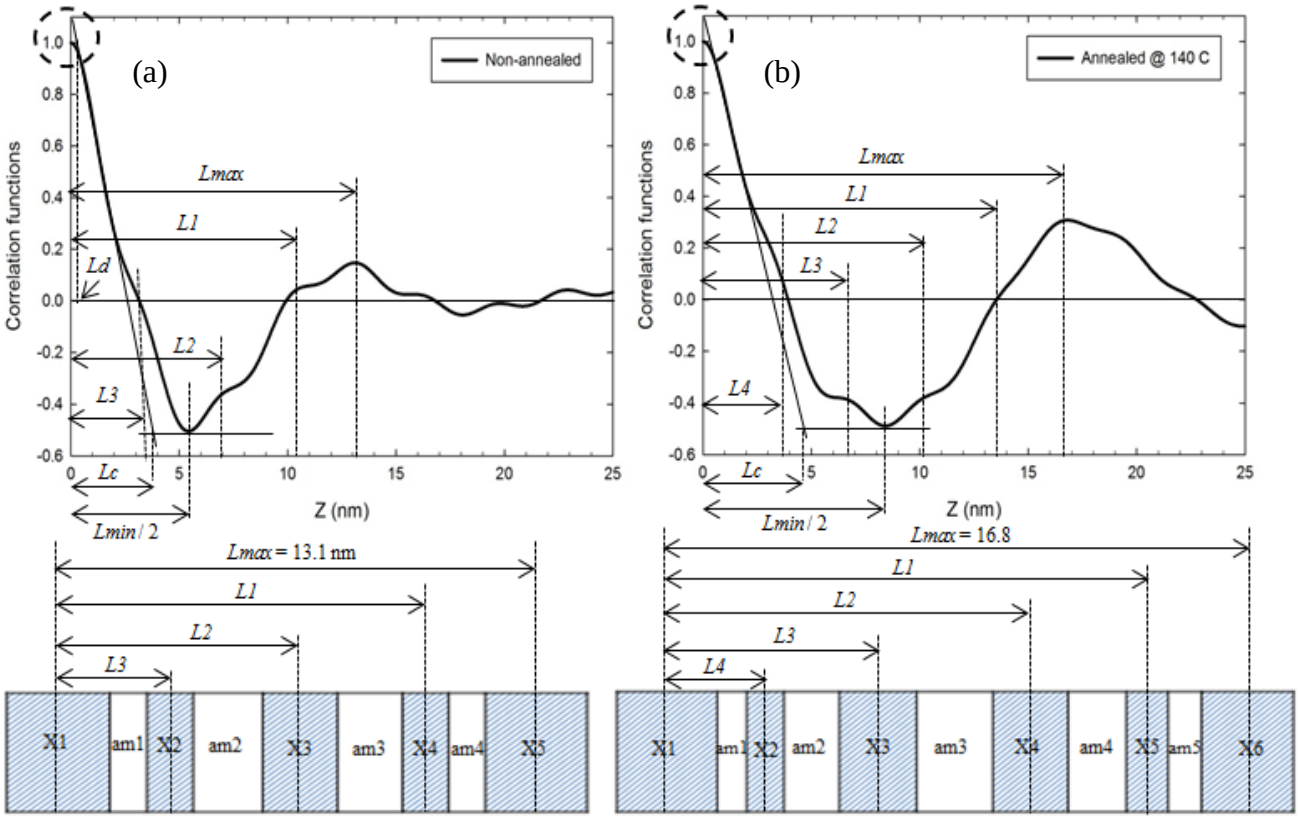

Figure 7-2: Schematic representation for the (a) non-annealed and (b) annealed crystal morphologies at 140 °C based on the SAXS correlation function results.

Figure 7-3 compares the DSC results for annealed and non-annealed precursor films. The development of a small peak is observed around the annealing temperature and below the melting peak for the annealed samples. It can be seen that the peak temperature of the shoulder became more prominent as the annealing temperature is increased. This shoulder has also been observed by other authors [15, 19, 21, 29]. This endothermic peak, referred to as annealing peak, can be ascribed to the melting of small crystallites, which are formed in the amorphous region between primary lamellae as confirmed by SAXS analysis (Figures 7-1 and 7-2) [15, 27]. Wide angle X-ray diffraction (WAXD) measurements for annealed and non-annealed samples showed no

intensity peaks corresponding to beta or any new crystals (data not shown here). This suggests that annealing does not affect the crystal lattice [2, 33].

The growth of crystalline lamellae involves a translational motion of the polymer chains [18]. As demonstrated by numerous investigations [2, 17, 27], the amorphous orientation increased slightly during the annealing process. This might be due to a slight movement of the molecules in the amorphous phase during annealing. By increasing the annealing temperature, the chain mobility in the amorphous phase is increased [18]. Thus, this might cause the generation of many microcrystals with random arrangements in the amorphous region between the primary lamellae during annealing [15, 18, 29].

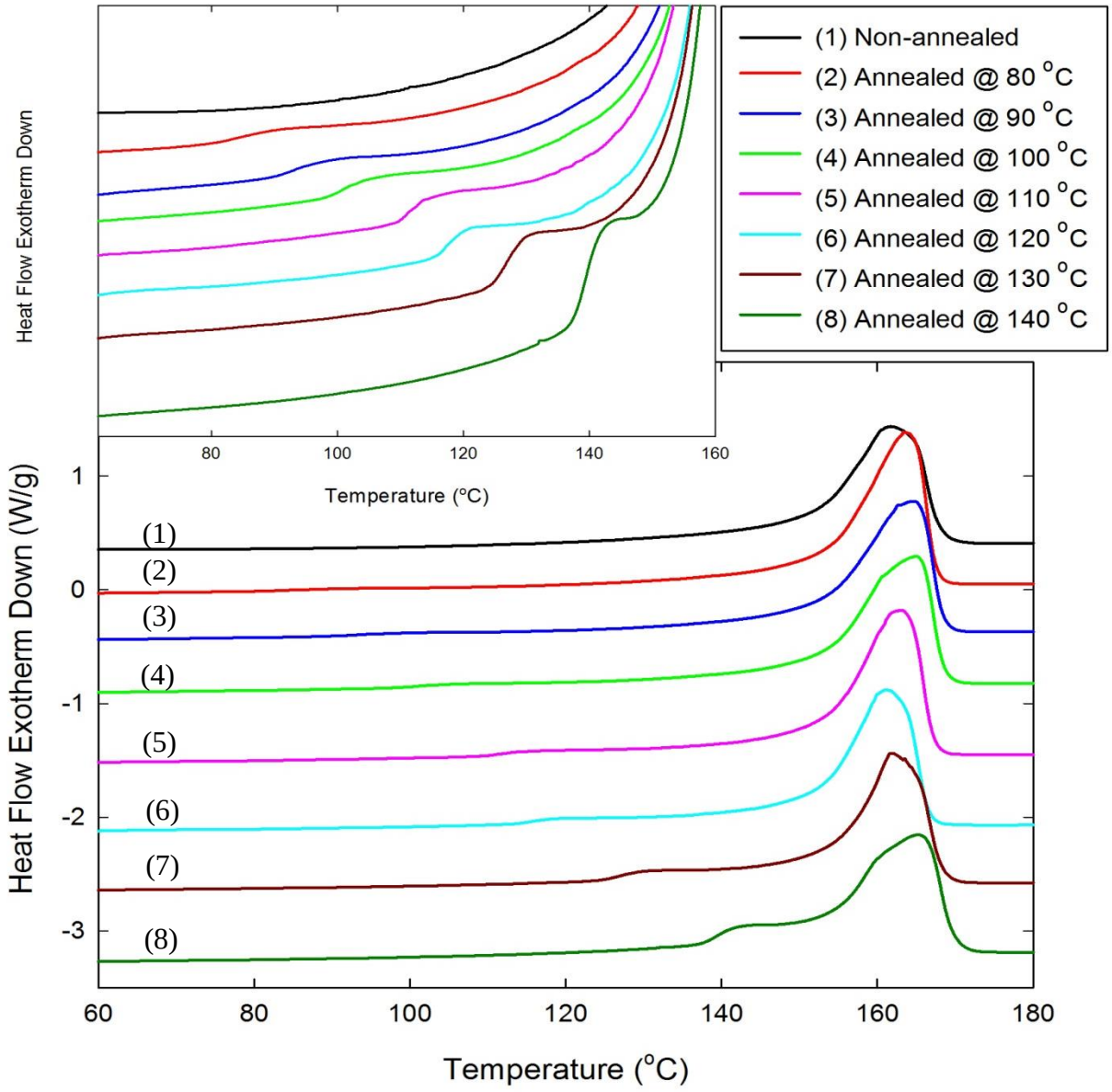

Figure 7-3: DSC thermograms of the annealed films at different annealing temperature (*t*=30min); (the inset shows details of the lower temperature range of the plot).

The tear resistance is the most sensitive mechanical property to crystalline structure changes [16, 35]. The relation between the crystalline orientation and the tear resistance along MD has been discussed elsewhere [2, 10, 16]. In summary, samples with high crystalline and amorphous

orientation rupture along MD at much smaller strains. This could be due to the arrangement of the lamellae blocks along MD, which increases the number of tie chains in this direction [35]. A reduction in the resistance of annealed samples can be seen in the range of 80 to 110 °C, while further increase of the annealing temperature hardly affects the tear resistance (see Figure 7-4a). Small changes of tear resistance are observed upon annealing above 110 °C, indicating a stronger crystal alignment at the initial stage of the annealing process.

The crystalline orientation and crystallinity of annealed and non-annealed samples are presented in Figure 7-4b. It is obvious that the annealed samples exhibit larger crystalline orientation and larger crystallinity than the non-annealed sample [2, 18, 29]. An increase in the annealing temperature further increases these parameters. This could be due to the reduction/elimination of crystal defects in crystalline regions during annealing and chain rearrangements in the machine direction as well [2, 15, 18]. This leads us to the hypothesis that the increase in the crystallinity during annealing, in addition to the formation the new lamellae, must be caused by the thickening of the primary lamellae, in agreement with the results presented in Figures 7-1 to 7-3 [18, 27, 29]. However, it should be noted that the initial crystalline lamellar structure might deteriorate by increasing the annealing temperature to a high value through local partial melting and re-crystallization or transformation into the non-crystalline region [17, 29].

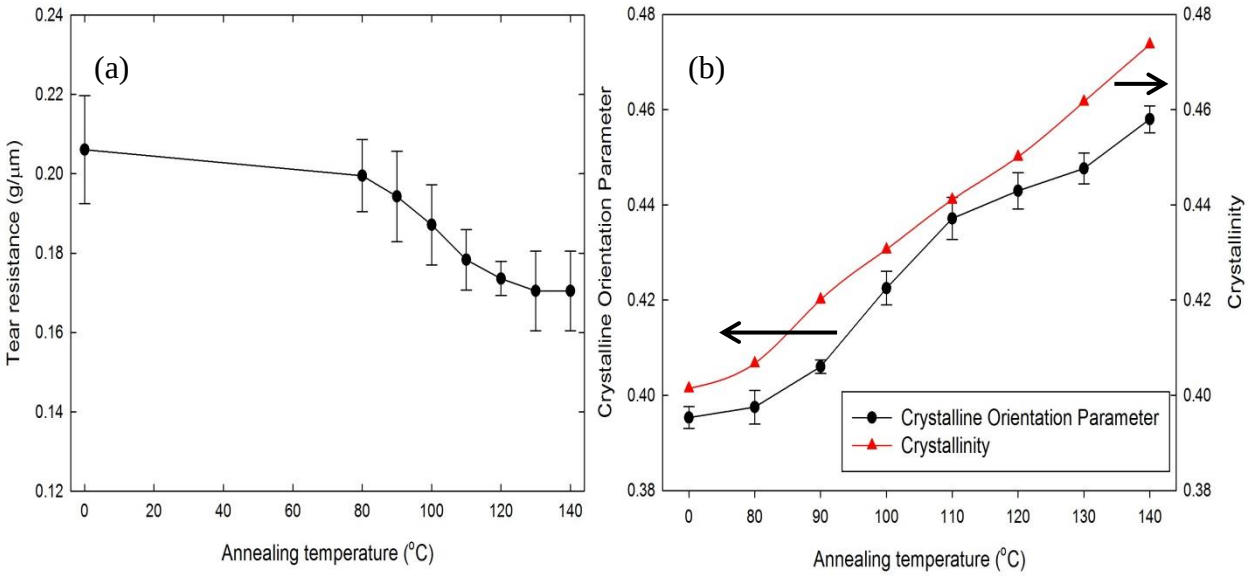

Figure 7-4: (a) Tear resistance along MD and (b) crystalline orientation parameter (obtained from FTIR) and crystallinity (obtained from DSC), as functions of the annealing temperature (*t*=30min).

It is well established that the structures of the crystalline and amorphous phases strongly influence the mechanical properties of the precursor films [16, 17, 36]. Tensile and puncture resistance tests were carried out to analyze the response of the annealed and non-annealed precursor films along machine and normal directions, respectively. The results are presented in Figure 7-5. As pointed out above, annealing has a significant impact on the crystalline structure, which leads to improvements of the mechanical properties of the films [11, 15, 17]. Figure 7-5a presents the results of the tensile stress as a function of deformation. Two yield points (double yield) are observed for the annealed samples compared to non-annealed sample, except for the sample annealed at 80 °C. This is probably due to the presence (and thickness) of the new secondary crystalline lamellae. The deformation mechanisms of both yield points can be

generally associated with fine and coarse chain slip, as schematically presented in Figure 7-5a. The fine chain slip, at the first yield point, is combined with a transformation and rearrangement within the lamellae being oriented in the stretching direction without breaking. However, the process of coarse chain slip results in lamellar fragmentation upon stretching at the second yield point [9, 15, 37]. In fact, the second yield point could be related to the deformation of the secondary crystalline lamellae. However, the size of the secondary lamellae is small and cannot remain stable under high stresses. Nevertheless, the secondary lamellae can act as entanglements or physical crosslink points in the molecular network, thus reducing the stretchability of the amorphous chains [15, 19, 38].

It should be noted that for highly oriented samples, which may possess more active tie chains, the stresses are mostly concentrated in stretching the tie chains in the space between the crystal blocks. However, for samples with low orientation levels, the stresses are mostly spent for reorienting the crystal blocks in the stretching direction. As shown in Figure 7-3, the non-annealed sample has a low crystalline orientation, which means its crystalline lamellae are not well aligned perpendicular to MD. By applying stresses during the tensile test, the lamellae align themselves perpendicular to MD after the first yield point and, consequently, a yield stress drop is observed before strain hardening [16, 37]. It should be noted that the yield stress drop is an amorphous phase property [37]. Annealing causes a decrease in the yield stress drop as a result of increasing crystallinity and decreasing amorphous regions. Apparently, 80 °C is not a high enough temperature to observe a double yield point and it just leads to an improved crystalline orientation. According to Figure 7-5a, 90 °C is the starting temperature to observe a double yield point while the strength of the double yield point increases as the annealing temperature

increases. This result could be attributed to the presence of thicker lamellae at high annealing temperatures.

The strain hardening modulus, which is defined as the slope of the stress vs. strain at large strains, is found to decrease during the annealing process (see Figure 7-5a). For example, the strain hardening modulus of the non-annealed sample is around 9 MPa while for the annealed samples at 110 and 140 °C it is around 6.5 and 3.5 MPa, respectively. These values demonstrate a negative linear correlation between strain hardening and crystallinity. For an amorphous polymer, strain hardening is generally attributed to the network density [37, 39]. However, for semi-crystalline polymers, especially as a result of the annealing process, the density of the inter-crystalline links should be analyzed in relation with the strain hardening behavior through stress transfer between adjacent crystallites [39]. An explanation could be that it originates from the formation of the new lamellae and increasing average crystal thickness caused by the annealing process. Indeed, during annealing, the chain mobility may be sufficient for the growing of the crystallites, which leads to a decrease of the density of inter-crystalline links and strain hardening as well [15, 39]. Meanwhile, stretching will continue until the stress reaches a value large enough to breakdown the lamellae and then rupture happens. The size and amount of lamellae after annealing, especially in high temperature annealed films (140 °C), are larger than in the non-annealed sample. Therefore, rupture for annealed samples occur at lower strains than for non-annealed ones [11, 15].

The results of puncture tests are presented in Figure 7-5b in terms of the normalized maximum puncture force. Each point is an average of over 10 samples. As pointed out earlier, the crystallinity as well as the alignment of the crystalline and amorphous phases increase with the annealing temperature, explaining the pronounced increases in the puncture resistance [14].

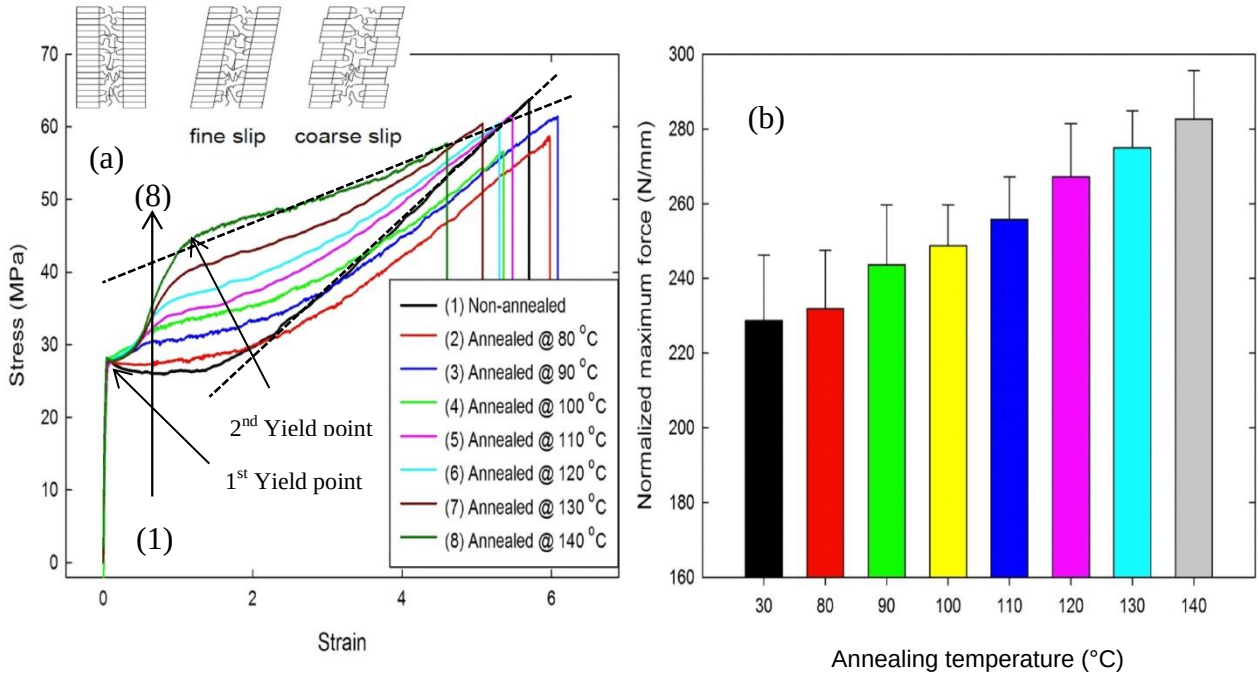

Figure 7-5: (a) Stress–strain curves along MD of the annealed films at different annealing temperature; strain rate = 50mm/min and (b) normalized maximum force for piercing as a function of the annealing temperature (t=30min); strain rate = 25mm/min.

7.3.2 Effect of annealing time on the crystalline structure and mechanical properties of the precursor films.

In this section, the effect of annealing time is investigated for the annealing temperature of 120 °C. The results are presented in Figs. 6-9. Figures 7-6a-d compare the SAXS patterns of annealed films with that of the non-annealed film. We observe that the meridian intensity, which is attributed to lamellae, increases substantially with time up to 10 min, whereas longer annealing times have little additional impact on the pattern. The appearance of a new peak before L_{max} in the correlation function curve of the samples annealed more than 10 min (see Figure 7-6e)

confirms the formation and presence of the thin crystalline lamellae in the amorphous region. Slight changes are seen in the features after 10 min, which suggests that 10 min is the optimum time for the annealing process.

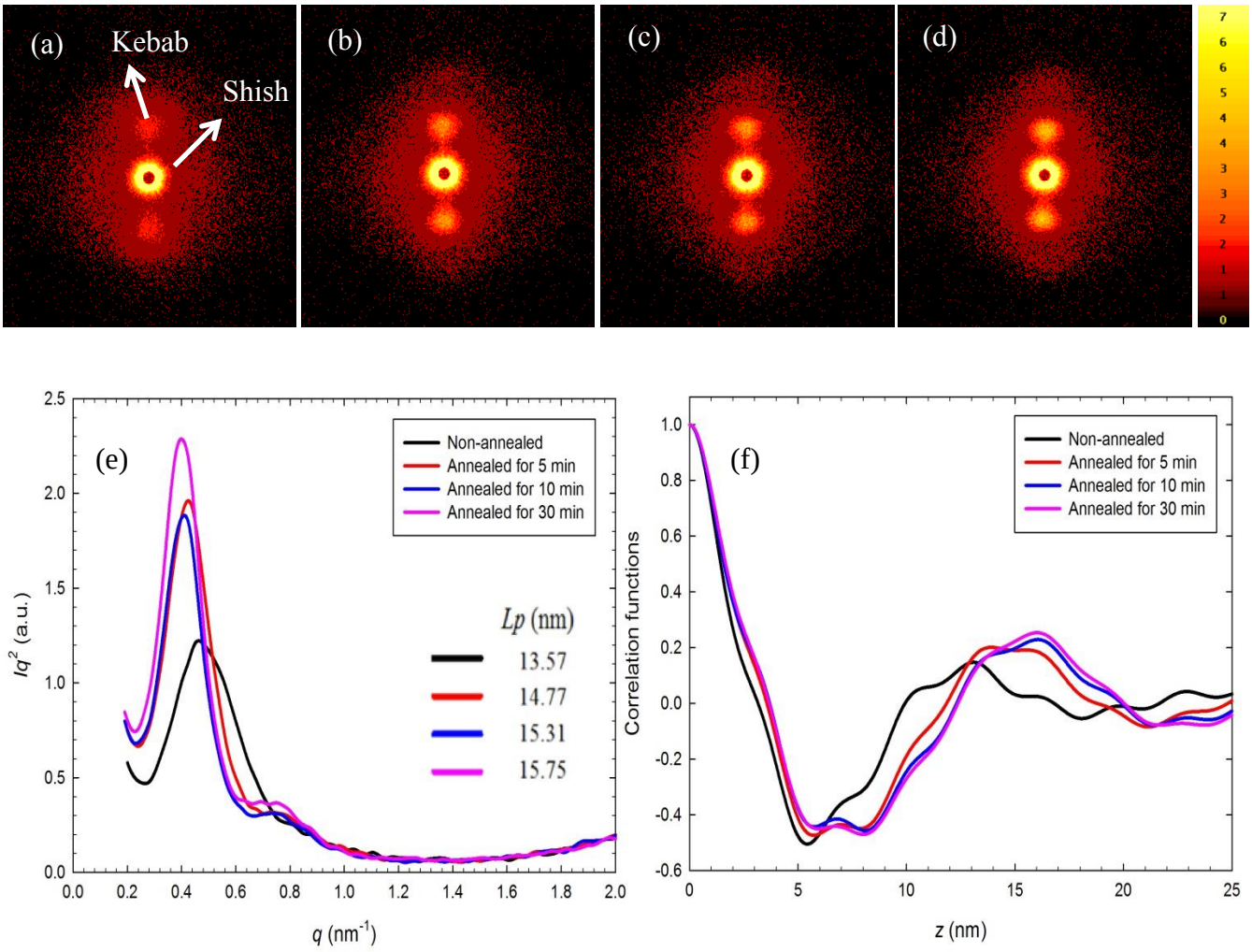

Figure 7-6: SAXS patterns of precursor films, (a) non-annealed, (b) annealed for 5 min, (c) annealed for 10 min, (d) annealed for 30 min and (e) SAXS intensity profiles and (f) SAXS correlation functions for non-annealed and annealed samples at different annealing times (T=120 °C).

DSC results are compared in Figure 7-7 for the non-annealed and annealed samples for different times (at *T*= 120 °C). We observe the formation of a small peak around 120 °C (the annealing temperature) for the annealed samples. The results suggest that secondary lamellae could be formed even at a short annealing time (2 min) in the amorphous phase between primary lamellae.

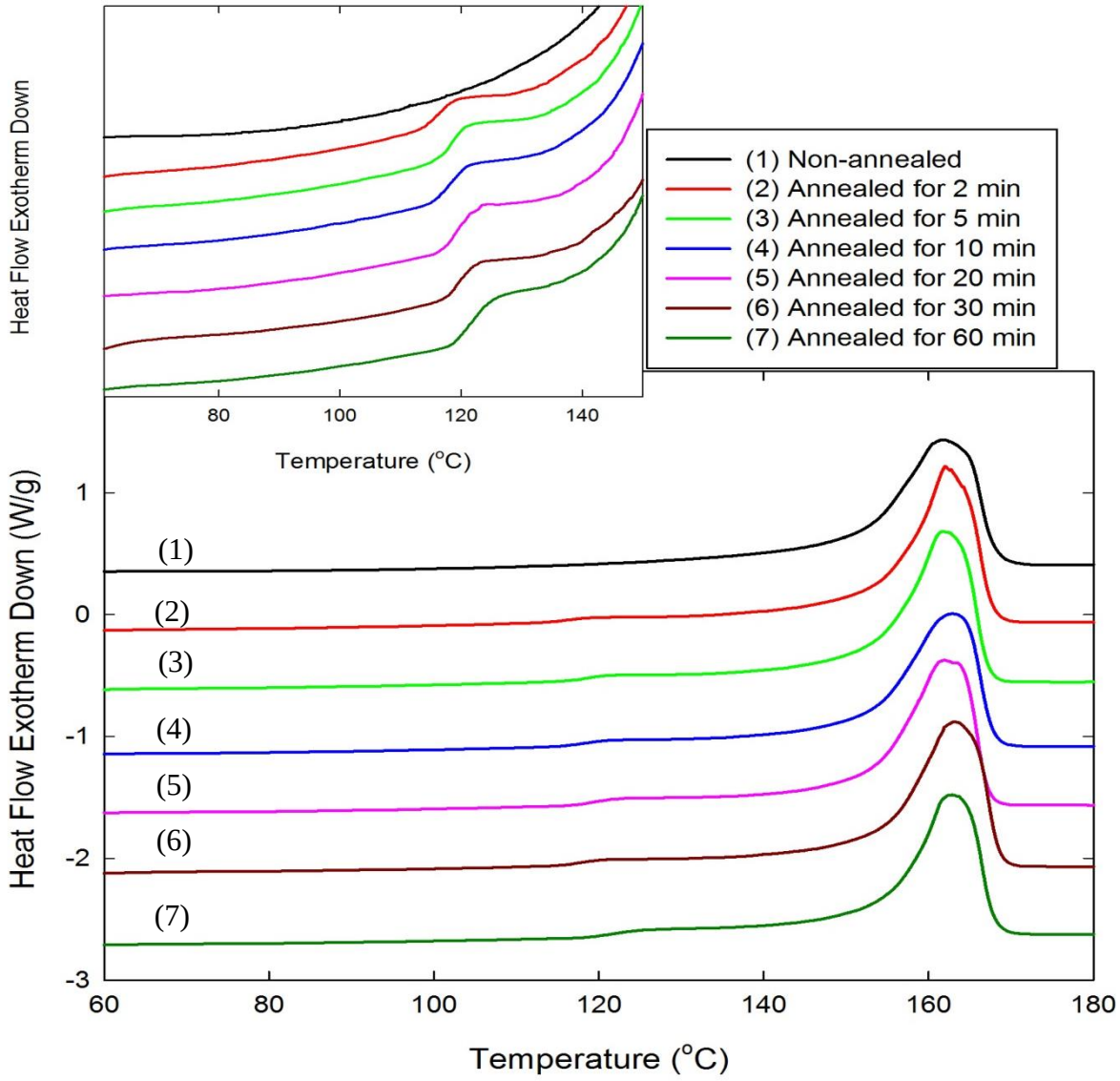

Figure 7-7: DSC thermograms of the annealed films at different annealing times (*T*=120 °C); (the inset shows details of the lower temperature range of the plot).

Figure 7-8a shows that the crystallinity and crystalline orientation of the precursor films increase predominantly within the first 10 min, followed by a slight increase and finally reach plateau values. This suggests again that 10 min is enough time for annealing the precursor film and beyond that, the structure parameters remain almost constant.

As mentioned previously, tear resistance is one of the most sensitive mechanical properties to the crystalline structure and it decreases with crystalline orientation [2, 10, 16]. Figure 7-8b shows that the only noticeable changes in the tear resistance along MD occur within the first 10 min annealing time and after that the changes are less pronounced.

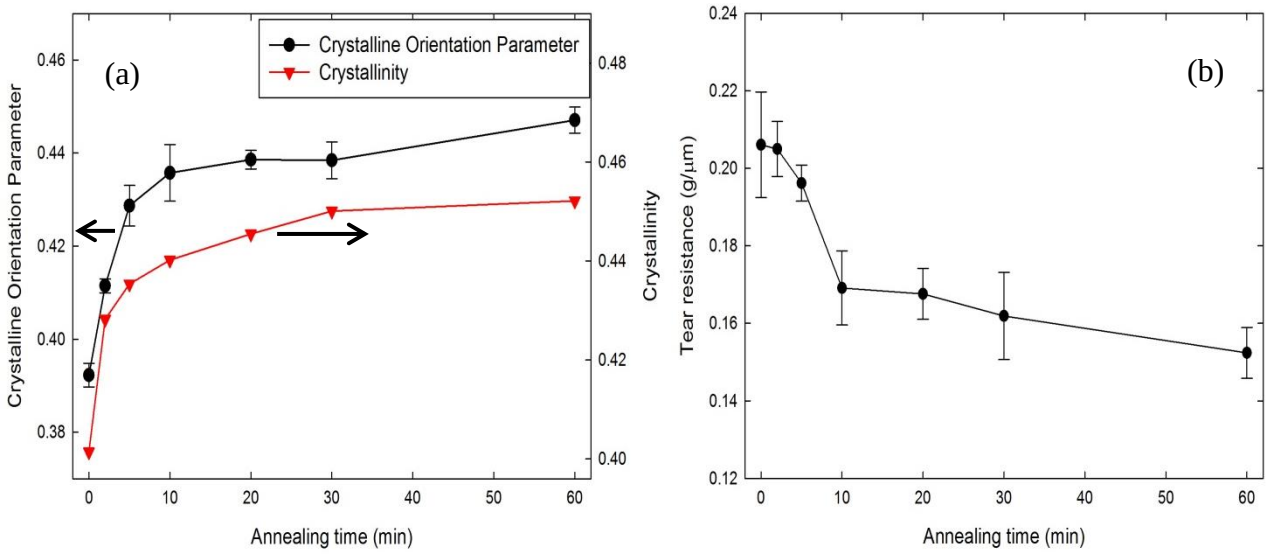

Figure 7-8: (a) Crystalline orientation parameter (obtained from FTIR) and crystallinity (obtained from DSC) and (b) tear resistance along MD as functions of the annealing time (T=120 °C).

Tensile and puncture resistance of the precursor films annealed for different times at 120 °C are presented in Figure 7-9 as functions of the deformation along MD and ND. The strength of second yield point and puncture resistance values of the annealed samples confirm again that the

crystalline structure does not change dramatically after 10 min annealing, supporting the previous results.

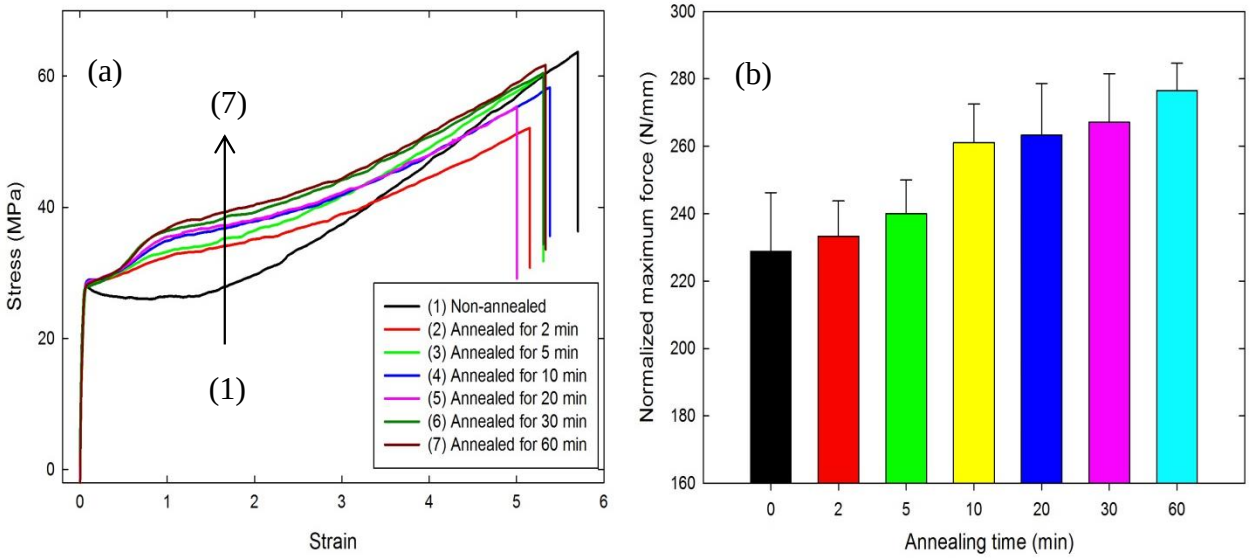

Figure 7-9: (a) Stress–strain curves along MD of the annealed films at different annealing time; strain rate = 50 mm/min and (b) normalized maximum force for piercing as functions of annealing time (T=120 °C); strain rate = 25 mm/min.

7.3.3 Relationship between the crystalline structure and the yield stress

The yield stress for semi-crystalline polymers has often been related to crystal thickness and crystallinity degree, by considering the thermal nucleation of the screw dislocation within the crystalline lamellae [39]. As mentioned above regarding yielding, the existence of two yield points (double yield) can be clearly observed in annealed samples and its stress increase with increasing crystal lamellae thickness. Figure 7-10 presents the second yield stress (obtained from tensile measurements) as a function of the crystalline lamellae thickness (obtained from SAXS and DSC). The results depict a reasonable linear correlation between the second yield stress and

thickness of the crystal lamellae. As mentioned earlier, the second yield point is considered to be associated with the secondary lamellae fragmentation. Thus, secondary lamellae believed to be the controlling parameter in the activation of the second yield stress and, subsequently, the linear correlation could be caused by the secondary lamellae thickness.

The peak positions in the SAXS profiles are taken to calculate the average lamellae thickness from [37, 39]:

$$l_c = L_P \times X_{vol} \tag{7-3}$$

where X_{vol} is the volumetric percentage of crystals calculated from the crystal weight percentage X:

$$X_{vol} = \frac{\frac{X}{\rho_c}}{\frac{X}{\rho_c} + \frac{100 - X}{\rho_A}} * 100\% \tag{7-4}$$

where X is obtained from DSC, ρ_C is the crystal density and ρ_A is the amorphous polymer density. The values for the amorphous and crystalline densities where taken as those of PP: ρ_C = 0.95 g/mL, ρ_A = 0.85 g/mL [18, 37]. Also, l_c^* is the lamellar thickness of the non-annealed precursor film.

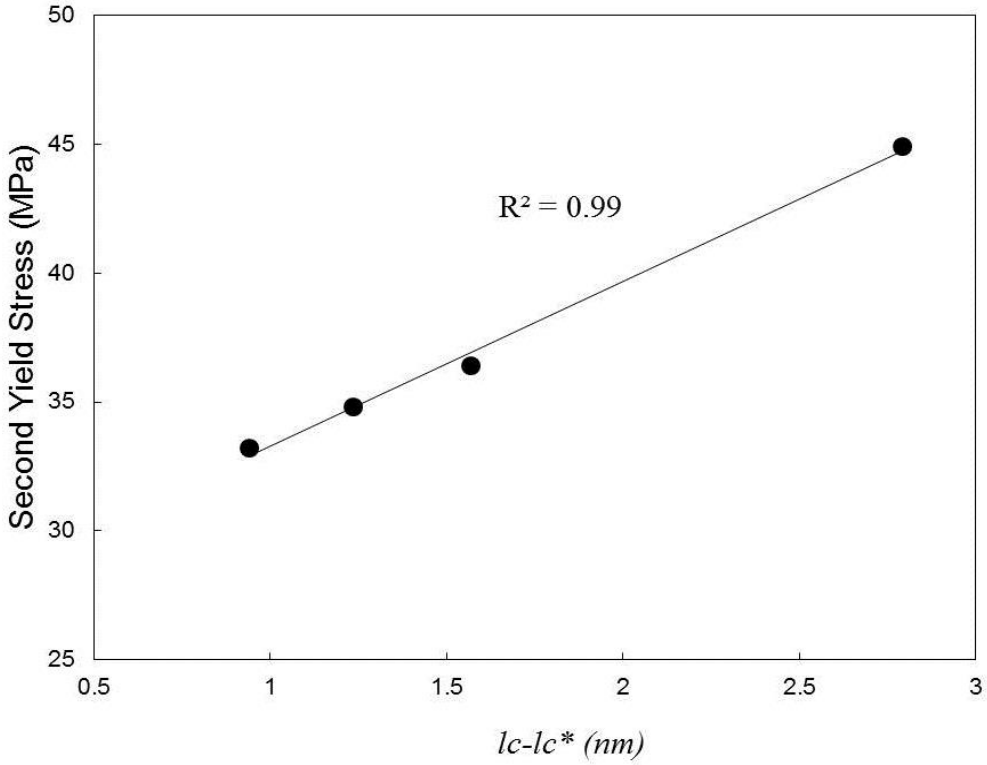

Figure 7-10: Relationship between the second yield stress of the tested samples and the relative lamellae thickness (lc- lc^*).

7.3.4 Effect of annealing temperature and time on the membrane morphology and performance

DSC data for the membranes produced from annealed and non-annealed samples are presented in Figure 7-11. These provide some information regarding the possible formation of the new lamellae between the amorphous sections. The evolution in the crystalline structure can be seen again after the annealing process. Two types of the lamellae distribution are expected after stretching the precursor films. One of those corresponds to crystals with interconnected bridges between the lamellae (I) and the other reflects the lamellae crystals (C). The interconnected

bridges are formed from stretching the tie chains during cold and hot stretching [17]. This means that the interconnected bridges act like shish crystals and have a melting temperature of about 5–10 °C higher than that of lamellae crystals (kebabs) [10, 17, 40, 41]. The presence of a double melting peak in the membrane of the non-annealed sample instead of one for the annealed one is believed to be related to the formation of secondary lamellae in the amorphous phase during annealing. This lamellae formation could decrease the number of the interconnected bridges and increase lamellae crystals as well. Therefore, the lamellae crystals to interconnected bridges ratio (C/I) in the annealed sample would be increased, and a single melting peak is obtained, instead of double melting point.

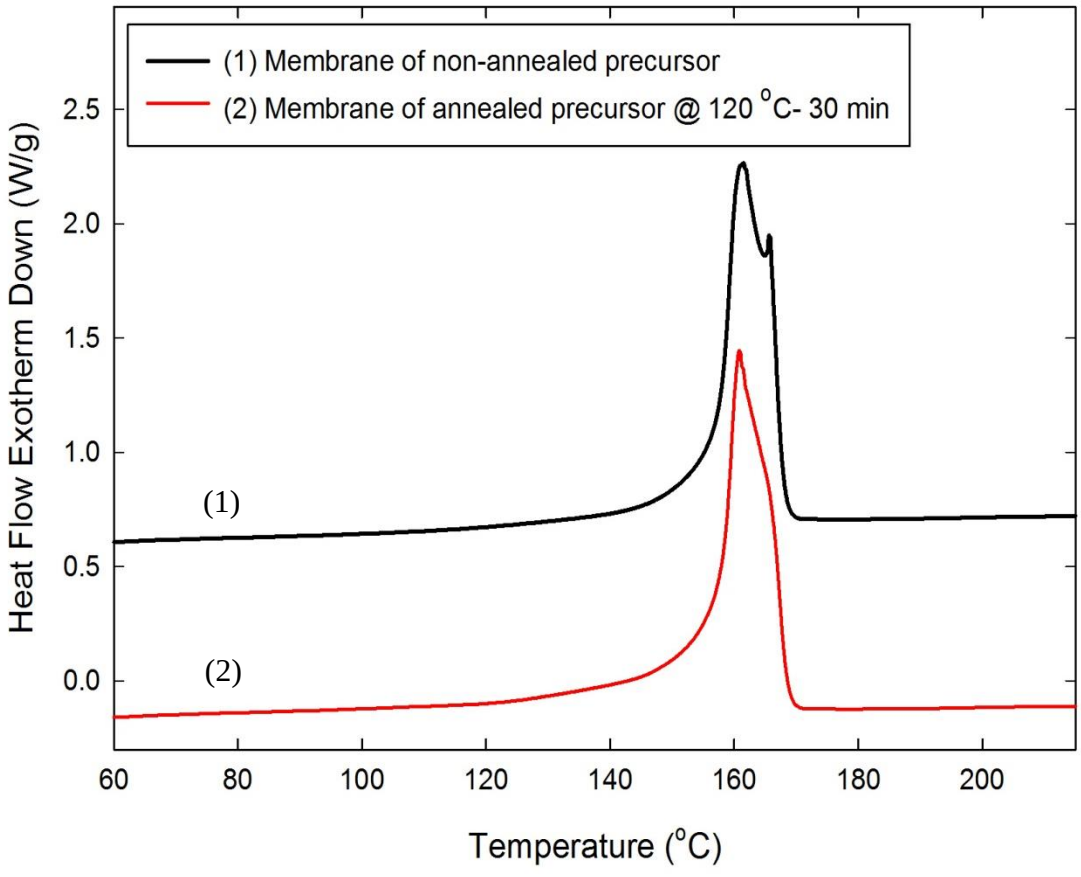

Figure 7-11: DSC of the final membranes prepared from the non-annealed and annealed samples.

SEM images of surface morphology of the developed membranes at different annealing conditions are presented in Figure 7-12. It is evident that increasing annealing time and temperature causes an increase in the size and number of pores.

Results of the mercury porosimetry analysis for the microporous membranes obtained using different annealing conditions are reported in Table 2. It is known that the mercury intrusion volume is directly related to the pore size and porosity due to interconnected pores [17, 42]. We observe that the total pore area and average pore diameter increase with annealing time and temperature, which is in agreement with the SEM results. However, annealing had a small influence on the peak position in the pore size distribution (data not shown here); all three samples revealed peaks around 0.1 μm. Furthermore, porosity values of 18.8, 25.3 and 27.5% were obtained for the samples annealed for 5 min (at 120 °C), 30 min (at 120 °C) and at 130 °C for 30 min membranes, respectively. The increasing porosity for a membrane prepared with longer annealing time and higher temperature is attributed to the formation of thicker secondary lamellae. Consequently, they are less resistant to lamellae separation, which results in more pore interconnection [2, 17, 42].

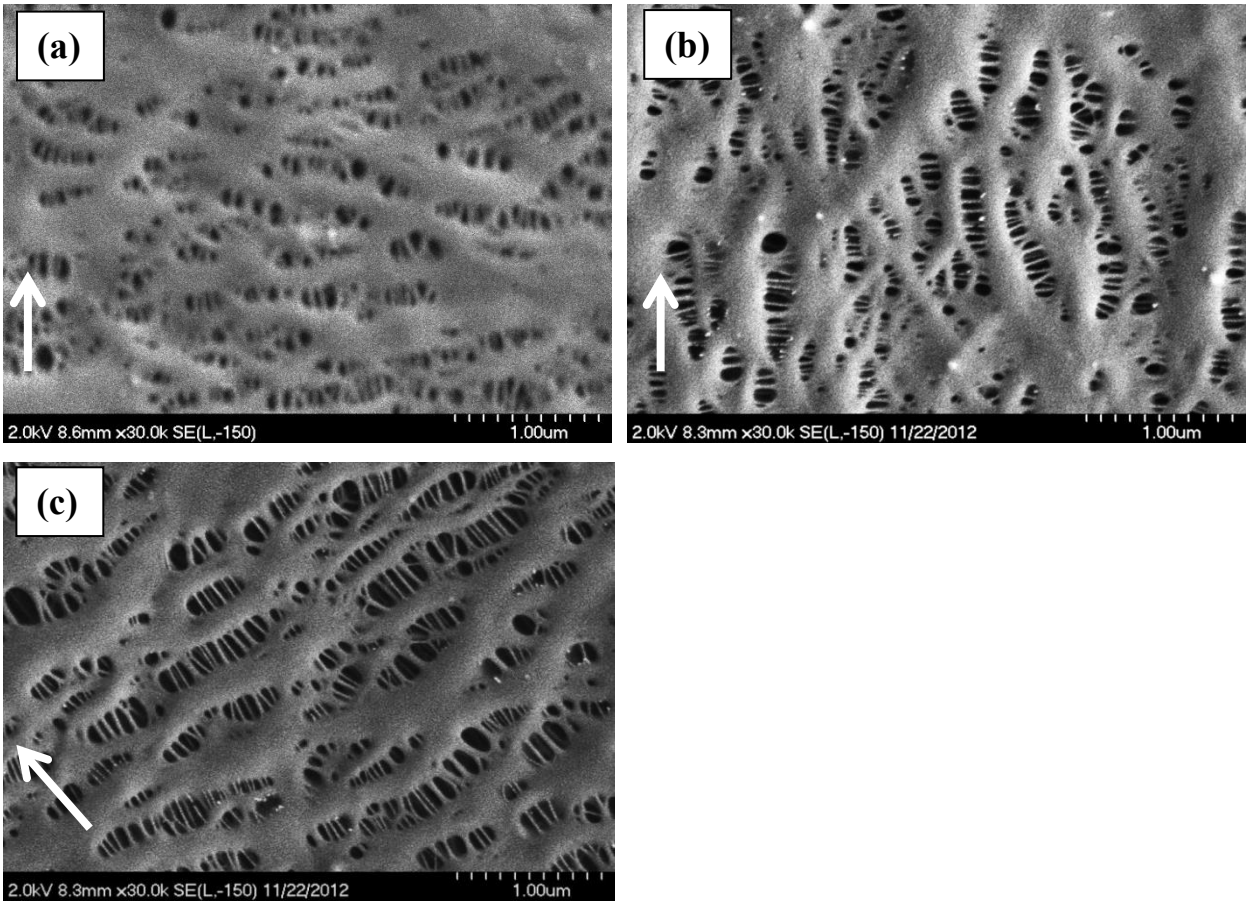

Figure 7-12: SEM micrographs of the surface of the microporous membranes for different annealing conditions, (a) 120 °C- 5 min, (b) 120 °C- 30 min, (c) 130 °C- 30 min; (the arrows indicate the stretching machine direction).

Table 7-2: Results of the mercury porosimetry analysis for the microporous membranes.

	Total pore area (m^2/g)	Average pore diameter (nm)	Porosity (%)
Annealed @ 120 °C- 5 min	14.5	60	18.8
Annealed @ 120 °C- 30 min	19.8	82	25.3
Annealed @ 130 °C- 30 min	22.1	93	27.5

Figure 7-13 presents the water vapor transmission rates (WVTR) of the produced microporous membranes. Low WVTR was measured for the 2 min annealed sample. However, interestingly, the WVTR increased by a factor of 6 when the film was subjected to 10 min annealing at 120 °C. This can be attributed to the formation of more pores, higher porosity and better interconnection between the pores as a result of increasing crystalline orientation and crystallinity of the precursor films (in agreement with the previous results) [2]. The small additional changes of the water vapor permeability for the samples annealed for more than 10 min indicate again that the lamellar structure does not change dramatically after 10 min annealing. Furthermore, the effect of the annealing temperature on the permeability of microporous membranes was investigated and the results are presented in Figure 7-13b. The water vapor permeability is observed to increase with the annealing temperature, which is in agreement with mercury porosimetry results and SEM observations.

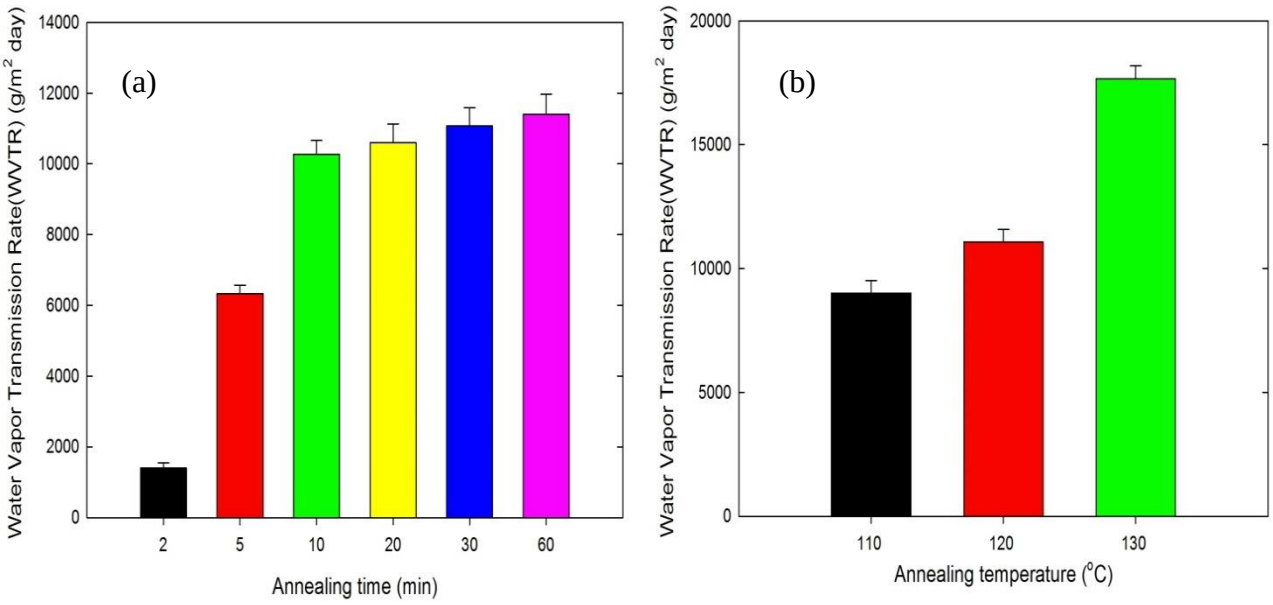

Figure 7-13: Water vapor transmission rate as a function of (a) annealing time *(T*= 120 °C) and (b) annealing temperature (*t*=30 min).

7.4 Conclusions

In this work, we investigated the structure of PP based cast films, in terms of orientation and crystalline structure after annealing under different conditions (temperature and time). The effects of annealing on the performances of precursor films and microporous membranes obtained by stretching the films were analyzed. Our findings can be summarized as follows:

Annealing changes the nano-scale structure of the precursor films, particularly the crystalline structure. FTIR, DSC, SAXS and mechanical analysis indicated that annealing forms secondary crystalline lamellae between the primary lamellae. SAXS results analysis, using indirect Fourier transformation of the scattering function, suggested that the lamellar morphology of the annealed samples consisted of lamellae and amorphous regions with a thickness distribution and a large variation in the long period distance.10 min was sufficient time for annealing the precursor films. Beyond that, the crystalline structure changed only slightly.The yield behavior in the stress-strain curves of the films was changed by annealing. Two characteristics could be distinguished in the annealed samples: 1) presence of the double yield point and 2) a linear dependence of second yield stress with the lamellae thickness.

The strain hardening modulus and elongation at break of the precursor films were found to decrease for annealed samples. Annealing had a dramatic effect on puncture resistance of the films probably as a result of increased crystallinity.

Microporous membranes having higher porosity, high pore density and consequently, higher water vapour permeability were obtained for the annealed films. Good agreement between water

vapor permeability, SEM and mercury porosimetry analysis was observed for the microporous membranes.

7.5 Acknowledgments

Financial support from NSERC Network for Innovative Plastic Materials and Manufacturing Processes (NIPMMP) is gratefully acknowledged. We are also thankful to Ms. Sylvie St-Amour and Ms. Sylvie Sauriol from FP Innovations (Paprican Division) for the use of and training on their AutoPore IV mercury intrusion porosimeter.

7.6 References

[1] E. Gérard, E. Bessy, C. Salvagnini, V. Rerat, M. Momtaz, G. Hénard, P. Marmey, T. Verpoort, J. Marchand-Brynaert, Surface modifications of polypropylene membranes used for blood filtration, Polymer, 52 (2011) 1223-1233.

[2] S.H. Tabatabaei, P.J. Carreau, A. Ajji, Microporous membranes obtained from polypropylene blend films by stretching, Journal of Membrane Science, 325 (2008) 772-782.

[3] M. Xu, X. Shi, H. Chen, T. Xiao, Synthesis and enrichment of a macromolecular surface modifier PP-b-PVP for polypropylene, Applied Surface Science, 256 (2010) 3240-3244.

[4] A.S. Gozdz, C.N. Schmutz, J.M. Tarascon, P.C. Warren, Method of making polymeric electrolytic cell separator membrane, in, 1997.

[5] M. Aoyama, M. Ito, S. Tsuji, T. Ishii, T. Tanaka, Method of forming a porous polyolefin film, in, 1990.

[6] G.-y. Shi, F. Chu, G.-e. Zhou, Z.-w. Han, Plastic deformation and solid-phase transformation in β-phase polypropylene, Die Makromolekulare Chemie, 190 (1989) 907-913.

[7] G.T. Offord, S.R. Armstrong, B.D. Freeman, E. Baer, A. Hiltner, D.R. Paul, Influence of processing strategies on porosity and permeability of β nucleated isotactic polypropylene stretched films, Polymer, 54 (2013) 2796-2807.

[8] G.T. Offord, S.R. Armstrong, B.D. Freeman, E. Baer, A. Hiltner, J.S. Swinnea, D.R. Paul, Porosity enhancement in β nucleated isotactic polypropylene stretched films by thermal annealing, Polymer, 54 (2013) 2577e2589.

[9] S.H. Tabatabaei, P.J. Carreau, A. Ajji, Microporous membranes obtained from PP/HDPE multilayer films by stretching, Journal of Membrane Science, 345 (2009) 148-159.

[10] S.H. Tabatabaei, P.J. Carreau, A. Ajji, Structure and properties of MDO stretched polypropylene, Polymer, 50 (2009) 3981-3989.

[11] F. Sadeghi, A. Ajji, P.J. Carreau, Analysis of row nucleated lamellar morphology of polypropylene obtained from the cast film process: Effect of melt rheology and process conditions, Polymer Engineering & Science, 47 (2007) 1170-1178.

[12] K.Y. Lin, Novel polypropylene based microporous membranes via spherulitic deformation, in, New Jersey Institute of Technology, Newark, 2008.

[13] J. Varga, G. Ehrenstein, Beta-modification of isotactic polypropylene, in: J. Karger-Kocsis (Ed.) Polypropylene, Springer Netherlands, 1999, pp. 51-59.

[14] A. Saffar, P.J. Carreau, A. Ajji, M.R. Kamal, Development of polypropylene microporous hydrophilic membranes by blending with PP-g-MA and PP-g-AA, Journal of Membrane Science, 462 (2014) 50-61.

[15] D. Liu, J. Kang, M. Xiang, Y. Cao, Effect of annealing on phase structure and mechanical behaviors of polypropylene hard elastic films, J Polym Res, 20 (2013) 1-7.

[16] S.H. Tabatabaei, P.J. Carreau, A. Ajji, Effect of processing on the crystalline orientation, morphology, and mechanical properties of polypropylene cast films and microporous membrane formation, Polymer, 50 (2009) 4228-4240.

[17] F. Sadeghi, A. Ajji, P.J. Carreau, Analysis of microporous membranes obtained from polypropylene films by stretching, Journal of Membrane Science, 292 (2007) 62-71.

[18] C. Hedesiu, D.E. Demco, R. Kleppinger, G.V. Poel, W. Gijsbers, B. Blümich, K. Remerie, V.M. Litvinov, Effect of Temperature and Annealing on the Phase Composition, Molecular Mobility, and the Thickness of Domains in Isotactic Polypropylene Studied by Proton Solid-State NMR, SAXS, and DSC, Macromolecules, 40 (2007) 3977-3989.

[19] H. Bai, H. Deng, Q. Zhang, K. Wang, Q. Fu, Z. Zhang, Y. Men, Effect of annealing on the microstructure and mechanical properties of polypropylene with oriented shish-kebab structure, Polymer International, 61 (2012) 252-258.

[20] H. Bai, F. Luo, T. Zhou, H. Deng, K. Wang, Q. Fu, New insight on the annealing induced microstructural changes and their roles in the toughening of β-form polypropylene, Polymer, 52 (2011) 2351-2360.

[21] D. Ferrer-Balas, M.L. Maspoch, A.B. Martinez, O.O. Santana, Influence of annealing on the microstructural, tensile and fracture properties of polypropylene films, Polymer, 42 (2001) 1697-1705.

[22] P. Järvelä, L. Shucai, P. Järvelä, Dynamic mechanical properties and morphology of polypropylene/maleated polypropylene blends, Journal of Applied Polymer Science, 62 (1996) 813-826.

[23] I.W. Hamley, V. Castelletto, Small-angle scattering of block copolymers: in the melt, solution and crystal states, Progress in Polymer Science, 29 (2004) 909-948.

[24] G.H. Michler, I. Naumann, F.J. Baltá Calleja, F. Ania, Problems relating to long period determination in polyethylene shish-kebab structures, Acta Polymerica, 48 (1997) 36-40.

[25] M.E. Myers, A.M. Wims, T.S. Ellis, J. Barnes, An investigation of the morphology of amorphous/semicrystalline nylon blends using small-angle x-ray scattering, Macromolecules, 23 (1990) 2807-2814.

[26] A.J. Ryan, I.W. Hamley, W. Bras, F.S. Bates, Structure Development in Semicrystalline Diblock Copolymers Crystallizing from the Ordered Melt, Macromolecules, 28 (1995) 3860-3868.

[27] V. Premnath, A. Bellare, E.W. Merrill, M. Jasty, W.H. Harris, Molecular rearrangements in ultra high molecular weight polyethylene after irradiation and long-term storage in air, Polymer, 40 (1999) 2215-2229.

[28] A. Bellare, H. Schnablegger, R.E. Cohen, A Small-Angle X-ray Scattering Study of High-Density Polyethylene and Ultrahigh Molecular Weight Polyethylene, Macromolecules, 28 (1995) 7585-7588.

[29] Q. Zhang, Z. Mo, S. Liu, H. Zhang, Influence of Annealing on Structure of Nylon 11, Macromolecules, 33 (2000) 5999-6005.

[30] B. Goderis, H. Reynaers, M.H.J. Koch, V.B.F. Mathot, Use of SAXS and linear correlation functions for the determination of the crystallinity and morphology of semi-crystalline polymers. Application to linear polyethylene, Journal of Polymer Science Part B: Polymer Physics, 37 (1999) 1715-1738.

[31] N. Stribeck, X–Ray Scattering of Soft Matter, in, Springer, Hamburg, 2007, pp. 26-32

[32] C. Santa Cruz, N. Stribeck, H.G. Zachmann, F.J. Balta Calleja, Novel aspects in the structure of poly(ethylene terephthalate) as revealed by means of small angle x-ray scattering, Macromolecules, 24 (1991) 5980-5990.

[33] Y.A. Akpalu, E.J. Amis, Effect of polydispersity on the evolution of density fluctuations to lamellar crystals in linear polyethylene, The Journal of Chemical Physics, 113 (2000) 392-403.

[34] A.J. Ryan, J.L. Stanford, W. Bras, T.M.W. Nye, A synchrotron X-ray study of melting and recrystallization in isotactic polypropylene, Polymer, 38 (1997) 759-768.

[35] F. Sadeghi, A. Ajji, P.J. Carreau, Study of Polypropylene Morphology Obtained from Blown and Cast Film Processes: Initial Morphology Requirements for Making Porous Membrane by Stretching, Journal of Plastic Film and Sheeting, 21 (2005) 199-216.

[36] X.M. Zhang, A. Ajji, Oriented structure of PP/LLDPE multilayer and blends films, Polymer, 46 (2005) 3385-3393.

[37] B.A.G. Schrauwen, R.P.M. Janssen, L.E. Govaert, H.E.H. Meijer, Intrinsic Deformation Behavior of Semicrystalline Polymers, Macromolecules, 37 (2004) 6069-6078.

[38] J.M. Samon, J.M. Schultz, B.S. Hsiao, Morphological Changes during the Annealing of Polybutene-1 Fiber, Macromolecules, 34 (2001) 2008-2011.

[39] D. Jauffrès, O. Lame, G. Vigier, F. Doré, How Nascent Structure of Semicrystalline Polymer Powders Enhances Bulk Mechanical Properties, Macromolecules, 41 (2008) 9793-9801.

[40] F. Sadeghi, S.H. Tabatabaei, A. Ajji, P.J. Carreau, Properties of uniaxially stretched polypropylene films: effect of drawing temperature and random copolymer content, The Canadian Journal of Chemical Engineering, 88 (2010) 1091-1098.

[41] R.H. Somani, L. Yang, L. Zhu, B.S. Hsiao, Flow-induced shish-kebab precursor structures in entangled polymer melts, Polymer, 46 (2005) 8587-8623.

[42] F. Sadeghi, A. Ajji, P.J. Carreau, Microporous membranes obtained from polypropylene blends with superior permeability properties, Journal of Polymer Science Part B: Polymer Physics, 46 (2008) 148-157.

CHAPTER 8 - ARTICLE 4:

THE INFLUENCE OF STRETCHING ON THE PERFORMANCE OF POLYPROPYLENE BASED MICROPOROUS MEMBRANES.

Amir Saffar[1], Pierre J. Carreau[1], Abdellah Ajji[1], Musa R. Kamal[2]

1) Research Center for High Performance Polymer and Composite Systems (CREPEC), Chemical Engineering Department, Polytechnique Montreal, PO Box 6079, Stn Centre-Ville, Montreal, Quebec, Canada, H3C 3A7.

2) CREPEC, Department of Chemical Engineering, McGill University, 3610 University Street, Montreal, Quebec, Canada, H3A 2B2.

This work was submitted to *Industrial & Engineering Chemistry Research*

Abstract

In this paper, we analyze the pore structure changes during the fabrication of polypropylene based microporous membranes via the stretching method. The membranes were prepared via melt extrusion followed by annealing, stretching at room temperature and at an elevated temperature (cold and hot stretching steps), respectively. Understanding the pore formation mechanisms is important for an effective control of the membrane performance. Hence, the pore structure along the membrane surface and across the thickness, which determined the size, number and interconnectivity of the pores, was analyzed to quantify the effect of stretching on the membrane performance. The cold stretching step was found to be the important one to promote interconnection between the pores. Furthermore, it was shown that applying a low strain rate improved the permeability of the membranes. Finally, no maximum was observed in the permeability by increasing the stretch ratio during the hot stretching step.

Keywords

Polypropylene films, Membranes by stretching, Morphology, Water vapor permeability.

8.1 Introduction

Polypropylene (PP) is a semi-crystalline polymer commonly used to produce porous membranes for various applications.[1-3] Membranes are usually made from a solution/phase separation process. In recent studies, PP porous membranes have been prepared by using a dry process (melt process) combining a specific crystalline morphology followed by annealing and stretching.[2, 4-6] Therefore, to obtain a satisfactory porous membrane using the stretching method, three consecutive stages need to be carried out: (1) creating a precursor film containing the desired lamellar morphology, i.e., an oriented shish-kebab structure, (2) annealing the precursor film at

elevated temperatures to improve the crystalline structure, and (3) stretching at room temperature to create the pores by lamellae separation and subsequently stretching at a high temperature to enlarge them.[2, 4-7] Polypropylene microporous membranes obtained via this method are commercially available under the trade name Celgard.[8]

The orientation and arrangement of the crystal lamellae are the key factors in controlling the properties of the precursor film and, consequently, the properties of the porous membrane.[2, 7, 9] The first step for controlling the crystalline orientation and generating the desired lamellar morphology in the cast film process is the selection of the right materials and the use of suitable processing conditions. These aspects are determined by several parameters, which can be summarized as follows. The material variables include molecular weight, molecular weight distribution and chain structure of the polymer, on the other hand, the applied processing conditions include air cooling of the film right at the exit of the die, chill roll temperature and draw ratio (ratio of the roll speed to the die exit velocity). These parameters have been investigated previously by our group[2, 6, 9-11] and other groups.[12-14] In fact, an initial orientation for the laminar structure is required (more than 0.3), in order to obtain a row-nucleated morphology suitable for the formation of porous membranes.[10]

The second step of the stretching method is annealing, which is an effective method to improve the crystalline structure by thickening the lamellae and re-arranging the molecular chains in the amorphous phase. In our previous work[15] a detailed investigation was performed to evaluate the influence of annealing conditions on the crystalline structure and the subsequent membrane properties for PP based films. We observed that annealing forms secondary crystalline lamellae between the primary lamellae. This improves the mechanical properties of the precursor film and the performances of the microporous membrane.

There are few examples in literature that examine how stretching, as the third step of the stretching method, affects the membrane performance of semi-crystalline polymers.[2, 4, 14, 16, 17] However, to our knowledge, little attention has been paid to the mechanisms of pore structure changes during each step of stretching. Understanding these mechanisms is important to prepare membranes with desired performances.

Hence, in this study, a detailed investigation is performed to evaluate the pore structure as a function of stretching and its impact on the microporous membrane performance. For example, we show that the water vapor permeability of a membrane can be increased by a factor up to 140 depending on the processing conditions. In addition, the separate effects of cold and hot stretching steps on the pore structure of the membrane are examined. Furthermore, the effect of stretching on the performance of membranes made of PP containing 2wt % of an acrylic acid grafted polypropylene (PP-g-AA) from our previous work [18] is determined.

8.2 Experimental

8.2.1 Materials

A commercial linear high molecular weight polypropylene (PP5341E1) supplied by ExxonMobil Company was selected. It had a melt flow rate (MFR) value of 0.8 g/10 min (under ASTM conditions of 230 °C and 2.16 kg). Its melting point, T_m, and crystallization temperature, T_c, obtained from differential scanning calorimetry (DSC) at a rate of 10 °C/min, were 161 °C and 115 °C, respectively. In the case of blend sample, a commercial linear polypropylene (PP4712E1, ExxonMobil) and an amphiphilic polymer consisting of a PP hydrophobic backbone and an acrylic acid grafted PP (PP-g-AA Polybond®1002, Chemtura Corporation) were selected. Their

MFR values were of 2.8 g/10 min under ASTM conditions of 230 ºC and 2.16 kg and 20 g/10 min, respectively.[18]

8.2.2 Film preparation

Precursor films from PP were prepared using a 45 mm diameter Killion single screw extruder equipped with a slit die of 0.7 mm opening. The temperature profile along the barrel was: 165/195/210/215 °C and the die temperature was 220 °C. For film cooling, an air knife was applied right at the exit of the die to supply air to the film surface. The extrusion was carried out using a screw speed of 12.5 rpm and a draw-down ratio (ratio of the roll speed to the die exit velocity) was set at 25 to produce precursor films having a thickness of around 30 μm. The distance between die exit to the nip cast roll was around 15 cm, and the cast roll temperature was constant at 50 $^{\circ}$C.

8.2.3 Membrane preparation

The dry-stretching method was used to prepare the microporous membranes as follows [18]:

The precursor films with a thickness, width and length of 30 μm, 8 cm, and 4 cm, respectively, were first annealed at 120 °C for 30 min. Then, the annealed samples were cold and hot stretched to different stretch ratios at room temperature and various hot stretching temperatures, respectively. Both annealing and stretching were performed using an Instron machine (ElectroPlus ^{TM} E3000) equipped with an environmental chamber.

8.2.4 Film and membrane characterization

8.2.4.1 Fourier transform infrared spectroscopy (FTIR)

For FTIR measurements, a Perkin Elmer infrared spectrometer with a spectral resolution of 4 cm^{-1} and a scanning rate of 32 kHz, was used. The data were collected in the range from 4000 to 600 cm^{-1}. The crystalline orientation, based on the difference in absorption of the plane-polarized radiation, was measured using a polarized radiation in parallel and perpendicular to the stretching machine direction (MD) in the transmission-FTIR mode. The Herman orientation function was calculated according to [2]:

$$f = \frac{D-1}{D+2} \tag{8-1}$$

where D is the dichroic ratio and defined as the ratio of the absorbencies parallel and perpendicular to MD at the specific vibration used. For PP, the absorption at the wavelength of 998 cm^{-1} is attributed to the crystalline phase only and can be used to obtain the crystalline orientation function, f_c.

8.2.4.2 X-Ray diffraction (XRD)

Wide angle X-ray diffraction (WAXD) measurements were performed using a Bruker D8 Discover equipped with a Hi-STAR two-dimensional area detector. The generator was set up at 40 kV and 40mA. A Cu source was used (K_α energy of 8.04 keV and wavelength of 1.542 Å) with a graphite monochromator. The detector was fixed at 9.95 cm distance from the sample. To get the maximum diffraction intensity, several layers of the film were stacked together to obtain the total thickness of about 2 mm.

The SAXS patterns were collected via a Bruker AXS Nanostar system. The instrument is equipped with a Microfocus Copper Anode at 45 kV / 0.65 mA. The MONTAL OPTICS and a VANTEC 2000 2D detector were located at 107.2 mm distance from the samples. The distance

was calibrated with a Silver Behenate standard prior to the measurements while four layers of the film were stacked together.

8.2.4.3 Differential scanning calorimetry (DSC)

Thermal properties of the specimens were analyzed using a TA Instruments differential scanning calorimeter (DSC) Q 1000. Samples were heated from 50 to 220 ºC at a heating rate of 10 °C/min.

8.2.4.4 Mercury intrusion porosimetry (MIP)

The porosity and pore distributions of the membranes were evaluated using an AutoPore IV 9500 mercury intrusion porosimeter developed by Micromeritics Instrument Corporation.

8.2.4.5 Water vapor transmission rate (WVTR)

The permeability to water vapor was measured via a MOCON PERMATRAN-W Model 101K at room temperature. The equipment is composed of three chambers. An upper chamber, which is separated from the center chamber by two porous films, contains liquid water. The center chamber is separated from the lower one by the test film. The water vapor diffuses from the first film to fill the space between the films (standard guard and test films), and is swept away by N_2 gas to a relative humidity (RH) sensor.

8.2.4.6 Morphology

The microporous membrane surfaces and cross-sections were observed using scanning electron microscopy (SEM). The samples were coated with a gold-palladium alloy and electron micrographs were then taken using a Hitachi (S4700) microscope operated at 2 kV accelerating voltage. To clearly observe the cross-sections of the samples, the specimens were cut in liquid nitrogen along the machine direction and then analyzed by SEM.

8.2.4.7 Tensile properties

Tensile tests were performed on the precursor films using an Instron universal tensile machine (Model 3365) with 500 N load-cell at room temperature. The tensile specimens having a rectangular geometry of 25 mm wide and 50 mm long were stretched at different cross-head speeds.

8.3 Results and discussion

8.3.1 Characterization of the PP precursor films

Orientation and arrangement of the crystal lamellae of the precursor films are the key factors in controlling the properties of the microporous membranes.[2, 7, 9] Therefore, WAXD and SAXS measurements were performed to examine the crystalline structure of the PP precursor films.

Figure 8-1a illustrates the WAXD patterns of the PP precursor films. The first and second rings of the pole figures show the patterns for the 110 and 040 crystalline planes, respectively.[2, 9] The normal to the 110 plane is the bisector of the *a* and *b* axes and 040 is along the *b*-axis of crystal unit cells [5]. The intense and sharp arcs in the equatorial zones imply high orientation and alignment for the crystal lamellae.[18] Furthermore, the large crystalline orientation factor obtained from FTIR test (f_c=0.55), which is larger than 0.3[10], confirms and suggests that the precursor film has a row-nucleated morphology suitable for the formation of a porous membrane.

Figure 8-1b presents the 2D SAXS pattern for the PP precursor films, which has a shish-kebab structure. The equatorial streak in the SAXS pattern is attributed to the formation of shishes aligned in MD, while the meridian maxima are attributed to lamellae or kebabs perpendicular to MD.[2] The long period distance, L_p, which is the thickness of the crystalline

lamellae plus amorphous interlayer have been estimated from Bragg's law[15] and found to be 14.11 nm for the precursor film. SAXS is also extensively used to identify morphologies from the sequence of Bragg reflections observed and the positions of the peaks in the structure.[15, 19] The localisation of the observed reflections in the SAXS data (Lorentz corrected SAXS intensity profiles), i.e., *nq* in which *n* =1, 2, 3, (not shown here), indicates that our system has a lamellar structure.

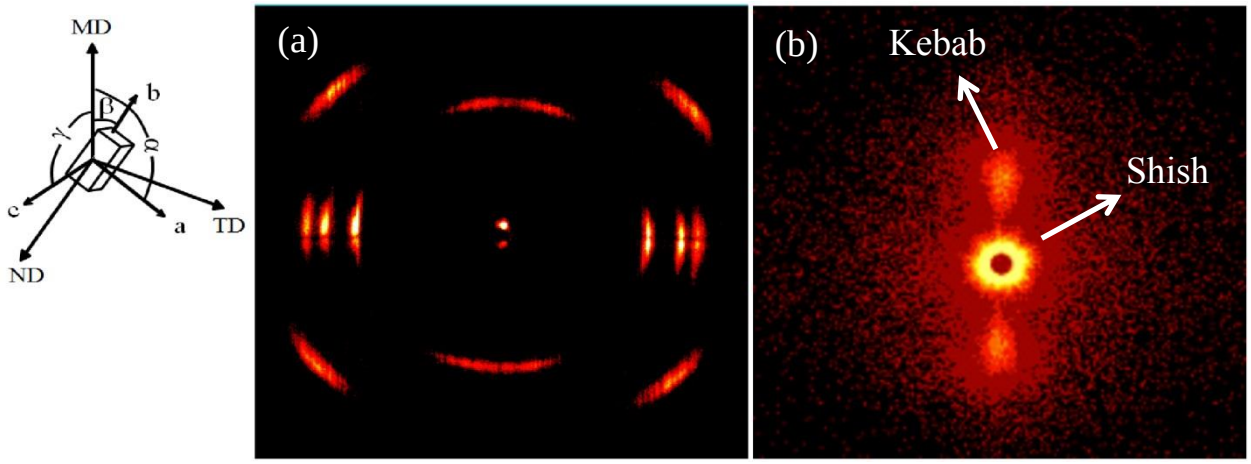

Figure 8-1: (a) WAXD patterns and (b) SAXS patterns of the PP precursor films, the schematic on the left represents the film production axes and crystal block coordinates.

8.3.2 Effect of strain rate on the membrane morphology and performance

It is well established that the structure of the crystalline and amorphous phases strongly influence the mechanical properties of the precursor films.[9, 16, 20] These macroscopic properties are known to depend on strain rate.[21] Thus, tensile tests at different strain rates were carried out to analyze the response of the annealed precursor films along MD and the results are presented in Figure 8-2. As pointed out earlier, annealing has a significant impact on the crystalline structure by creating new secondary lamellae in the amorphous region. This leads to improvements of the mechanical properties of the films.[15] Two yield points (double yield) are observed for annealed

films and are probably due to the presence (and thickness) of the newly formed secondary crystalline lamellae. The deformation mechanisms at both yield points can be generally associated with fine and coarse chain slips. The fine chain slip, at the first yield point, is combined with a transformation and rearrangement within the lamellae, which are being oriented in the stretching direction without breaking. However, coarse chain slip results in lamellae fragmentation upon stretching at the second yield point.[4, 7, 22] In fact, the second yield point could be related to the deformation of the secondary crystalline lamellae.[15] However, the size of the secondary lamellae is small and cannot remain stable under high stresses.

Pores are formed in the precursor films by cold stretching and enlarged by subsequent hot stretching[4] as a consequence of inter lamellar separation. It can be seen from Figure 8-2 that increasing strain rate shifts the curves to larger stresses. Therefore, a lower stress is required to achieve the strain of 35% (used during the cold stretching step) stretching at 5 mm/min. This can be explained in terms of the decreasing molecular motion with increasing strain rate,[8, 23, 24] which results in changing the pore formation behavior as discussed below.

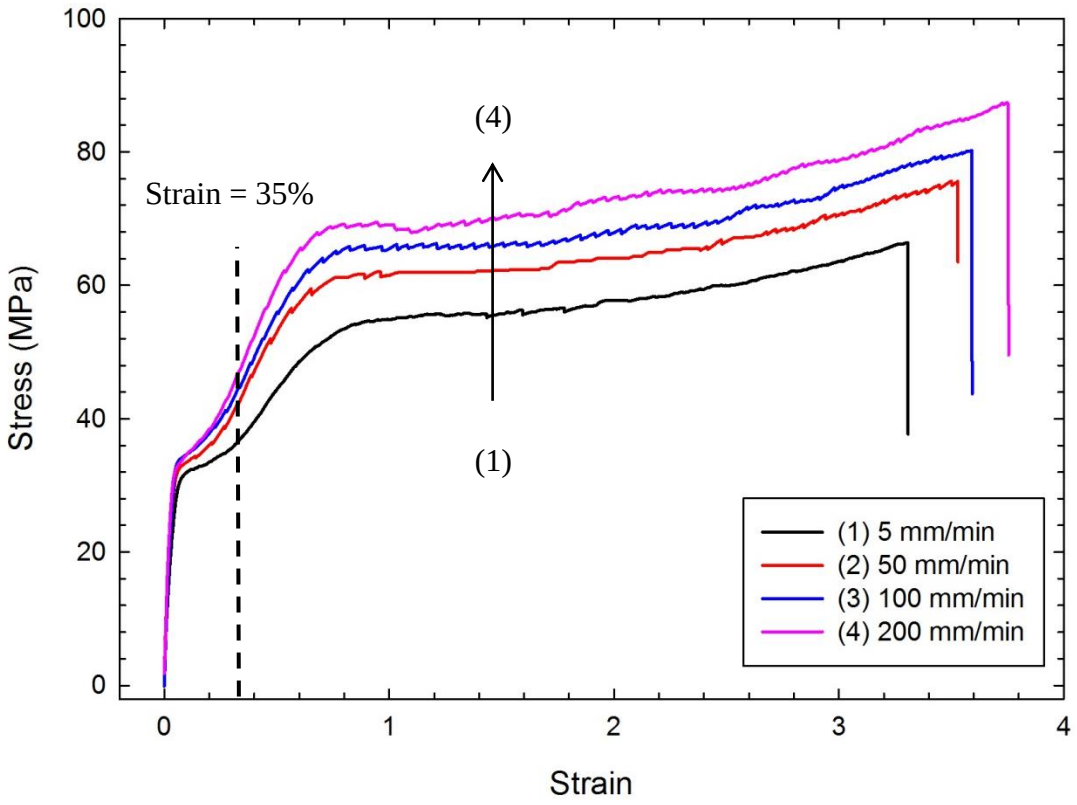

Figure 8-2: Stress–strain curves along MD of the annealed precursor films at different strain rates.

Figure 8-3 illustrates SEM micrographs of the cross-section of the precursor films after cold stretching only at different strain rates. The annealed samples were cold stretched up to 35% of their initial length and heated up to 120 °C for 2 min to fix the pore structure. The figure shows clearly that applying a lower strain rate produces a larger pore number and more interconnectivity of the pores along the thickness, which can be attributed to more lamellae separation. In fact, the interconnection between the pores determines the effective pore diameter and the membrane performance.[16]

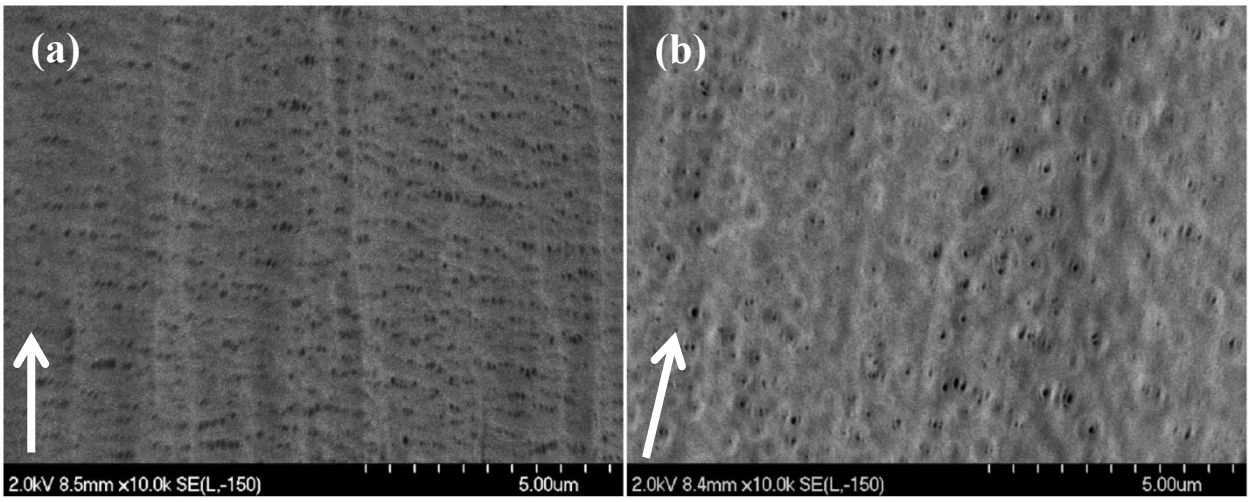

Figure 8-3: SEM micrographs of the cross-section of the precursor films after cold stretching only up to 35% of their initial length at (a) strain rate = 5 mm/min and (b) strain rate = 200 mm/min, (the arrows indicate the stretching machine direction).

Figure 8-4 reveals that the water vapor permeability of the precursor films after cold stretching only increases predominantly with strain rate up to 50 mm/min, whereas larger strain rates have little additional impact. An explanation could be that a larger number of pores and better interconnectivity of the pores across the thickness are obtained when applying a low strain rate (see Figure 8-3). Figure 8-4 presents water vapor permeability of the produced microporous membranes. The membranes produced at a 5 mm/min strain rate exhibit larger permeability values compared with those formed at the larger strain rates. As mentioned above, applying a low strain rate during the cold stretching step enhances the lamellae separation due to the creation of more pores, higher porosity and better interconnection between the pores. Thus, applying hot stretching enlarges all initiated pores and, consequently, raises permeability. It is also observed that increasing strain rate above 50 mm/min decreases the permeability slightly. This indicates again that the pore structure does not change dramatically for strain rates larger

50 mm/min. Furthermore, the effect of the heating time during the hot stretching step on the permeability of the microporous membranes was investigated and some membranes obtained at 200 mm/min were kept 5 min longer under high temperature (120 °C) before and after the hot stretching step. No noticeable changes were observed in the WVTR results. This suggests that the decreasing trend for the microporous membranes observed in Figure 8-4 is clearly related to the strain rate.

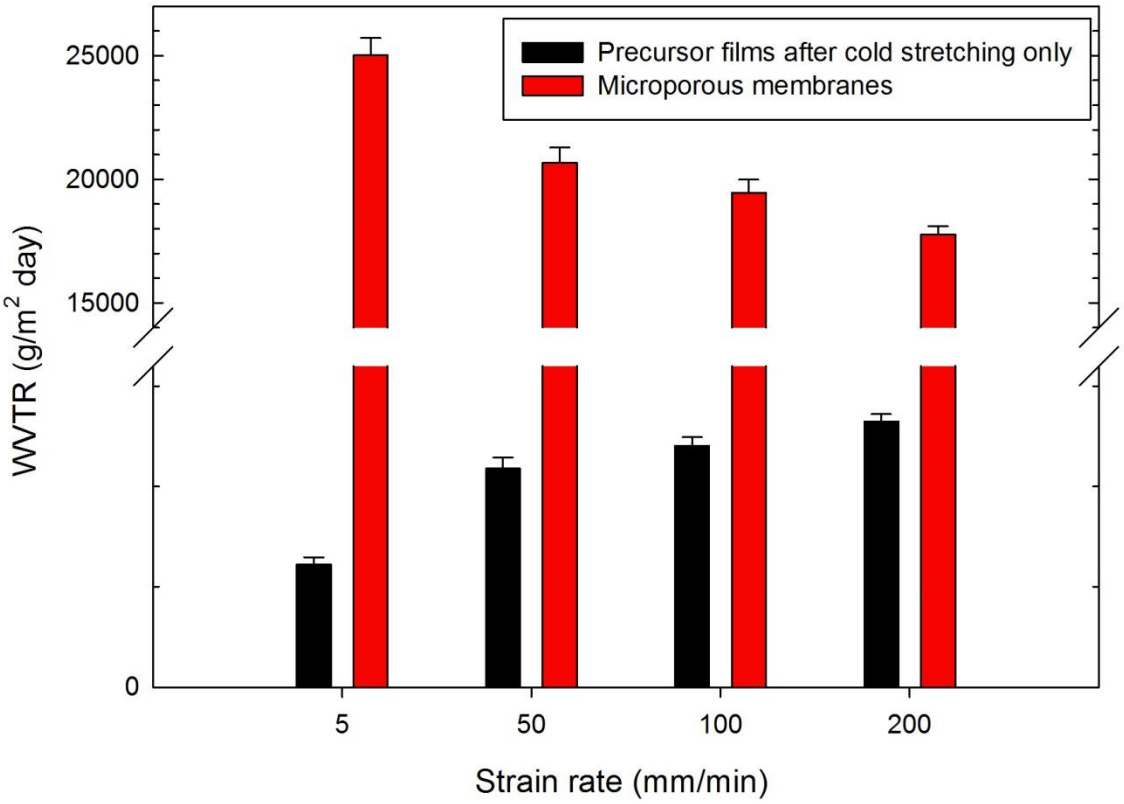

Figure 8-4: Water vapor transmission rate as a function of strain rate for the precursor films after cold stretching only up to 35% of their initial length and microporous membranes obtained from cold stretching of 35% followed by hot stretching of 60%.

Figure 8-5 presents SEM micrographs of the surface and cross-section of the developed microporous membranes at different strain rates. It is clear that the size and number of the pores

in the membrane prepared at the lower strain rate (Figures 8-5a) are much larger than those obtained at the larger strain rate (Figures 8-5b). We believe that applying a lower strain rate during stretching steps yields a better lamellae separation and interconnectivity of the pores, as can be observed in Figure 8-5a2 compared to Figure 8-5b2.

Results of the mercury porosimetry analysis for the microporous membranes made of the neat PP0.8 and blend of PP2.8 containing 2wt % PP-g-AA at different strain rates are reported in Table 1. We observe that the total pore area and average pore diameter decrease with strain rates, which is in agreement with the SEM results. Furthermore, porosity values of 35.7 and 28.3% were obtained for neat PP0.8 samples stretched at 5 and 200 mm/min, respectively. The increasing porosity for a membrane prepared at lower strain rate is attributed to a lower resistance to lamellae separation, which results in more pore interconnections.[2, 11, 16] Therefore, the SEM observations and mercury porosimetry results support the permeability data. The similar trends were observed for the blend sample with lower molecular weight (M_w) PP matrix and containing polar groups on its surface.

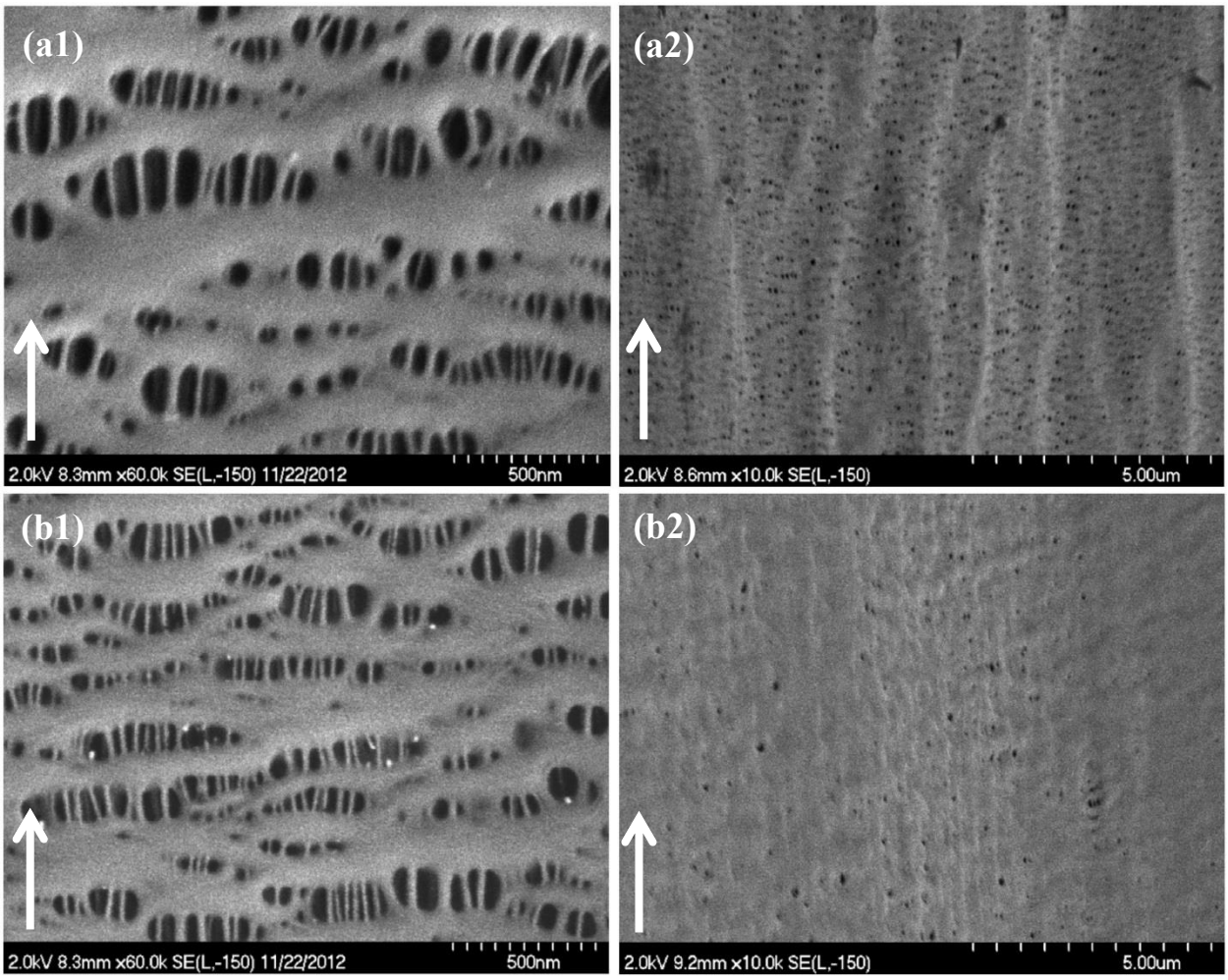

Figure 8-5: SEM micrographs of the surface (left images) and cross-section (right images) of the microporous membranes prepared at (a) strain rate = 5 mm/min and (b) strain rate = 200 mm/min; cold stretching of 35% followed by hot stretching of 60%, (the arrows indicate the stretching machine direction).

Table 8-1: Results of the mercury porosimetry for the microporous membranes.

	Total pore area (m^2/g)	Average pore diameter (nm)	Porosity (%)
PP0.8 @ 5 mm/min	28.7	90	35.7
PP0.8 @ 200 mm/min	23	81	28.3
PP2.8+PPAA20 (2wt%) @ 5 mm/min	22.5	85	26.6
PP2.8+PPAA20 (2wt%) @ 200 mm/min	15.2	65	19

8.3.3 Effect of cold and hot stretch ratio on the membrane morphology and performance

To find the optimum cold stretch ratio, cold drawing was carried out for different stretch ratios while hot stretching was kept constant at 60%. Figure 8-6 reports water vapor transmission rate (WVTR) of microporous membranes as a function of the applied cold stretch ratio for the PP porous membranes. According to Figure 8-2, 15-50% stretch ratios are between the first and second yield points, 75% stretch ratio is the one corresponding to the second yield point, 100% stretch ratio is after the second yield point and before strain hardening and 250% stretch ratio occurs during strain hardening. It is obvious that by applying 25-50% stretch ratios during cold stretching, the lamellae began to separate and an increased stretch ratio enlarged the pore size; while further stretching resulted in a reduction of WVTR. It is believed that the continuous increase in the stretch ratio after the second yield point during the cold stretching step caused lamellae fragmentation [15]. This results in a reduction of the crystal alignment and collapse of the pore structure. Furthermore, it is observed that 15% stretch ratio, compare to 25-50% stretch ratios, was not enough to initiate pores formation. It was also found that membranes prepared by hot stretching only exhibit lower permeability values. Its WVTR value was 140 times lower than

membranes obtained from 35% cold stretch ratio followed by 60% hot stretch ratio; while, it was 6 times lower than the precursor films prepared from cold stretching only (see Figure 8-4). These results indicate that the cold stretching step plays an important role in the preparation of microporous membranes.

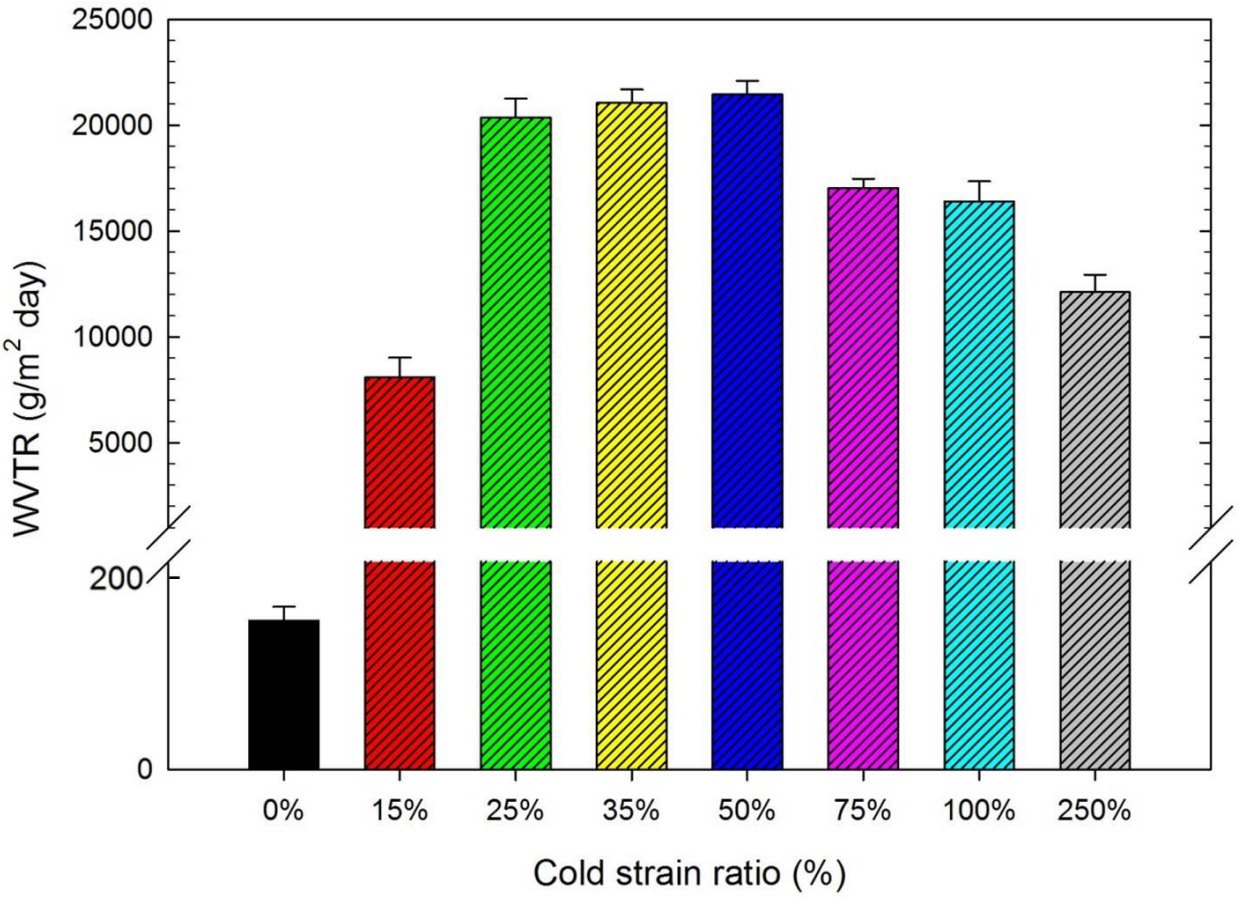

Figure 8-6: Water vapor transmission rate as a function of cold stretch ratio, hot stretching of 60% and strain rate = 50 mm/min.

The surface morphology of the developed membranes at different cold stretch ratios was investigated using SEM and the images are presented in Figure 8-7. For the membrane prepared without the cold stretching step (Figure 8-7a) a more uniform pore size and better morphology

are observed. This behavior will be explained below. Comparing the surface of the membrane prepared at different cold stretch ratios (see Figures 8-7 b-f), the size and number of pores are found to increase up to a strain of 50% and then decrease. This confirms the water vapor permeability results.

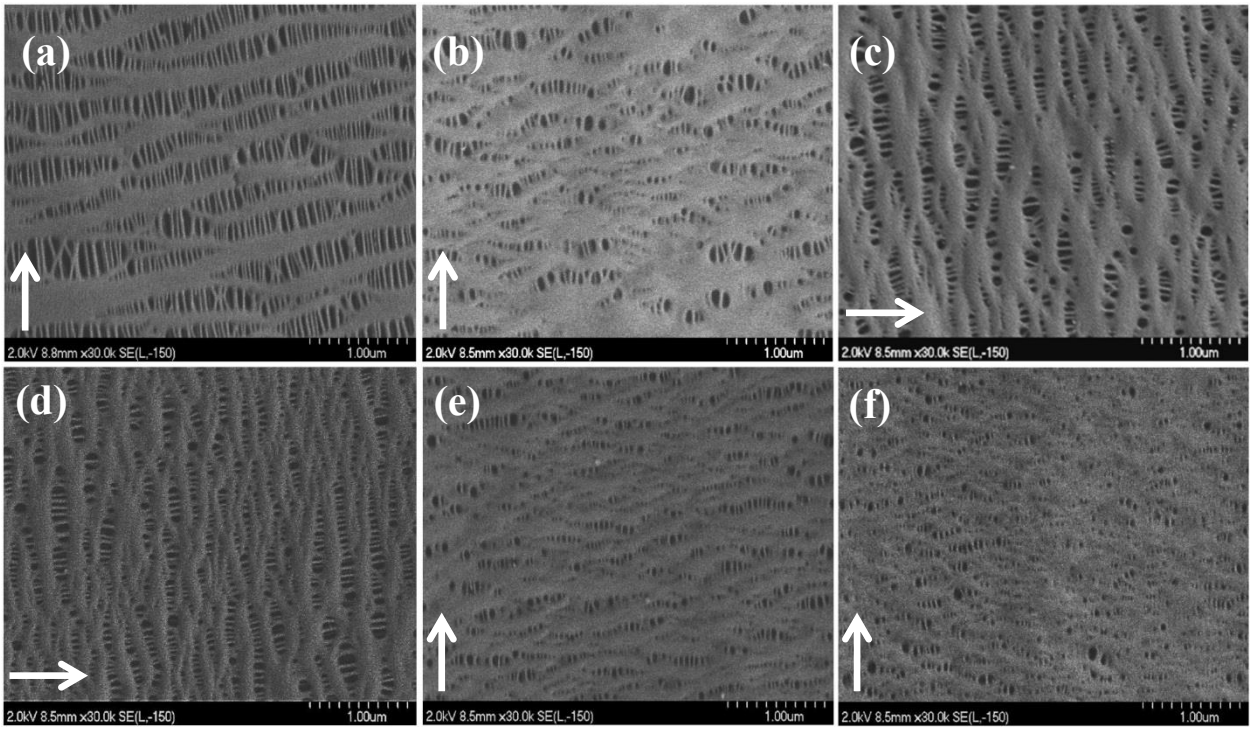

Figure 8-7: SEM micrographs of the surface of the microporous membranes as a function of cold stretch ratio, (a) 0%, (b) 15%, (c) 35%, (d) 50%, (e) 100%, (f) 250%; hot stretching of 60% and strain rate = 50 mm/min, (the arrows indicate the stretching machine direction).

In order to explain the WVTR data and SEM image of the precursor film after hot stretching only (Figures 8-6 and 8-7a), the pore structure along its thickness were observed. Compared with the micrographs of the cross-section for the precursor films after cold stretching only and the microporous membranes (Figure 8-3 and Figures 8-5 a2-b2), Figure 8-8a shows larger pore size and lower number of the pores across the thickness, resulting in a lower interconnectivity of the pores. This is attributed to the less efficient lamellae separation, resulting

in a lower porosity as well as smaller WVTR values.[4] The effect of the cold stretching step on the pore size distribution and porosity was also considered using mercury porosimetry data, as illustrated in Figure 8-8b. It is known that the mercury intrusion volume is directly related to the pore size and porosity due to interconnected pores.[16] The results show that applying the cold stretching step increases dramatically the area under the curve, indicating that the number of pores and the porosity increase.[2] A porosity value of 6 % was obtained for the membranes prepared with hot stretching only (60%) compared 31.5 % for the membrane prepared by cold stretching of 35% followed by hot stretching of 60%. This supports the observed information in the SEM images and water vapor permeability results and suggests again that cold stretching is an important step for developing microporous membranes.

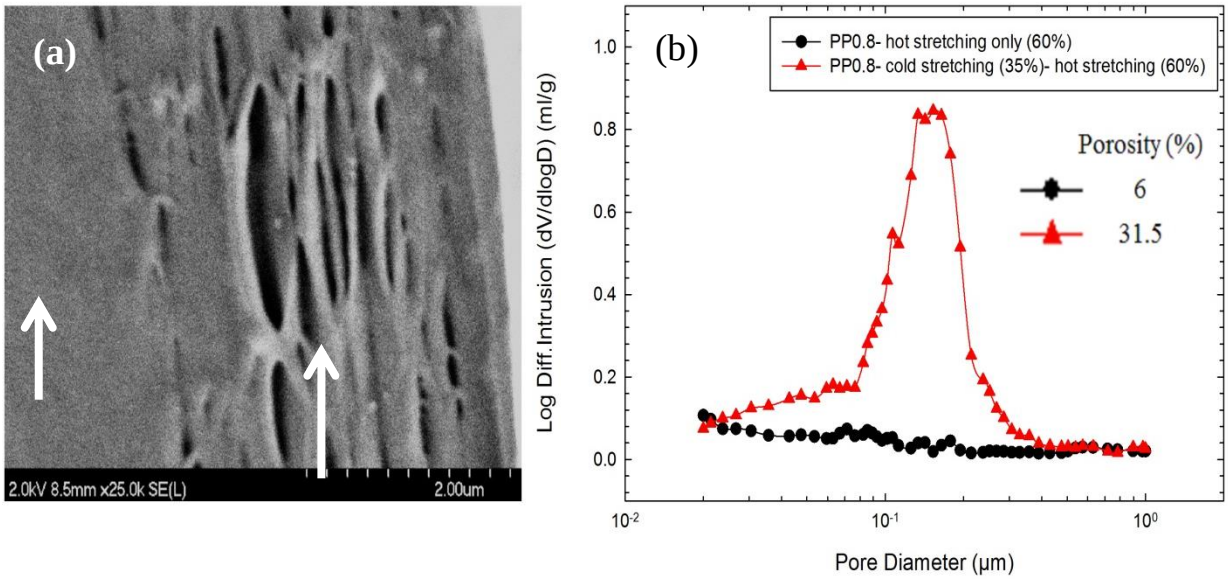

Figure 8-8: (a) SEM micrographs of the cross-section of the precursor film after hot stretching only (60%), (the arrows indicate the stretching machine direction), and (b) pore size distribution via MIP for the membranes obtained using two different stretching conditions; (the legend shows the porosity values), strain rate = 50 mm/min.

In this section, the influence of the hot stretch ratio was investigated while the cold stretch ratio was kept constant at 35%. Figure 8-9 illustrates the surface morphology of membranes prepared at different hot stretch ratios. Very large pores can be observed for the samples prepared at high stretch ratios, which could be attributed to the higher flexibility of the amorphous and tie chains at high temperatures, resulting in an easier lamellae separation. In contrast to the cold stretching behavior, no maximum is observed in the permeability results as shown in Figure 8-10a. The continuing increase of pore size with increasing stretch ratio (see Figure 8-9) can explain the improvement of the permeability results of Figure 10a.

DSC results for the microporous membranes prepared at different hot stretch ratios are presented in Figure 8-10b. Two types of the lamellae distribution are expected after stretching the precursor films. One of those corresponds to crystals with interconnected bridges between the lamellae (I) and the other reflects the lamellae crystals (C). The interconnected bridges are formed from stretching the tie chains situated between the lamellae during the cold and hot stretching steps.[15, 16] This means that the interconnected bridges act like shish crystals and have a melting temperature of about 5–10 °C higher than that of lamellae crystals (kebabs).[16, 25, 26] The presence of a double melting peak in the membrane prepared at the larger stretch ratio compared to that prepared at the lower ones is believed to be related to the formation of a larger number of interconnected bridges. Therefore, the interconnected bridges to the lamellae crystals ratio (I/C) would be increased, and a double melting peak is obtained.

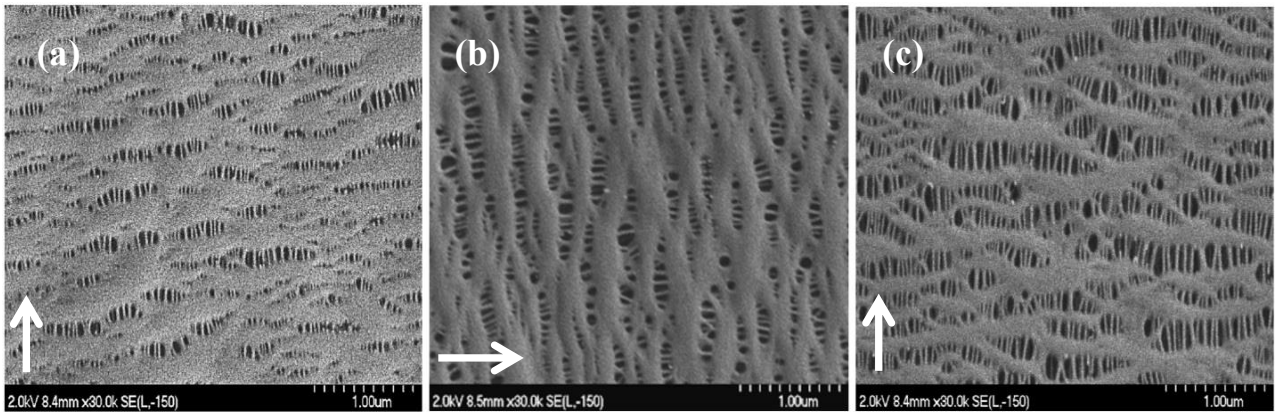

Figure 8-9: SEM micrographs of the surface of the microporous membranes as a function of hot stretch ratio at 120 °C, (a) 30%, (b) 60%, (c) 100%; cold stretching of 35% and strain rate = 50 mm/min, (the arrows indicate the stretching machine direction).

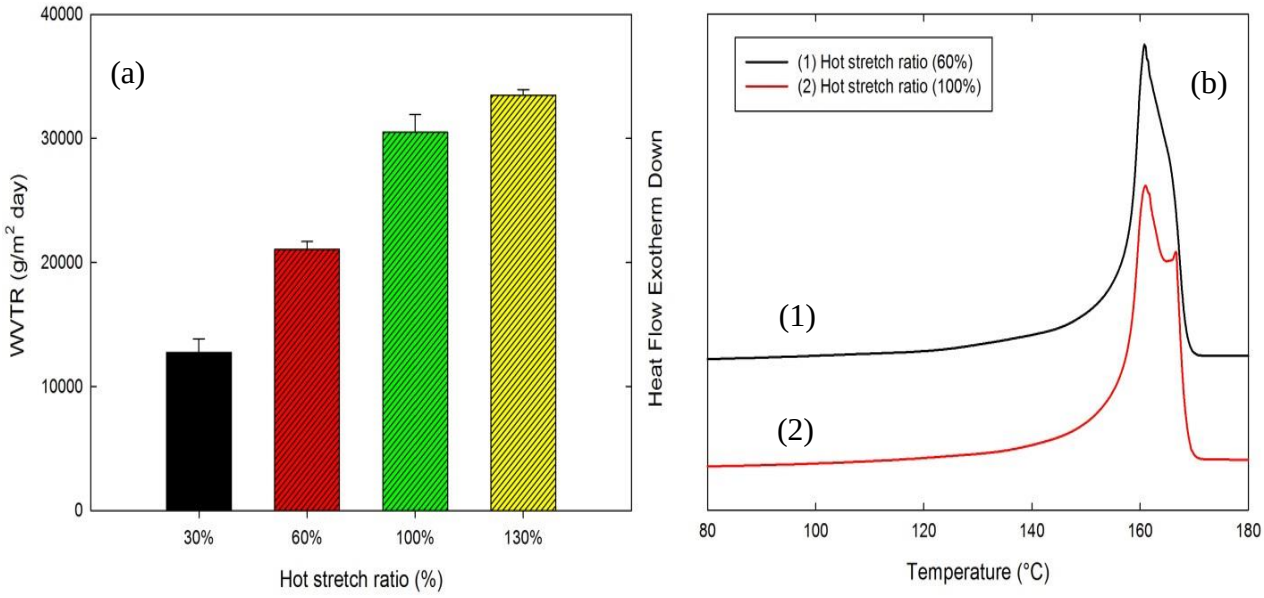

Figure 8-10: (a) Water vapor transmission rate and (b) DSC thermograms of the membranes prepared under different hot stretch ratios at 120 °C; cold stretching of 35% and strain rate = 50mm/min.

8.3.4 Effect of hot stretching temperature on the membrane morphology and performance

The effect of hot stretching temperature on microporous membranes obtained at 35% cold stretch ratio followed by 60% hot stretching was investigated, while the strain rate was maintained at 50 mm/min. The results of permeability tests and SEM observations are presented in Figures 8-11 and 8-12, respectively. They show that increasing the hot stretching temperature increases the permeability as a result of increasing the size and number of pores. It was also found that hot stretching at 140 °C yields longer interconnected bridges. This is believed to be due to the higher flexibility of the amorphous and tie chains at higher temperature.

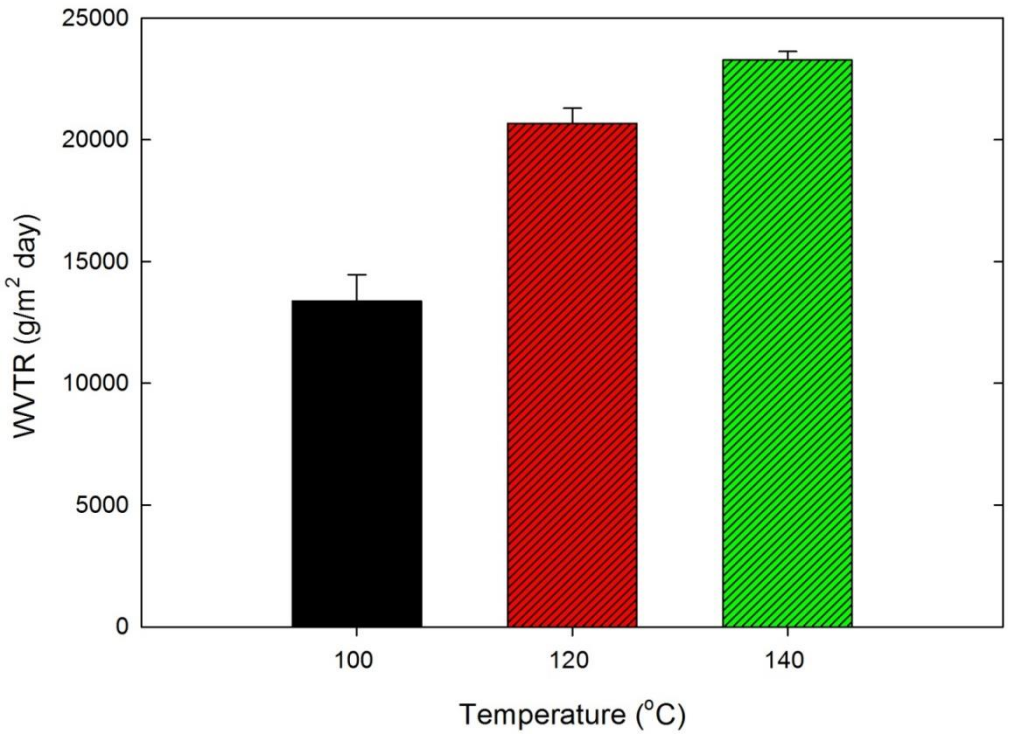

Figure 8-11: Water vapor transmission rate as a function of hot stretching temperature; cold stretch ratio of 35% followed by hot stretch ratio of 60% and strain rate = 50mm/min.

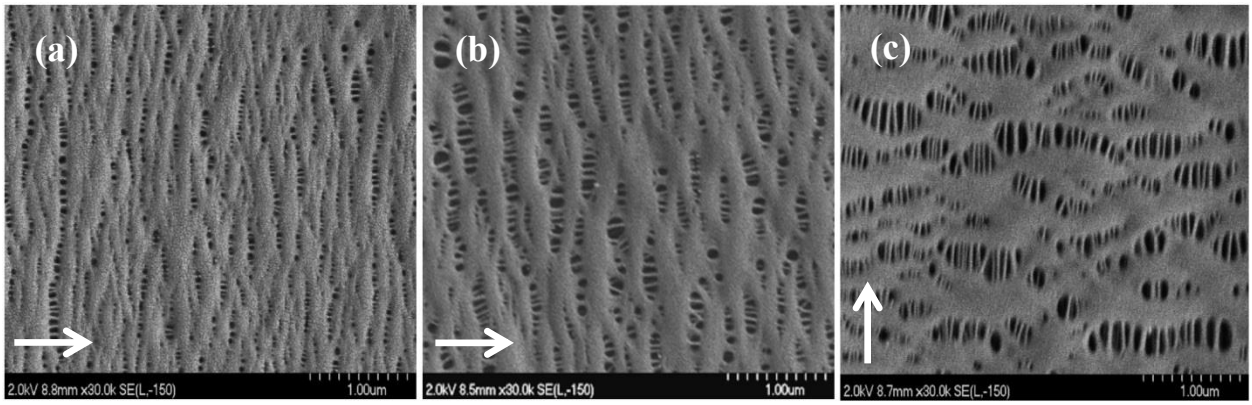

Figure 8-12: SEM micrographs of the surface of the microporous membranes as a function of hot stretching temperatures, (a) 100 °C, (b) 120 °C, (c) 140 °C; cold stretch ratio of 35% followed by hot stretch ratio of 60% and strain rate = 50mm/min, (the arrows indicate the stretching machine direction).

8.4 Conclusions

In this work, we investigated the influence of the stretching variables on the pore structure and performance of microporous membrane made from polypropylene based film. Our findings can be summarized as follows:

Microporous membranes having larger porosity, high pore density and, consequently, larger water vapor permeability values were obtained by stretching at low strain rate. This was attributed to a better lamellae separation and more interconnectivity of the pores.

Compared to membranes prepared without cold stretching, the permeability of the membranes obtained from 35% cold stretch ratio (under the same conditions) increased by a factor of 140. This indicates that the cold stretching step plays an important role in the preparation of microporous membranes.

The stretch ratio for the cold stretching step should be chosen below the strain corresponding to the second yield point of the polymer. Beyond that, non-uniform pores and a small number of pores were observed. This resulted in lamellae fragmentation and collapse of the pore structure.

Compared to the cold stretching step, no maximum was observed in the permeability results by increasing the hot stretch ratio, which was confirmed by SEM images. Also, by increasing the hot stretching temperature, pore size and permeability values increased. This could be due to the higher flexibility of the amorphous phase and tie chains at high temperatures, which resulted in more lamellae separation.

The effects of stretching for a blend membrane of PP containing 2 wt % of PP-g-PAA were very similar to those observed for the neat PP membrane.

8.5 Acknowledgments

Financial support from NSERC Network for Innovative Plastic Materials and Manufacturing Processes (NIPMMP) is gratefully acknowledged. We are also thankful to Ms. Sylvie St-Amour and Ms. Sylvie Sauriol from FP Innovations (Paprican Division) for the use of and training on their AutoPore IV mercury intrusion porosimeter.

8.6 Reference

(1) Gérard, E.; Bessy, E.; Salvagnini, C.; Rerat, V.; Momtaz, M.; Hénard, G.; Marmey, P.; Verpoort, T.; Marchand-Brynaert, J. Surface modifications of polypropylene membranes used for blood filtration. *Polymer*. **2011**, *52*, 1223.

(2) Tabatabaei, S.H.; Carreau, P.J.; Ajji, A. Microporous membranes obtained from polypropylene blend films by stretching. *J. Membr. Sci.* **2008**, *325*, 772.

(3) Xu, M.; Shi, X.; Chen, H.; Xiao, T. Synthesis and enrichment of a macromolecular surface modifier PP-b-PVP for polypropylene. *Appl. Surf. Sci*. **2010**, *256*, 3240.

(4) Tabatabaei, S.H.; Carreau, P.J.; Ajji, A. Microporous membranes obtained from PP/HDPE multilayer films by stretching. *J. Membr. Sci.* **2009**, *345*, 148.

(5) Tabatabaei, S.H.; Carreau, P.J.; Ajji, A. Structure and properties of MDO stretched polypropylene. *Polymer*. **2009**, *50*, 3981.

(6) Sadeghi, F.; Ajji, A.; Carreau, P.J. Analysis of row nucleated lamellar morphology of polypropylene obtained from the cast film process: Effect of melt rheology and process conditions. *Polym. Eng. Sci.* **2007**, *47*, 1170.

(7) Liu, D.; Kang, J.; Xiang, M.; Cao, Y. Effect of annealing on phase structure and mechanical behaviors of polypropylene hard elastic films. *J. Polym. Res*. **2013**, *20*, 1.

(8) Offord, G.T.; Armstrong, S.R.; Freeman, B.D.; Baer, E.; Hiltner, A.; Paul, D.R. Influence of processing strategies on porosity and permeability of β nucleated isotactic polypropylene stretched films. *Polymer*. **2013**, *54*, 2796.

(9) Tabatabaei, S.H.; Carreau, P.J.; Ajji, A. Effect of processing on the crystalline orientation, morphology, and mechanical properties of polypropylene cast films and microporous membrane formation. *Polymer*. **2009**, *50*, 4228.

(10) Sadeghi, F.; Ajji, A.; Carreau, P.J. Study of Polypropylene Morphology Obtained from Blown and Cast Film Processes: Initial Morphology Requirements for Making Porous Membrane by Stretching. *J. Plast. Film. Sheet*. **2005**, *21*, 199.

(11) Sadeghi, F.; Ajji, A.; Carreau, P.J. Microporous membranes obtained from polypropylene blends with superior permeability properties. *J. Polym. Sci., Part B: Polym. Phy*. **2008**, *46*, 148.

(12) Kim, J.; Kim, S.S.; Park, M.; Jang M. Effects of precursor properties on the preparation of polyethylene hollow fiber membranes by stretching. *J. Membr. Sci*. **2008**, *318*, 201.

(13) Huang, L.T.; Hsu, P.S.; Kuo, C.Y.; Chen, S.C.; Lai, J.Y. Pore size control of PTFE membranes by stretch operation with asymmetric heating system. *Desalination*. **2008**, *233*, 64.

(14) Caihong, L.; Shuqiu, W.; Ruijie, X.; Xinlong, P.; Wenqiang, S.; Bing, H. Influence of low molecular weight tail of polypropylene resin on the pore structure by room-temperature stretching. *Polym. Eng. Sci.* **2013**, *53*, 2594.

(15) Saffar, A.; Ajji, A.; Carreau, P.J.; Kamal, M.R. The Impact of New Crystalline Lamellae Formation during Annealing on the Properties of Polypropylene Based Films and Membranes. *Polymer*. http://dx.doi.org/10.1016/j.polymer.2014.05.017

(16) Sadeghi, F.; Ajji, A.; Carreau, P.J. Analysis of microporous membranes obtained from polypropylene films by stretching. *J. Membr. Sci*. **2007**, *292*, 62.

(17) Caihong, L.; Shuqiu, W.; Ruijie, X.; Qi, C.; Bing, H.; Xinlong, P.; Wenqiang, S. Formation of stable crystalline connecting bridges during the fabrication of polypropylene microporous membrane. *Polym. Bull.* **2013**, *70*, 1353.

(18) Saffar, A.; Carreau, P.J.; Ajji, A.; Kamal, M.R. Development of polypropylene microporous hydrophilic membranes by blending with PP-g-MA and PP-g-AA. *J. Membr. Sci*. **2014**, *462*, 50.

(19) Hamley, I.W.; Castelletto, V. Small-angle scattering of block copolymers: in the melt, solution and crystal states. *Prog. Polym. Sci.* **2004**, *29*, 909.

(20) Zhang, X.M.; Ajji, A. Oriented structure of PP/LLDPE multilayer and blends films. *Polymer*. **2005**, *46*, 3385.

(21) Sahin, S.; Yayla, P.; Effects of testing parameters on the mechanical properties of polypropylene random copolymer. *Polym. Test*. **2005**, *24*, 613.

(22) Schrauwen, B.A.G.; Janssen, R.P.M.; Govaert, L.E.; Meijer, H.E.H. Intrinsic Deformation Behavior of Semicrystalline Polymers. *Macromolecules*. **2004**, *37*, 6069.

(23) Mulliken, A.D.; Boyce, M.C. Mechanics of the rate-dependent elastic–plastic deformation of glassy polymers from low to high strain rates. *Int. J. Solids. Struct.* **2006**, *43*, 1331.

(24) Richeton, J.; Ahzi, S.; Vecchio, K.S.; Jiang, F.C.; Adharapurapu, R.R. Influence of temperature and strain rate on the mechanical behavior of three amorphous polymers: Characterization and modeling of the compressive yield stress. *Int. J. Solids. Struct.* **2006**, *43*, 2318.

(25) Sadeghi, F.; Tabatabaei, S.H.; Ajji, A.; Carreau, P.J. Properties of uniaxially stretched polypropylene films: effect of drawing temperature and random copolymer content. *Can. J. Chem. Eng.* **2010**, *88*, 1091.

(26) Somani, R.H.; Yang, L.; Zhu, L.; Hsiao, B.S.; Flow-induced shish-kebab precursor structures in entangled polymer melts. *Polymer*. **2005**, *46*, 8587.

CHAPTER 9 GENERAL DISCUSSION

To produce microporous membranes by the stretching technique, one must obtain precursor films with an adequate orientation and alignment of the crystal lamellae. The process for the formation of such a lamellar structure is based on the elongation of the chains in the melt state followed by a rapid crystallization. It has been pointed out for most of the researchers working in this field that the higher the crystalline alignment in the precursor film, the better is expected the lamellae separation and, as a consequence, the larger the porosity and permeability of the microporous membranes. However, the intrinsic hydrophobic character of the polymer limits its applications as membranes separator and leads to the irreversible membrane fouling. The presence of polar groups in the precursor film and membrane surface can form hydrogen bonds with the surrounding water molecules and produce a water boundary on the surface. Therfore, it is difficult for hydrophobic solutes to approach the water boundary and break the orderly structure due to the energy required to remove the water boundary and expose the membrane surface. Also, presence of those polar groups increase wettability of the surface. However, hydrophobic materials have higher mechanical and chemical stability than hydrophilic materials, which are used in membrane applications. Thus, the ideal membrane would combine the superior bulk properties of hydrophobic materials with the surface chemistry of hydrophilic materials.

Several techniques such as plasma treatment, coating and grafting method to improve the membrane surface have been extensively reported in the literature. But, these techniques usually result in economical or recycling issues. Blending hydrophilic modifier with hydrophobic matrix is another potential method which has attracted a great attention over years. It is known that the crystalline structure of the precursor film and consequently, the porosity and pore size of the membrane is decreased by blending with low molecular weight polymers or blending with an

immiscible and incompatible polymer. This behavior could be due to the reduction in chain regularity. A minimum crystalline orientation factor of 0.3 (*c*-axis with respect to the machine direction) for the precursor film is necessary in order to obtain a row-nucleated morphology suitable for porous membrane formation (Sadeghi 2006). It is obvious that the chains should preserve their elongated form to be able to act as initial nuclei. The relaxation time of the chains is the most important factor for this stage. Therefore, it is important to select and blend at optimum concentrations hydrophilic modifiers in order to generate films with the desired lamellar morphology as well as having hydrophilic characteristics. The thermodynamic incompatibility between hydrophobic and hydrophilic polymers cause the hydrophilic compound release from the surface when contacted with a polar chemical solvent. Thus, the hydrophilicity achieved by blending this modifiers are not permanent and changes with time.

In the first phase of this study, amphiphilic copolymers (PP-g-MA and PP-g-AA) were used in a large range of concentrations as hydrophilic modifiers which the hydrophobic tail (PP) anchors into the PP matrix. The result showed that by increasing the modifier content, the changes in the crystalline structure, which governs the final membrane performance, might be the dominating factor for the decreased permeability. While, the enhanced permeability at low modifiers content might be mainly attributed to the improved surface hydrophilicity since the membranes possess a similar structure. Also, the addition of the modifiers did not show a dramatic effect on the mechanical properties of the precursor films and membranes along MD and ND in the range of low modifier contents. Based on these results, it was established that the polar groups of the amphiphilic modifiers can play an important role and act as surface functional groups on the precursor film surface.

It was shown that these groups can graft with other hydrophilic groups, without affecting the crystalline and pore structure. So, in order to increase even further the hydrophylic properties, in the second phase of this study, TiO2 nanoparticles was employed. There are two main approaches to prepare polymer/TiO_2 nanoparticles composite membranes: blending the nanoparticles with a polymer or dipping the prepared polymer film in a suspension of TiO_2 nanoparticles and fabricate the hydrophilic membrane via grafting. As mentioned, the crystalline structure of the precursor film is affected by blending with low molecular weight polymers. Furthermore, several studies showed that preparing polymer/TiO_2 nanoparticles composite membranes via blending results in noticeable changes in the crystalline structure and, subsequently, in the pores structure of the membranes. Therefore, the immersion method (dipping the prepared film in a suspension of TiO_2 nanoparticles) was used for grafting TiO_2 nanoparticles, with the functional groups on the surface. Strong bonds between COOH groups and TiO_2 nanoparticles at the interface of the film were confirmed by ATR-FTIR spectrum and EDS analysis, resulting in a stable hydrophilic precursor film. This method decreased significantly the water contact angle of the films (by a factor of 2.5), meanwhile the water vapor permeability of the microporous membranes prepared from those films increased without affecting the bulk properties of the matrix. As mentioned above, we used the stretching technique for fabricating microporous membranes, which includes extrusion, annealing, and stretching. It was also shown that nanoparticles were not dislodged by high temperature and stretching during the preparation of microporous membranes.

The uniaxial stretching a polymer film containing a row-nucleated lamellar structure (lamellae separation) was developed 30 years ago for some semi-crystalline polymers. It involves extrusion, annealing and stretching. However, most of the detailed information-processing

remains proprietary to the companies and is not available to the scientific community. Understanding the mechanisms is important to prepare membranes with desired performances. As mentioned, after the production of the precursor films with a proper structure and orientation, annealing, as the second step, should be performed before application of cold and hot stretching.

Two key factors in this stage are time and temperature of annealing. Annealing is performed at temperatures above the onset of mobility in the crystalline structure (T_α), and below the melting temperature of the precursor film. In order to understand the factors promoting the crystalline structures during annealing, the one-dimensional (1D) correlation function method was examined by means of SAXS technique. These measurements indicated that annealing caused formation of a secondary crystalline lamellae between the primary lamellae as well as primary kebabs thickening. So, it was shown that annealing is an effective method to improve the physical properties of semi-crystalline polymers by improving the crystalline structure. The temperature was more effective and it was found that there is an optimum time for the annealing process, beyond that, the the changed in the crystalline structure of the films and their membrane performance was only slightly. Also, the effect of the new lamellae formation on the mechanical properties of the precursor films and consequently membrane performace was investigated. The results showed that the annealed films exhibited double yield points in the tensile deformation curves. The second yield point was related to the deformation of the secondary crystalline lamellae. This information can be used to understand and control pore formation mechanisms during stretching step.

As mentioned before, in the preparation of porous membranes using the stretching technique, pores are formed by cold stretching and enlarged by subsequent hot stretching. The microporous morphologies produced via this method are a consequence of interlamellar separation, which

takes place at temperatures above T_g of the specific semi-crystalline polymers. The behavior in cold stretching, in comparison to that in hot stretching, is different since the temperature is low. In hot stretching flexibility of the amorphous phase and tie chains is higher while the crystallization can also take place. Extensive morphological analysis by means of SEM of the cross-section for the precursor films as well as porosity value using mercury porosimetry data led to conclude that cold stretching step is the important step to promote interconnection between the pores. Larger number of pores, better porosity and consequently, better permeability were obtained when applying a low strain rate, which can be attributed to more lamellae separation. The tensile deformation curves can help to undrestand and explain the reason. Lower stress required to achieve the strain corresponding to cold stretching step was observed by stretching at low strain rate. Also, the optimum stretch ratio for the cold stretching step was found to be below the strain corresponding to the second yield point of the polymer; beyond that strain, a reduction in the permeability was observed and explained in terms of lamellae fragmentation.

CHAPTER 10 CONCLUSIONS AND RECOMMENDATIONS

10.1 Conclusions

In this dissertation, the development of hydrophilic microporous polypropylene membranes through cast film extrusion followed by annealing and uniaxial stretching has been investigated. We have studied the structure and performance of the microporous membranes from blends of linear low and high molecular weight PPs with amphiphilic modifiers at different concentrations. FTIR, WAXD, and SAXS were employed to measure the orientation and lamellar long spacing of crystalline phase. Adding the amphiphilic modifiers decreased the crystalline orientation and degree of the crystallinity as a result of reduction in chain regularity. SEM micrographs of the membrane surface revealed less uniform pores and a worse distribution as the modifier content increased. But, amphiphilic copolymers, PP-g-MA and PP-g-AA, enhanced the surface hydrophilicity of PP membranes. The optimum concentration was found to be 2wt % modifier to achieve membranes having good hydrophilic characteristics, with enough polar groups on the surface and causing a minimal change in the crystalline structure compared to neat PP film. Finally, the water vapor permeability of the membranes, which reflects the pore interconnection and hydrophilicity of the surface, was checked for the blends as well as for the neat polymers and it was consistent with SEM and XPS results.

The hydrophilic segments of the amphiphilic modifiers can act as surface functional groups on the film surface and graft with other hydrophilic groups. The effects of grafted TiO_2 nanoparticles on the hydrophilicity of the PP/PP-g-AA blend microporous membranes were investigated. ATR-FTIR results confirmed that TiO_2 nanoparticles were successfully grafted on the surfaces of the precursor films during immersion method. After TiO_2 modification, the water contact angle of the

precursor films was significantly decreased and the water vapor permeability of the membranes was increased. SEM micrographs of the surface of ungrafted and TiO_2 grafted blend membranes indicated that grafting TiO_2 nanoparticles did not have a dramatic effect on the pore structure of the membranes surface.

Annealing was found to be a crucial stage for the membrane production and have a dramatic effect on the crystalline structure of the PP based film. A detailed investigation was performed to evaluate the influence of annealing conditions on the crystalline structure, morphology, and mechanical properties of cast films and formation of microporous membranes. FTIR, DSC, SAXS and mechanical analysis indicated that annealing forms secondary crystalline lamellae between the primary lamellae. The yield behavior in the stress-strain curves of the films was changed by annealing. The annealed films exhibited double yield points in the tensile deformation curves. A direct linear relationship was also found between the strength of the second yield point and the fraction of the lamellae. The strain hardening modulus and elongation at break of the precursor films were found to decrease for annealed samples. Also, 10 min was sufficient time for annealing the precursor films. Beyond that, the crystalline structure and membrane performance changed only slightly.

Microporous membranes from the films possessing well oriented shish-kebab crystal morphology were produced after annealing and subsequent stretching in the machine direction.. The pore structure along the membrane surface and across the thickness, which determined the size, number and interconnectivity of the pores, was also analyzed to quantify the effect of the stretching variables on membrane performance. Microporous membranes having larger porosity, high pore density and consequently, larger water vapor permeability values were obtained by stretching at low strain rate. Compared to membranes prepared without cold stretching, the

permeability of the membranes obtained from 35% cold stretch ratio (under the same conditions) increased by a factor of 140. This indicated that the cold stretching step plays an important role in the preparation of microporous membranes. It was found that stretch ratio for the cold stretching step should be chosen below the strain corresponding to the second yield point of the polymer. Beyond that, non-uniform pores and a small number of pores were observed. This resulted in lamellae fragmentation and collapse of the pore structure. Also, compared to the cold stretching step, no maximum was observed in the permeability results by increasing the hot stretch ratio, which was confirmed by SEM images.

10.2 Original contributions

To our knowledge, no study has been performed on the development of hydrophilic microporous membranes microporous polypropylene membranes fabricated by extrusion followed by stretching through blending with amphiphilic polymers, and grafting TiO_2 nanoparticles on its surface.

In view of our experimental results, we observed that employing low content of the amphiphilic polymers not only increased the hydrophilic properties of the membrane, but it also caused a slight change in the crystalline structure of neat PP which led to better membrane performance. The polar groups of the modifiers can act as surface functional groups on the precursor film surface for grafting with TiO_2 nanoparticles. We observed that, compared to PP and PP/PP-g-AA blend films, the water contact angle decreased by a factor of 2.5 after grafting TiO_2 onto the surface of the precursor films, meanwhile the water vapor permeability of the microporous membranes prepared from those films increased.

Little attention has been paid in the literature to the annealing of flow-oriented polymers and stretching of the precursor films, especially to the mechanisms of the microstructural changes during each individual step.

In the third part of this study we observed that annealing process created secondary lamellae in the amorphous region and the crystal morphologies of the annealed and non-annealed films were presented. It was shown that the annealed films exhibited double yield points in the tensile deformation curves which explained in term of deformation of the secondary crystalline lamellae. Also, the individual stages of the stretching step were examined in details to understand pore formation mechanisms as well as to optimize the stretching conditions. The cold stretching step was found to be the important step to promote interconnection between the pores. Furthermore, the optimum stretch ratio for the cold stretching step was found and explained using tensile deformation curves.

10.3 Recommendations

For the continuation of this work and future research, the following unexplored topics are recommended:

1) The conditions of the immersion method need to be optimized in order to decrease the grafting time.

2) Extending the grafting method to some other hydrophilic polymers. As mentioned, the hydrophilic segments of the amphiphilic modifiers can act as surface functional groups on the film surface and graft with other hydrophilic groups. Bovine serum albumin (BSA) is a protein, which is often used to evaluate the protein-resistant characteristics of the prepared membranes

(Fang et al. 2009). It is reasonable to predict that the modified membrane by BSA may have a promising future for applications in the biomedical field.

3) Some researchers (Tjong et al. 1999; Zhu et al. 2008) reported that maleic anhydride (MA) and poly(ethylene glycol) (PEG) can be grafted via esterification between anhydride and hydroxyl groups. Therefore, this new amphiphilic modifier (PP-g-MA-g-PEG) could be used as a modifier to investigate its effect on the crystalline structure and membrane performance.

4) Developing multilayer hydrophilic microporous membranes with polyoxymethylene (POM) and blends made of PP containing 2wt % of an acrylic acid grafted polypropylene (PP-g-AA). Compared to the PP film, the polyoxymethylene (POM) film is hydrophilic and possesses approximately identical annealing and melting temperatures. Amphiphilic modifiers could be used to solve the adhesion problem between POM and PP at the interface.

5) Although a few authors have investigated the modeling of crystallization of various resins under different flow magnitudes, no study has been considered the flow-induced crystallization under cooling in the cast film process. Therefore, developing a thermo-mechanical model that describes polymer crystallization and predict the final morphology of the precursor film under flow and cooling using air and cast roll is recommended.

REFERENCES

Agarwal, P. K., R. H. Somani, et al. (2003). "Shear-Induced Crystallization in Novel Long Chain Branched Polypropylenes by in Situ Rheo-SAXS and -WAXD." Macromolecules **36**(14): 5226-5235.

Aoyama, M., M. Ito, et al. (1990). Method of forming a porous polyolefin film. **US Patent 4921653**.

Bae, T.H. and T.M. Tak (2005). "Preparation of TiO2 self-assembled polymeric nanocomposite membranes and examination of their fouling mitigation effects in a membrane bioreactor system." Journal of Membrane Science **266**(1–2): 1-5.

Baker, R. W. (2004). Front Matter. Membrane Technology and Applications, John Wiley & Sons, Ltd**:** i-xiii.

Bashir, Z., J. A. Odell, et al. (1986). "Stiff and strong polyethylene with shish kebab morphology by continuous melt extrusion." Journal of Materials Science **21**(11): 3993-4002.

Bischoff White, E., H. Henning Winter, et al. (2012). "Extensional-flow-induced crystallization of isotactic polypropylene." Rheologica Acta **51**(4): 303-314.

Bongiovanni, R., B. Gagnor, et al. (1998). "Surface properties and adhesion of maleinized polyethylene films." Journal of Materials Science **33**(6): 1461-1464.

Capecchi, G., M. Faga, et al. (2007). "Adsorption of CH3 COOH on TiO2: IR and theoretical investigations." Research on Chemical Intermediates **33**(3-5): 269-284.

Chandavasu, C. (2001). Microporous polymeric membranes via melt processing'. Ph.D., New Jersey institute of technology.

Chen, H., X. Shi, et al. (2009). "Surface functionalization of polypropylene by entrapment of polypropylene-grafted-poly(ethylene glycol)." Journal of Applied Polymer Science **114**(4): 2461-2468.

Custodio, F., R. J. A. Steenbakkers, et al. (2009). " Model development and validation of crystallization behavior in injection molding prototype flows." Macromolecular Theory and Simulations **18**(9): 469-494.

Dang, T. H. (2009). Surface modifying macromolecules (SMM) - incorporated ultrafiltration membranes for natural organic matter (NOM) removal: characterization and cleaning. Ph.D., University of Ottawa.

Datla, V. M. (2008). Surface modification of fibers and nonwovens with melt additives. Ph.D., North Carolina State University.

Fang, B., Q. Ling, et al. (2009). "Modification of polyethersulfone membrane by grafting bovine serum albumin on the surface of polyethersulfone/poly(acrylonitrile-co-acrylic acid) blended membrane." Journal of Membrane Science **329**(1–2): 46-55.

Goel, N. K., Y. K. Bhardwaj, et al. (2009). "Physicochemical and electrochemical characterization of battery separator prepared by radiation induced grafting of acrylic acid onto microporous polypropylene membranes." eXPRESS Polymer Letters **3**(5): 268-278.

Gozdz, A. S., C. N. Schmutz, et al. (1997). Method of making polymeric electrolytic cell separator membrane. **US Patent 5607485**.

Hester, J. F., P. Banerjee, et al. (1999). "Preparation of Protein-Resistant Surfaces on Poly(vinylidene fluoride) Membranes via Surface Segregation." Macromolecules **32**(5): 1643-1650.

Hester, J. F., P. Banerjee, et al. (2002). "ATRP of Amphiphilic Graft Copolymers Based on PVDF and Their Use as Membrane Additives." Macromolecules **35**(20): 7652-7661.

Iervolino, R. (2006). Rheology and morphology of the flow induced crystallization in polymers. Ph.D., Universita` degli Studi di Salerno.

Kazimi, M. R., I. Ahmed, et al. (2011). A Short Review of Hydrophilic Surface Modification Methods for Low Density Poly Ethylene. International Conference on Chemical Innovation (ICCI 2011). TATI University College.

Kim, J. Y. and D. Y. Lim (2010). "Surface-Modified Membrane as A Separator for Lithium-Ion Polymer Battery." Energies **3**(4): 866-885.

Kim, S. H., S.Y. Kwak, et al. (2003). "Design of TiO2 nanoparticle self-assembled aromatic polyamide thin-film-composite (TFC) membrane as an approach to solve biofouling problem." Journal of Membrane Science **211**(1): 157-165.

Kundu, P. P. and S. Choe (2003). "Transport of Moist Air Through Microporous Polyolefin Films." Journal of Macromolecular Science, Part C **43**(2): 143-186.

Lamberti, G. (2011). "Flow-induced crystallization during isotactic polypropylene film casting." Polymer Engineering & Science **51**(5): 851-861.

Li, E., Z. Du, et al. (2013). "Properties of a water layer on hydrophilic and hydrophobic self-assembled monolayer surfaces: A molecular dynamics study." Science China Chemistry **56**(6): 773-781.

Li, J.H., Y.-Y. Xu, et al. (2009). "Fabrication and characterization of a novel TiO2 nanoparticle self-assembly membrane with improved fouling resistance." Journal of Membrane Science **326**(2): 659-666.

Lin, K. Y. (2008). Novel polypropylene based microporous membranes via spherulitic deformation. Ph.D., New Jersey Institute of Technology.

Liu, D., J. Kang, et al. (2013). "Effect of annealing on phase structure and mechanical behaviors of polypropylene hard elastic films." Journal of Polymer Research **20**(5): 1-7.

Liu, F., N. A. Hashim, et al. (2011). "Progress in the production and modification of PVDF membranes." Journal of Membrane Science **375**(1–2): 1-27.

Meier-Haack, J., M. Valko, et al. (2004). "Microporous membranes from polyolefin-polyamide blend materials." Desalination **163**(1–3): 215-221.

Nady, N., M. C. R. Franssen, et al. (2011). "Modification methods for poly(arylsulfone) membranes: A mini-review focusing on surface modification." Desalination **275**(1–3): 1-9.

Nagō, S., S. Nakamura, et al. (1992). "Structure of microporous polypropylene sheets containing CaCO3 filler." Journal of Applied Polymer Science **45**(9): 1527-1535.

Nogales A., Hsiao B.S., et al. (2001). "Shear-induced crystallization of isotactic polypropylene with different molecular weight distributions: in situ small- and wide-angle X-ray scattering studies." Polymer **42**(12): 5247–5256.

Park, J. Y., M. H. Acar, et al. (2006). "Polysulfone-graft-poly(ethylene glycol) graft copolymers for surface modification of polysulfone membranes." Biomaterials **27**(6): 856-865.

Paul, S. (2009). Surface modification of polypropylene nonwovens to improve adhesion to elastomers. Ph.D., North Carolina State University.

Persson, P., M. J. Lundqvist, et al. (2006). "Quantum Chemical Calculations of the Influence of Anchor-Cum-Spacer Groups on Femtosecond Electron Transfer Times in Dye-Sensitized Semiconductor Nanocrystals." J Chem Theory Comput **2**(2): 441-451.

Rezaei Kolahchi, A., A. Ajji, et al. (2014). "Enhancing hydrophilicity of polyethylene terephthalate surface through melt blending." Polymer Engineering & Science: n/a-n/a.

Sadeghi, F. (2006). Development of microporous polypropylene by stretching. Ph.D., École Polytechnique de Montreal.

Seki, M., D. W. Thurman, et al. (2002). "Shear-Mediated Crystallization of Isotactic Polypropylene: The Role of Long Chain−Long Chain Overlap." Macromolecules **35**(7): 2583-2594.

Shi, G.Y., F. Chu, et al. (1989). "Plastic deformation and solid-phase transformation in β-phase polypropylene." Die Makromolekulare Chemie **190**(4): 907-913.

Somani, R. H., B. S. Hsiao, et al. (2000). "Structure Development during Shear Flow-Induced Crystallization of i-PP: In-Situ Small-Angle X-ray Scattering Study." Macromolecules **33**(25): 9385-9394.

Somani, R. H., L. Yang, et al. (2006). "Effects of high molecular weight species on shear-induced orientation and crystallization of isotactic polypropylene." Polymer **47**(15): 5657–5668.

Steenbakkers, R. J. A. (2009). Precursors and nuclei, the early stages of flow-induced crystallization. Ph.D., Technische Universiteit Eindhoven.

Suk, D. E., G. Chowdhury, et al. (2002). "Study on the Kinetics of Surface Migration of Surface Modifying Macromolecules in Membrane Preparation." Macromolecules **35**(8): 3017-3021.

Tabatabaei, S. H. (2009). Development of microporous membranes from PP/HDPE films through cast extrusion and stretching. Ph.D., École Polytechnique de Montreal.

Tjong, S. C., Y. Xu, et al. (1999). "Compatibility and degradation of blends of poly(caprolactone)–poly(ethylene glycol) block copolymer and polypropylene." Polymer **40**(13): 3703–3710.

Van der Meer, D. W. (2003). Structure-property relationships in isotactic polypropylene. Ph.D., University of Twente.

Williams JL, Gunther H, et al. (1974). Process for the preparation of opencelled microporous films. **US patent 3839516**.

Xanthos, M., C. Chandavasu, et al. (2002). "Melt processed microporous films from compatibilized immiscible blends with potential as membranes." Polymer Engineering & Science **42**(4): 810-825.

Xu, M., X. Shi, et al. (2010). "Synthesis and enrichment of a macromolecular surface modifier PP-b-PVP for polypropylene." Applied Surface Science **256**(10): 3240-3244.

Xu, Q., J. Yang, et al. (2013). "Hydrophilization of porous polypropylene membranes by atomic layer deposition of TiO2 for simultaneously improved permeability and selectivity." Journal of Membrane Science **448**(0): 215-222.

Yamazaki, S., K. Watanabe, et al. (2005). "Formation mechanism of shish in the oriented melt (I)—bundle nucleus becomes to shish." Polymer **46**: 1675–1684.

Yu, T. (1995). Processing and structure-property behavior of microporous polyethylene-from resin to final film. Ph.D., Virginia Polytechnic Institute and State University.

Zhang, C., Y. Bai, et al. (2010). "Preparation of hydrophilic HDPE porous membranes via thermally induced phase separation by blending of amphiphilic PE-b-PEG copolymer." Journal of Membrane Science **365**(1–2): 216-224.

Zhang, R. C., Y. Xu, et al. (2008). "Shear-induced crystallization of poly(phenylene sulfide)." Polymer **49**: 2604–2613.

Zhou, H. (1997). Structure-property relationship: model studies on melt extruded uniaxially oriented high density polyethylene films having well defined morphologies. Ph.D., Virginia Polytechnic Institute and State University.

Zhou, Y.-G., L.-S. Turng, et al. (2010). "Morphological evolution and orientation development of stretched iPP films: Influence of draw ratio." Journal of Polymer Science Part B: Polymer Physics **48**(11): 1223-1234.

Zhu, L.P., L. Xu, et al. (2007). "Preparation and characterization of improved fouling-resistant PPESK ultrafiltration membranes with amphiphilic PPESK-graft-PEG copolymers as additives." Journal of Membrane Science **294**(1–2): 196-206.

Zhu, L.P., Y.Y. Xu, et al. (2009). "Amphiphilic PPESK-graft-P(PEGMA) copolymer for surface modification of PPESK membranes." Materials Chemistry and Physics **115**(1): 223-228.

Zhu, L.P., Z. Yi, et al. (2008). "Amphiphilic graft copolymers based on ultrahigh molecular weight poly(styrene-alt-maleic anhydride) with poly(ethylene glycol) side chains for surface modification of polyethersulfone membranes." European Polymer Journal **44**(6): 1907-1914.